Abschlußbericht des Vorhabens 03G0190A und B „SINDBAD I & II“

Zuwendungsempfänger: Leibniz-Institut für Meereswissenschaften (IFM-GEOMAR)
Wischhofstr. 1-3
24148 Kiel

und

Bundesanstalt für Geowissenschaften und Rohstoffe (BGR)
Postfach 51 01 53
30631 Hannover

Förderkennzeichen: 03G0190A (IFM-GEOMAR)
03G0190B (BGR)

Projektleiter: Prof. Dr. Heidrun Kopp (IFM-GEOMAR)
Dr. Christian Müller (BGR)

Vorhabenbezeichnung: SO 190 SINDBAD I & II

Laufzeit des Vorhabens: 01.09.2006 bis 31.12.2008 (IFM-GEOMAR)
01.08.2006 bis 30.11.2008 (BGR)

Berichtszeitraum: 01.08.2006 bis 31.05.2009

1. Aufgabenstellung

Im Rahmen des Forschungsprojektes SINDBAD (Seismische und geoakustische Untersuchungen entlang des Übergangs vom Sunda- zum Banda-Bogen) wurden marin-geophysikalische Untersuchungen mit FS SONNE vor dem östlichen Sundabogen und im Übergangsbereich zum Bandabogen vor Indonesien durchgeführt. Während der Fahrten SO 190 wurden - neben bathymetrischen und Potentialfeldmessungen – refraktionsseismische und reflexionsseismische Daten auf identischen Profilen mit dem Ziel gewonnen, strukturelle Wechselwirkungen zwischen Unter- und Oberplatte zu untersuchen.

2. Voraussetzungen

Die SONNE-Fahrten SO190 I und II wurden in den Zeiträumen vom 09.10.2006 bis zum 09.11.2006 (BGR) sowie vom 10.11.2006 bis zum 24.12.2006 (IFM-GEOMAR) planmäßig und erfolgreich durchgeführt.
Ein regelmäßiger Austausch zwischen den Arbeitsgruppen in Hannover (BGR) und Kiel (IFM-GEOMAR) sowie die enge Zusammenarbeit und Absprache der Projektleiter bildete die Grundlage für den erfolgreichen Abschluss der wissenschaftlichen Arbeiten, die in den unten aufgeführten Publikationen detailliert dargestellt sind. Die Aufteilung der Datenbearbeitung auf die beiden Standorte Hannover und Kiel setzte einen koordinierten wissenschaftlichen Austausch voraus, der aufgrund der guten Kooperation der Arbeitsgruppen erfolgreich und effektiv umgesetzt werden konnte.

3. Planung und Ablauf

Der vorgelegte Zeitplan wurde eingehalten.

4. Wissenschaftlich-technischer Stand

Der wissenschaftlich-technische Stand ist im Antrag ausführlich dargelegt.

5. Zusammenarbeit mit anderen Stellen

Neben den Kollegen des Verbundprojektes SINDBAD waren Wissenschaftler aus Indonesien an den Ausfahrten beteiligt. Als Gastwissenschaftler hat Dr. Leonardo Seeber vom Lamont-Doherty Earth Observatory am ersten Fahrtabschnitt SO190 I teilgenommen.

Die Arbeiten des Vorhanbens profitierten maßgeblich von einem Austausch mit laufenden sowie abgeschlossenen Projekten basierend auf FS SONNE-Fahrten entlang des Sunda-Kontinentrandes (SO137-139, SO179, SO186), so dass die Ergebnisse nicht nur im Hinblick auf das Untersuchungsgebiet, sondern im Rahmen des plattentektonischen Systems einzuordnen sind.

Die Daten des SINDBAD Projektes flossen zudem in die Modellierungen des GITEWS-Vorhabens zur Tusnami-Frühwarnung mit ein und unsere Arbeitsgruppen (BGR und IFM-GEOMAR) haben mit den Kollegen des GFZ Potsdam (S. Brune, A. Babeyko, S. Sobolev) zusammengearbeitet, um eine Abschätzung des Tsunamipotentials des Untersuchungsgebietes zu erarbeiten. Die Ergebnisse sind im Manuskript von S. Brune et al. dargelegt.

Die im SINDBAD Projekt datierten magnetischen Anomalien sind bei der FS SONNE-Fahrt SO199 nach Westen hin bis zum Investigator Ridge fortgesetzt und interpretiert worden. In der Region südlich des Arbeitsgebietes von SINDBAD werden die Anomalien in Zusammenarbeit mit der University von Sydney (A. Gibbons, D. Müller) neu interpretiert.

Eine weitere Zusammenarbeit hat sich mit der SE Asia Research Group des Royal Holloway College, London, entwickelt und fokussiert sich auf Untersuchungen der 'SE Asian Gateway Evolution'. U. a. werden die Ergebnisse des SINDBAD Projektes direkt in ein entsprechendes Symposium in London im Sept. 2009 einfliessen (eingeladener Vortrag H. Kopp et al., Variations in subduction style offshore Java, SAGE2009 Conference - Southeast Asian Gateway Evolution, 14-17 September 2009: Royal Holloway University of London).

6. Eingehende Darstellung der wissenschaftlichen Ergebnisse

Das Untersuchungsgebiet des SINDBAD-Projektes am Sunda-Banda-Bogen (Indonesien) stellt ein natürliches Labor da, um die Wechselwirkungen zwischen den tektonischen Strukturen der Unterplatte und der Segmentierung der Oberplatte zu untersuchen. Diese Prozesse wurden mittels einer seismischen Weitwinkeltomographie untersucht, für die ebenfalls die Informationen aus der Reflexionsseismik sowie Schweredaten berücksichtigt wurden. Die ozeanische Unterplatte südlich der Inseln Lombok und Sumba weist eine Mächtigkeit von 8.5-9.0 km auf. Tiefreichende Verwerfungen in der Nähe des Tiefseegrabens prägen die Kruste und gehen mit niedrigen Mantelgeschwindigkeiten von bis zu 7.5 km /s einher. Das Äußere Hoch ist durch seismische Geschwindigkeiten typisch für kompaktierte Sedimente charakterisiert und erfährt einen Volumenzuwachs hauptsächlich durch Unterplattungsprozesse. Die abtauchende Platte wird über eine Distanz von 70-100 km unterhalb des Vorderbogens verfolgt. Während das Lombok-Becken von einem serpentinisierten Mantelkeil unterlegt ist, sind ähnliche Strukturen seewärts der Insel Sumba nicht anzutreffen. Eine detaillierte Darstellung der Ergebnisse ist im Manuskript von Planert et al., 2009, JGR zusammengefasst.

Der Übergang vom Sunda- zum Banda-Bogen stellt eine der wenigen Regionen weltweit dar, wo die Anfangsphase einer Kontinent-Inselbogen-Kollision beobachtet wird. Die Kollision des australischen Kontinents mit dem Inselbogen führt hier zu großen Überschiebungssystemen. Eine kombinierte Analyse und Interpretation der im Rahmen des SINDBAD-Projektes gewonnenen Refraktions- und Reflexionsdaten mit den Schweredaten konnte zum ersten Mal die komplexe Tiefengeometrie des Gebietes südlich der Insel Sumba abbilden. Der 10-12 km mächtigen australischen Kruste südlich des Timorgrabens steht nördlich davon der 22-24 km mächtige Sumba-Rücken gegenüber. Dazwischen findet sich ein etwa 130 km breites Akkretionsprisma. Die strukturelle Diversität dieses Transektes könnte exemplarisch für junge Kollisionssysteme beim Übergang von ozeanischer Subduktion zu Kontinent-Inselbogen-Kollision stehen. Die detaillierten Ergebnisse sind in der Veröffentlichung Shulgin et al., 2009, GRL, dargestellt.

Die Sedimentmächtigkeit auf der abtauchenden ozeanischen Lithosphärenplatte von wenigen hundert Metern und damit auch der Sedimenteintrag in das Subduktionssystem ist, im Vergleich zum westlichen Sundabogen vor Sumatra, äußert gering. Das äußere Hoch liegt am östlichen Sundabogen gänzlich unterhalb des Meeresspiegels und die Ausprägung des äußeren Hochs bezüglich Tiefenlage und Volumen nimmt im Untersuchungsgebiet nach

Osten signifikant ab. Dieses ermöglichte eine gute Abbildung der Internstruktur des äußeren Hochs und auch der abtauchenden ozeanischen Lithosphärenplatte bis zu 70 km nördlich des Tiefseegrabens unterhalb des äußern Hochs. Die reflexionsseismischen Daten zeigen, dass nicht nur der jüngste seewärtige Teil des äußeren Hochs tektonisch aktiv ist. Überschiebungsstörungen im gesamten äußeren Hoch stellen Migrationswege für Fluide von der Plattengrenze bis zum Meeresboden dar. Eine rezente tektonische Aktivität des gesamten äußeren Hochs wird auch durch deutlich verkippte Sedimentsequenzen in Hangbecken auf dem äußeren Hoch als auch an der seewärtigen Flanke des Lombok-Beckens dokumentiert. Dadurch ergeben sich Hinweise auf ein ähnlich hohes Erdbeben- und Tsunamiriskio wie am westlichen Sundabogen. Weitere Details sind in der Veröffentlichung Müller et al., 2008, EOS, aufgeführt.
Die Reflexionsseismischen Daten zeigen zudem, dass die seewärts des Tiefseegrabens durch die Krümmung der abtauchenden ozeanischen Kruste angelegten Abschiebungen nach dem Eintritt in das Subduktionssystem unterhalb des äußeren Hochs als Überschiebungen reaktiviert werden. Die in 5-10 km breite Segmente zerbrochenen Krustenblöcke bilden Duplexstrukturen, die von unten an dem Akkretionskeil angelagert werden und dadurch zum Wachstum des Akkretionskeils betragen. Ein weiterer Hinweis auf die tektonische Aktivität des gesamten Subduktionskomplexes im Untersuchungsgebiet ergibt sich aus der Abbildung von Schlammdiapiren im östlichen Lombok-Becken. Eine Diapirstruktur erhebt sich etwa 40 m über den Meeresboden und steht in Verbindung mit einer seismisch transparenten Zone, welche Hinweise auf thermisch überprägte und mobile Sedimente im östlichen Lombok-Becken gibt. Weitere Details sind im Manuskript von Lüschen et al., 2009, Tectonophysics, dargestellt.

7. Fortschreibung des Verwertungsplans

- Es sind keine Erfindungen/Schutzrechtsanmeldungen gemacht oder Schutzrechte erteilt worden.

- Wirtschaftliche Verwertungskonzepte sind derzeit nicht konkret.

- Wissenschaftliche Ergebnisse wurden in Publikationen und auf nationalen und internationalen Tagungen mit Kurzfassungen von Postern und Vorträgen verwertet. Diese sind Ansatzpunkte für zukünftige Forschungsarbeiten und eröffnen bzw. vertiefen unsere internationale wissenschaftliche Zusammenarbeit in der marinen Geophysik (aktive Kontinentalränder). Bisher erschienene und eingereichte Publikationen sind im Anhang gelistet. Publikationen mit peer-review Verfahren finden sich in Kopie im Anhang.

- Wissenschaftliche Anschlussfähigkeit für eine mögliche nächste Phase: Eine weitergehende Untersuchung des Messgebietes, die Lücken schließt und offene Fragen angeht, wäre aus unserer Sicht eine sinnvolle nächste Phase.

8. Ergebnisse von dritter Seite mit Relevanz zum laufenden Projekt

- Wir stehen in engem Austausch mit internationalen Gruppen, die sich mit der Systemforschung an aktiven Kontinenträndern befassen und haben laufend Ergebnisse von dritter Seite in unsere Arbeiten integriert (z.B. neue Untersuchungen der Hikurangi-Zone des GNS Neuseeland (S. Henrys, R. Sutherland), die viele Korrelationen mit dem Äußeren Hoch im SINDBAD-Arbeitsgebiet aufweisen oder auch vulkanologische Untersuchungen auf Java (Macquarie-University, Sydney, H. Handley) um eine Anbindung an die onshore-Geologie zu ermöglichen.

9. Publikationen

Begutachtete Publikationen:

C. Mueller, H. Kopp, Y. S. Djajadihardja, U. Barckhausen, A. Ehrhardt, M. Engels, E. R. Flueh, C. Gaedicke, H. Keppler, R. Lutz, E. Lüschen, S. Neben, L. Seeber, D. P. S. Dzulkarnaen, From Subduction to Collision: The Sunda-Banda Arc Transition, EOS Transactions, Vol. 89, No. 6, P. 49-50, 2008.

Shulgin, A., H. Kopp, C. Mueller, E. Lueschen, L. Planert, M. Engels, E. R. Flueh, A. Krabbenhoeft, and Y. Djajadihardja (2009), Sunda-Banda arc transition: Incipient continent-island arc collision (northwest Australia), Geophys. Res. Lett., 36, L10304, doi:10.1029/2009GL037533.

E. Lueschen, C. Mueller, H. Kopp, M. Engels, R. Lutz, L. Planert, A. Shulgin, Y. Djajadihardja, Structure, Evolution and Tectonic Activity of the Eastern Sunda Forearc, Indonesia, from Marine Seismic Investigations, Tectonophysics, in review, 2009.

S. Brune, S. Ladage, A. Y. Babeyko, C. Mueller, H. Kopp, S. V. Sobolev, Submarine landslides at the eastern Sunda margin: observations and tsunami impact assessment, Natural Hazards, in review, 2009.

L. Planert, H. Kopp, E. Lueschen, C. Mueller, E. R. Flueh, A. Shulgin, Y. Djajadihardja, A. Krabbenhoeft, Lower plate structure and upper plate deformational segmentation at the Sunda-Banda arc transition, Indonesia, resolved from the analysis of seismic and gravity data, submitted to JGR, 2009.

Publikationen in Vorbereitung:

Shulgin, A., H. Kopp, C. Mueller, L. Planert, E. Lueschen, E. R. Flueh, A. Krabbenhoeft, and Y. Djajadihardja, Geophysical investigations of the 1994 tsunamogenic earthquake slip area offshore Java.

W. Weinrebe, H. Kopp, Globale Auslöser von Tsunamis: Erdbeben, Vulkane, Hangrutuschungen, eingeladener Beitrag für 'Geologische Rundschau', Sonderheft 12/2009.

Krabbenhöft, A., Weinrebe, W., Kopp, H., Flueh, E. R., Ladage, S., Djajadihardja, Y., Bathymetry in the Indian Ocean, Natural Hazards and Earth System Sciences, 2009.

Vorträge / Poster:

EGU-Jahrestagung, Wien, 19.-24. April 2009

L. Planert, A. Shulgin, H. Kopp, E. Lueschen, C. Mueller, E. Flueh, Y. Djajadihardja, and M. Engels, Crustal structure of the Sunda-Banda arc transition: results from marine geophysical investigations offshore eastern Indonesia

A. Shulgin, H. Kopp, C. Mueller, E. Lueschen, L. Planert, M. Engels, E.R. Flueh, A. Krabbenhoeft, and Y. Djajadihardja, The Australia - Indonesia continent to island arc collision: a case study of the Sunda-Banda Arc based on seismic and gravity modeling

DGG-Jahrestatung, Kiel, 23.-26. March 2009

Planert, L., H. Kopp, A. Shulgin, E. Lueschen, C. Mueller, E. Flueh, M. Engels, Y. Djajadihardja, Crustal structure of the Sunda-Banda arc transition: linking lower plate variability and forearc deformation

Shulgin, A., H. Kopp, C. Mueller, E. Lueschen, L. Planert, M. Engels, E.R. Flueh, A. Krabbenhoeft, and Y. Djajadihardja, The Sunda-Banda Arc Transition (northwest Australia): seismic and gravity modeling of the incipient continent-island arc collision

SONNE Statusseminar, Bremerhaven, 12.-13. Feb. 2009

Christian Müller, Heidrun Kopp, Ewald Lüschen, Martin Engels, Lars Planert, Alexey Shulgin, Y. Djajadihardja, und die SINDBAD Arbeitsgruppe, Seismische und geoakustische Untersuchungen entlang des Übergangs vom Sunda- zum Banda-Bogen

Lars Planert, Alexey Shulgin, Heidrun Kopp, Ewald Lüschen, Christian Müller, Ernst Flüh, Martin Engels, Y. Djajadihardja, und die SINDBAD Arbeitsgruppe, SO190 SINDBAD, Leg 2: Refraktionsseismische Untersuchungen entlang des Übergangs vom Sunda- zum Banda-Bogen

Ewald Lüschen, Christian Müller und die SINDBAD Arbeitsgruppe, SO190 SINDBAD, Leg 1: Reflexionsseismische Untersuchungen entlang des Übergangs vom Sunda- zum Banda-Bogen

AGU-Jahrestagung, San Francisco, 15.-19. Dec. 2008:

Planert, L., Kopp, H., Shulgin, A., Lueschen, E., Mueller, C., Djajadihardja, Y., Flueh, E., R., Engels, M., the SINDBAD Working Group: Crustal Structure of the Sunda-Banda Arc Transition: Linking Forearc Deformation and Lower Plate Variability VORTRAG

Lueschen, E., Mueller, C., Kopp, H., Djajadihardja, Y., Ehrhardt, M.,Engels, M., Lutz, M.,Planert, L, Shulgin, A., Working Group:, Sunda-Banda Arc Transition: Marine Multichannel Seismic Profiling POSTER

Shulgin, A., Planert, L., Kopp, H., Mueller, C. Lueschen, E., Engels, M., Flueh, E. R., Djajadihardja, Y., SINDBAD Working Group, Sunda-Banda Arc Transition: Marine Wide-Angle Seismic Modeling POSTER

International Geological Congress, Oslo, 6.- 14. Aug. 2008:

Shulgin, A., Planert, L., Kopp, H., Müller, C., Lüschen, E. and Flüh, E.R. Sunda-Banda Arc Transition: Wide-angle seismic modeling POSTER

Seismix Meeting, 13th Internal. Symposium on 'Deep seismic profiling of the continents and their margins', June 8-13, 2008, Saariselkä, Finland

Shulgin, A., Planert, L., Kopp, H., Müller, C., Lüschen, E. and Flüh, E.R. Sunda-Banda Arc Transition: Wide-angle seismic modeling POSTER

Lüschen, E., Müller, C., Kopp, H., Planert, L., Engels, M., Shulgin, A. and Djajadihardja, Y.S, Subduction along the Sunda-Banda Arc Transition VORTRAG

Lüschen, E., Müller, C., Kopp, H., Planert, L., Engels, M., Shulgin, A. and Djajadihardja, Y.S. Sunda-Banda Arc Transition: Marine multichannel seismic profiling POSTER

EGU-Jahrestagung, Wien, 13.-18. April. 2008:

Shulgin, A; Planert, L; Kopp, H; Müller, C; Lüschen, E; Flüh, E Subduction along the Sunda-Banda Arc Transition: Marine Wide-Angle Seismic Modelling POSTER

Mueller, C.; Kopp, H.; Djajadihardja, Y.; Engels, M.; Flueh, E.; Gaedicke, C.; Lueschen, E.; Neben, S.; Planert, L.; Shulgin, A, Subduction along the Sunda-Banda Arc transition: Marine multichannel seismic profiling POSTER

DGG-Jahrestagung, Freiberg, 3.-6. März 2008:

L Planert, A Shulgin, H Kopp, C Mueller, E Lueschen, M Engels, The Sunda-Banda Arc Transition: New Insights From Marine Wide-Angle Seismic Data Offshore Eastern Indonesia POSTER

AGU-Jahrestagung, San Francisco, 10.-14. Dec. 2007:

H. Kopp, D. Hindle, Structure and Evolution of the Accretionary Margin of Java-Sumatra. Seismic Data and Numerical Modeling Comparisons VORTRAG

L Planert, A Shulgin, *H Kopp, C Mueller, E Flueh, E Lueschen, M Engels, M Dayuf Jusuf, The Sunda-Banda Arc Transition: New Insights From Marine Wide-Angle Seismic Data POSTER

C Mueller, H Kopp, Y Djajadihardja, M Engels, E Flueh, C Gaedicke, E Lueschen, R Lutz, L Planert, A Shulgin, D D Soemantri, SINDBAD Working Group, The Sunda-Banda Arc Transition: New Insights from Marine Multichannel Seismic Data POSTER

EGU-Jahrestagung, Wien, 15.-20. April. 2007:

Mueller, C.; Kopp, H.; Djajadihardja, Y. S.; Engels, M.; Flueh, E. R.; Gaedicke, C.; Lueschen, E.; Soemantri, D.; The SINDBAD Working Group, The Sunda-Banda Arc Transition - First results from recent marine geophysical investigations offshore eastern Indonesia (Part 1) POSTER

Shulgin, A; Planert, L; Mueller, C; Flueh, E; Kopp, H; Krabbenhoeft, A; Lueschen, E; Yusuf, D; SINDBAD Working Group, The Sunda-Banda Arc Transition - First results from recent marine geophysical investigations offshore eastern Indonesia (Part 2) POSTER

DGG-Jahrestagung, Aachen, 26.-29. März 2007:

Christian Müller, Heidrun Kopp, Yusuf Djajadihardja, Martin Engels, Ernst Flueh, Christoph Gaedicke, Ewald Lüschen, Dzulkarnaen D. P. Soemantri, SINDBAD Working Group, The Sunda-Banda Arc Transition - First results from recent marine geophysical investigations offshore eastern Indonesia (Part 1) POSTER

Alexey Shulgin Lars Planert, Christian Müller, Ernst Flueh, Heidrun Kopp, Anne Krabbenhöft, Ewald Lüschen, M. Dayuf Yusuf, SINDBAD Working Group, The Sunda-Banda Arc Transition - First results from recent marine geophysical investigations offshore eastern Indonesia (Part 2) POSTER

EOS
EOS, TRANSACTIONS, AMERICAN GEOPHYSICAL UNION

VOLUME 89 NUMBER 6
5 FEBRUARY 2008
PAGES 49–60

From Subduction to Collision: The Sunda-Banda Arc Transition

PAGES 49–50

In the aftermath of the M_w 9.3 Indian Ocean earthquake and tsunami of 26 December 2004, which killed more than 250,000 people, numerous investigations have been commissioned near the epicenter offshore northern Sumatra to evaluate future earthquake and tsunami hazards. These projects have mapped seafloor morphology and imaged deep structures and faults in order to better understand the origin of megathrust earthquakes and tsunamis in the western portion of the Sunda Arc subduction system offshore northern Sumatra [e.g., *Henstock et al.*, 2006].

In contrast, the eastern part of the arc has received relatively little attention, even though it may be just as hazardous. Our geophysical data from the eastern Sunda Arc and the transition to the Banda Arc (Figure 1) provide evidence for recent tectonic activity and thus for a similar earthquake and tsunami risk.

Project Goals: Seismic and Geoacoustic Investigations

Our investigations are part of the joint German-Indonesian project SINDBAD (Seismic and Geoacoustic Investigations Along the Sunda-Banda Arc Transition), whose main goal is to quantify key parameters about seafloor sediments, oceanic crust (continental crust at the western Banda Arc), and mantle lithosphere that enter the subduction system at the trench. This study area is quite variable: The Roo Rise, the Argo Abyssal Plain, and the continental lithosphere of Australia highlight variations in morphology and composition of the subducting plate from west to east along the Sunda-Banda arc transition zone (Figure 1).

We investigate the influence of the incoming plate (Roo Rise, Argo Abyssal Plain, and Australian continental lithosphere) on the evolution of the overriding plate by imaging deep and shallow crustal structures using a suite of geophysical methods. These methods include analyses of multichannel reflection seismic (MCS), magnetic, and gravity data, as well as analyses of data collected through ocean bottom seismometers (OBS), swath bathymetry, and sediment echo sounders. Our data were collected on cruise SO190-SINDBAD, which was carried out on the German R/V *Sonne* during two consecutive legs from October until December 2006.

Because modern seismic and acoustic imaging has not been conducted in detail in the area of the Sunda-Banda arc transition, much of our study's efforts were focused on gaining a clearer picture of the area's tectonic setting.

Tectonic Setting

The orientation of the 7000-kilometer-long Sunda Arc gradually bends from east-west along Java to north-south along the Andaman Islands off Myanmar. The relative plate motion between the subducting Indo-Australian plate and the overriding Eurasian plate is thus nearly perpendicular in the study area at the eastern end of the arc, but is highly oblique at the western end, where plate motion is partitioned into thrust and strike-slip movement. The subduction rate of the Indo-Australian plate increases gradually eastward, reaching about 76 millimeters each year at the eastern end of the arc, compared with 60 millimeters each year at Sumatra's northern coast (Figure 1, inset).

While the overriding lithosphere is continental along Sumatra and Java, it is oceanic farther east along Lombok and Sumbawa (see Figure 1 for locations). The subducting oceanic lithosphere is characterized by two

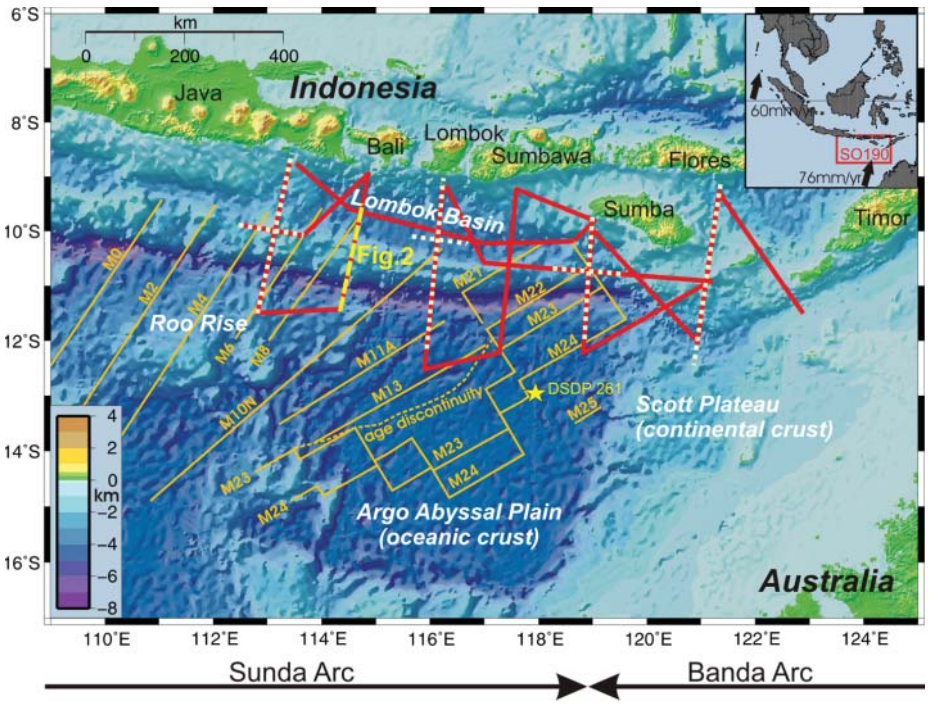

Fig. 1. Location map of the SO190-SINDBAD survey area with 4933 kilometers of geophysical lines (red) and reinterpreted magnetic anomalies modified from Heine et al. *[2004] in orange. Dotted lines (white) indicate the locations of seven refraction seismic lines augmented with ocean bottom seismometer stations. The locations of the multichannel reflection seismic section shown in Figure 2 are marked yellow. The inset shows the location of the survey area and convergence rates according to a global velocity model (NUVEL-1A).*

By C. Müller, H. Kopp, Y. S. Djajadihardja, U. Barckhausen, A. Ehrhardt, M. Engels, E. R. Flueh, C. Gaedicke, H. Keppler, R. Lutz, E. Lüschen, S. Neben, L. Seeber, and Dzulkarnaen D. P.S.

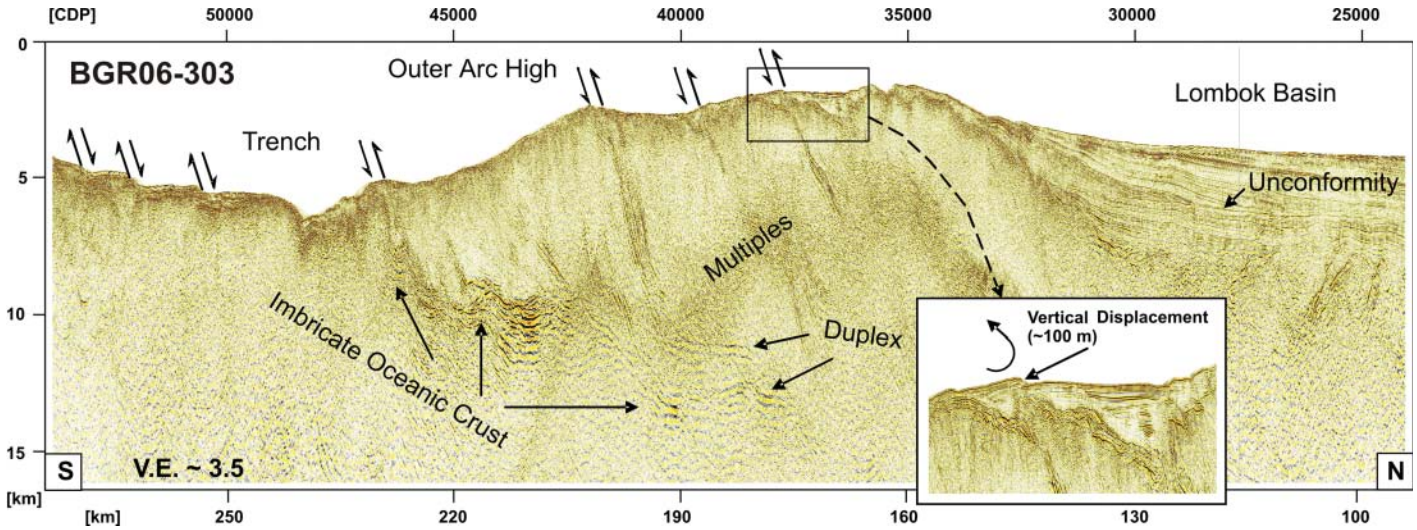

Fig. 2. Section of seismic line BGR06-303 (location shown in Figure 1) imaging major splay faults originating from duplex structures at the boundary between the overriding and the subducting plate and connecting to the seafloor, where they control small sedimentary basins. One of these basins is characterized by a pronounced vertical seafloor displacement of about 100 meters (inset). The fore-arc Lombok Basin is characterized by a major unconformity and tilted sedimentary strata. Data acquisition has been carried out using a 51-liter tuned airgun array, a 50-meter shot point interval, and a 3-kilometer active streamer length with 240 recording channels. Seismic data processing including poststack Kirchhoff-time migration was followed by time-to-depth conversion.

distinct provinces at the eastern part of the Sunda Arc. Offshore eastern Java, the oceanic Roo Rise is characterized by rough and high relief, while offshore Lombok and Sumbawa the Argo Abyssal Plain is smooth and about 1500 meters deeper. Still farther to the east, the continental lithosphere of Australia is colliding with the western Banda Arc along the islands of Flores, Sumba, and Timor.

The thickness of the sediment covering the incoming oceanic lithosphere, including the deep sea trench, decreases with increasing distance from the thick alluvial fan at the northern end of the Bay of Bengal (Bengal Fan), from about 4 kilometers offshore Sumatra to about 1.3 kilometers offshore western Java, and finally to less than 1 kilometer along the eastern Sunda Arc. Both sediment thickness and the nature of the underlying lithosphere are important factors affecting the tectonics of the arc.

A thick sedimentary section, composed mainly of deposits from the Bengal Fan, enters the subduction system at the trench offshore Sumatra and is largely accreted to the overlying Eurasian plate. This sedimentary section clearly contributes to the growth of the outer arc in the western part of the Sunda Arc. In the eastern part, incoming sediment is derived mostly from normal ocean sedimentation (pelagic), is about an order of magnitude thinner, and proportionally less of it may be accreted.

Subduction Factory and Tsunami Hazard

Despite major and systematic differences in kinematic and geologic parameters, the sizes and rates of earthquakes and tsunamis appear to be similar along all parts of the Sunda Arc [e.g., *Puspito*, 2002]. While the huge earthquake and tsunami disaster of 2004 as well as the recent 12 September 2007 M_w 8.4 event are still fresh in the minds of people worldwide, the 17 July 2006 M_w 7.8 tsunamigenic earthquake offshore Java is a reminder that 2004-like events may occur elsewhere along the Sunda Arc.

Magnetic seafloor-spreading anomalies of Late Jurassic age (155–145 million years ago) in the Argo Abyssal Plain represent the oldest crust along the entire Sunda Arc. Our magnetic data generally confirm the overall interpretation of the magnetic anomalies by *Heine et al.* [2004], but we suggest some significant modifications to Heine et al.'s conclusions. For example, through interpretation of our data, anomalies on the subducting crust can now be traced landward of the trench: In the northeastern part of the Argo Abyssal Plain, we map several Late Jurassic magnetic reversals (M24 through M21; see Figure 1) between two fracture zones.

Our MCS profiles image the bending of the oceanic crust down into the Earth's mantle as well as the associated normal faulting that results from this bending. Landward of the trench, profiles image the subducting slab beneath the outer arc high (highest elevation of seafloor in front of the volcanic arc), where the former bending-related normal faults (where the hanging block moves down) appear to be reactivated as reverse faults (where the hanging block is thrust up), causing vertical displacement and relief on the subducting slab. The accretionary prism and the outer arc high are characterized by a northward dipping system of overlapping (imbricate) thrust sheets with major thrust faults connecting seafloor and detachment (see fault structure in Figure 2).

On seismic profile BGR06-303 (Figure 2), a broad fault zone around kilometer 170 approaches the seafloor of the outer arc high. Evidence for recent deformation suggests this is an out-of-sequence splay fault (a fault that branches from the megathrust between the subducting and the overriding plate). The strong reflectivity of this fault can be related to alteration of the sediment by fluids rising along this fault. These fluids originate from subducted sediments as they lose their water at depth through dewatering processes such as those, for example, observed on the northern Barbados Ridge [*Shipley et al.*, 1994]. Close to the seafloor, this fault system controls a small basin (Figure 2, inset) that piggybacks the outer arc high. This piggyback basin is characterized by seaward-tilted sediment layers and a pronounced vertical seafloor displacement of about 100 meters.

Compression results in the shortening and steepening of the imbricate thrust sheets, contributing to buildup of the outer arc high. This continuing process is represented in tilted piggyback basin sediments and the observed seafloor displacement. North of the outer arc high, a thick upper sequence of landward-tilted sediments characterizes the southern Lombok Basin (Figure 2). This sequence of steeper dipping strata terminates against an underlying sedimentary sequence of lower dip (a pronounced unconformity) and also gives evidence for recent relative uplift of the landward and thus oldest part of the outer arc high. These clear seismic indications of continuous and abrupt uplift create the hazard for major earthquakes and tsunamis in the eastern part of the Sunda Arc.

Future Work

One of the general goals of this and other recent projects along the Sunda subduction

system is the improved characterization of future damaging earthquakes. Additionally, fore-arc basin evolution and the potential for hydrocarbon resources will be addressed in subsequent stages of our project. Geometries and dimensions of key elements of the subduction system will be obtained by the integration of depth models from MCS and OBS data. Our findings may also provide targets for in situ probing of active thrust faults.

Acknowledgments

We thank Captain Oliver Meyer and his crew for excellent cooperation and support during the cruise. The cruise and project SO190-SINDBAD are funded by the German Ministry of Education and Research (BMBF) under projects 03G0190A and 03G0190B. We gratefully acknowledge the continuous support for marine sciences with the outstanding research vessel *Sonne*. We are grateful to the Indonesian government for allowing us to work in its territorial waters.

References

Heine, C., R. D. Müller, and C. Gaina (2004), Reconstructing the lost Tethys Ocean basin: Convergence history of the SE Asian margin and marine gateways, in *Continent-Ocean Interactions Within East Asian Marginal Seas, Geophys. Monogr. Ser.*, vol. 149, edited by P. Clift et al., pp. 37–54, AGU, Washington, D.C.

Henstock, T. J., L. C. McNeill, and D. R. Tappin (2006), Seafloor morphology of the Sumatran subduction zone: Surface rupture during megathrust earthquakes?, *Geology, 34*, 485–488.

Puspito, N. T. (2002), Tsunami and earthquake activity in Indonesia, in *Proceedings of the International Workshop: Local Tsunami Warning and Mitigation*, edited by B. W. Levin and M. A. Nasov, pp. 138–145, Janus-K, Moscow.

Shipley, T. H., G. F. Moore, N. L. Bangs, J. C. Moore, and P. L. Stoffa (1994), Seismically inferred dilatancy distribution, northern Barbados Ridge decollement: Implications for fluid migration and fault strength, *Geology, 22,* 411–414.

Author Information

Christian Müller, Udo Barckhausen, Axel Ehrhardt, Martin Engels, Christoph Gaedicke, Hans Keppler, Rüdiger Lutz, Ewald Lüschen, and Sönke Neben, Federal Institute for Geosciences and Natural Resources (BGR), Hanover, Germany; E-mail: Christian.Mueller@bgr.de; Heidrun Kopp and Ernst R. Flueh, Leibniz Institute of Marine Sciences at University of Kiel (IFM-GEOMAR), Kiel, Germany; Yusuf S. Djajadihardja and Dzulkarnaen D. P. Soemantri, Agency for the Assessment and Application of Technology (BPPT), Jakarta, Indonesia; and Leonardo Seeber, Lamont-Doherty Earth Observatory (LDEO), Palisades, N.Y.

NEWS

Science News for the U.S. Hispanic Audience

PAGE 50

A science and health news service targeted toward the U.S. Hispanic community was launched on 23 January. ConCiencia, billed as the first Spanish-language science newswire service in the United States, provides free weekly news feeds to media targeting the U.S. Hispanic population. The news feeds, available to Spanish-language newspapers and radio stations, include newspaper features, radio segments, and online news content.

ConCiencia science advisor Bob Russell said it is critical to provide Hispanic media with an ongoing source of high-quality science news that meets the needs and interests of Hispanics. He noted that "Latinos currently achieve lower-than-average math and science scores in public schools and are significantly underrepresented in science and engineering professions."

AGU education program manager Inés Cifuentes, who received the Hispanic Heritage Foundation's 2007 Math and Science Hispanic Heritage Award, also addressed the media at the ConCiencia launch. She said there are a lot of bright schoolchildren whose talents are being wasted, and she hopes that the news service helps to educate them about science.

"Science is lots of fun, and kids love it, especially between the ages of three and when hormones hit," Cifuentes said. "It's not that we want to make all of them scientists, but we want to make all of them thinkers, and [ConCiencia] is a good way to do that."

ConCiencia, which is funded by the U.S. National Science Foundation, is a project of the Self-Reliance Foundation and the Hispanic Communications Network.

For more information, contact Duly Fernandez at duly.fernandez@hcnmedia.com.

—RANDY SHOWSTACK, Staff Writer

GEOPHYSICAL RESEARCH LETTERS, VOL. 36, L10304, doi:10.1029/2009GL037533, 2009

Sunda-Banda arc transition: Incipient continent-island arc collision (northwest Australia)

A. Shulgin,[1] H. Kopp,[1] C. Mueller,[2] E. Lueschen,[2] L. Planert,[1] M. Engels,[2] E. R. Flueh,[1] A. Krabbenhoeft,[1] and Y. Djajadihardja[3]

Received 29 January 2009; revised 15 April 2009; accepted 17 April 2009; published 27 May 2009.

[1] The eastern Sunda arc represents one of the few regions globally where the early stages of continent-arc collision can be studied. We studied along the western limit of the collision zone at the Sunda-Banda arc transition, where the Australian margin collides with the Banda island arc, causing widespread back arc thrusting. We present integrated results of a refraction/wide-angle reflection tomography, gravity modeling, and multichannel reflection seismic imaging using data acquired in 2006 southeast of Sumba Island. The composite structural model reveals the previously unresolved deep geometry of the collision zone. Changes in crustal structure encompass the 10–12 km thick Australian basement in the south and the 22–24 km thick Sumba ridge in the north, where backthrusting of the 130 km wide accretionary prism is documented. The structural diversity along this transect could be characteristic of young collisional systems at the transition from oceanic subduction to continent-arc collision. **Citation:** Shulgin, A., H. Kopp, C. Mueller, E. Lueschen, L. Planert, M. Engels, E. R. Flueh, A. Krabbenhoeft, and Y. Djajadihardja (2009), Sunda-Banda arc transition: Incipient continent-island arc collision (northwest Australia), *Geophys. Res. Lett.*, *36*, L10304, doi:10.1029/2009GL037533.

1. Introduction

[2] The convergence of the Indo-Australian plates and Eurasia and resulted in the formation of the Sunda and Banda island arcs. The transitional zone between the arcs is located south of Flores Island and is characterized by the change in the tectonic regime along the boundary. This segment of the plate boundary was only little investigated previously. In the scope of this study we address the problem of constraining the entire crustal scale structure and current geodynamic regime at the transitional zone using seismic reflection and wide-angle investigations and gravity modeling.

2. Tectonic Setting

[3] The plate boundary south of Sumba Island, Indonesia, is marked by a change in the tectonic regime (Figure 1) from subduction of the Indo-Australian oceanic lithosphere along the Sunda margin in the west that began ~45 m.y. ago [*Hall*, 2002] to continent - island arc collision along the Banda arc in the east [*Audley-Charles*, 1975; *Katili*, 1989; *Milsom*, 2001; *Audley-Charles*, 2004]. This margin experiences the early stages of continent-island arc collision as a result of the interaction between the Australian margin and the Banda island arc in the Pliocene [*Hall and Smyth*, 2008].

[4] Our goal is to constrain the deep crustal structure and tectonic evolution of the forearc using geophysical data collected during the RV Sonne SO-190 cruise in 2006. Our profile starts at ca. 12.5°S at the transition from the Late Jurassic oceanic lithosphere of the Argo Abyssal plain to the rifted Triassic continental crust of the Scott plateau [*van der Werff*, 1995] that is marked by the eastern termination of the Java trench at the transition to the Timor trough (Figure 1). Northwards, the oblique collision of the rifted continental crust of the Scott plateau with the forearc commenced 3–5 Ma ago [*Harris*, 1991] at a rate of ~7 cm/yr [*Curray*, 1989]. The current convergence rate at the Timor trough is ~15 mm/yr [*Bock et al.*, 2003] and it is manifested in back arc thrusting [*Silver and Reed*, 1988]. The Sumba Block, farther north, is believed to be an isolated tectonic block trapped between the trench and the volcanic arc (see *Rutherford et al.* [2001] and *Hall and Smyth* [2008] for discussion). Ridge structures of the Sumba Ridge include the submarine basement high, extending from Sumba Island to Savu Island and then merging with outer high crest towards Timor Island (Figure 1) [*Silver et al.*, 1983]. The basement of the ridge is dated from >80 to ~18 Ma, as inferred from the outcrops of intrusives and volcanic rocks together with sediments on Sumba and Savu Islands [*Karig et al.*, 1987], which might have been a part of the Paleogene Sumba-Banda forearc [*Hall and Smyth*, 2008].

[5] The origin of the abnormal width of the forearc south of Flores Island is enigmatic (Figure 1). Seismicity deeper than 30 km is absent between the islands of Sumba and Timor, while further north common earthquakes deeper than 100 km [*Engdahl and Villaseñor*, 2002] suggest the presence of the subducting slab below the Banda island arc, further confirmed by geochemical data from Flores Island [*Elburg et al.*, 2004]. However, most volcanic rocks of the Banda islands consist of primitive basalts typical of a volcanic arc built on oceanic lithosphere [*Hamilton*, 1988]. The complex basement thus reflects different periods of extension, subduction, and collision in Eastern Indonesia [*Hall and Smyth*, 2008].

3. Data Acquisition and Modeling

[6] Here we present a Vp seismic tomography model along the Sunda - Banda arc transition, further constrained by gravity modeling. Marine seismic investigations (Figure 1) were carried out by multichannel seismic reflection profiling (MCS), accompanied by gravity measurements, and seismic refraction profiling with ocean-bottom seismometers (OBS)

[1]Leibniz Institute of Marine Sciences, IFM-GEOMAR, Kiel, Germany.
[2]Federal Institute for Geosciences and Natural Resources, Hannover, Germany.
[3]Agency for the Assessment and Application of Technology, Jakarta, Indonesia.

0094-8276/09/2009GL037533$05.00

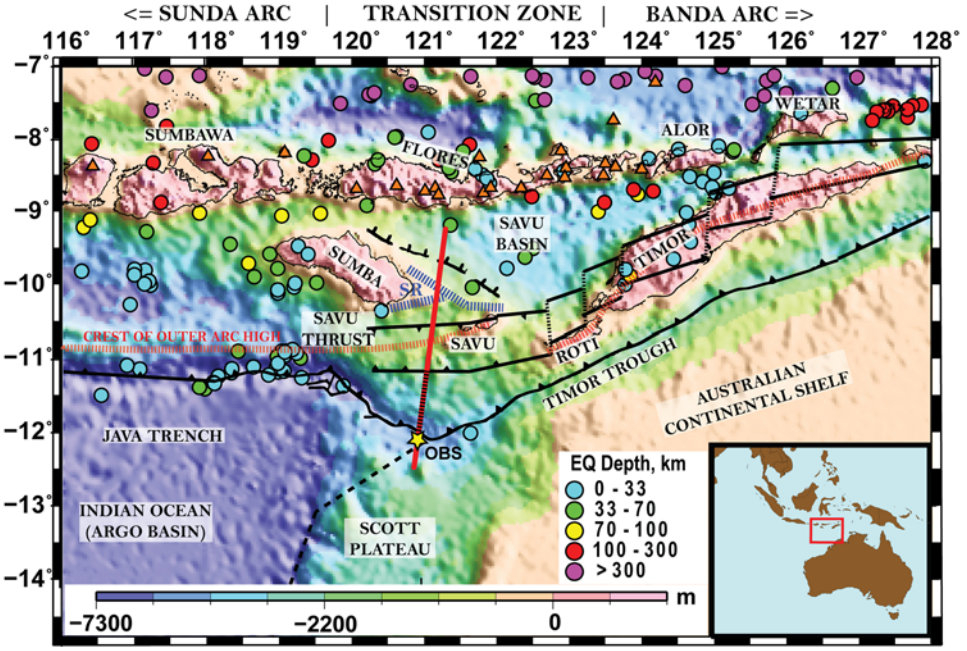

Figure 1. Simplified tectonic and bathymetric map of the Sunda-Banda Arc transition. Red line - seismic profile discussed in this study. Dashed red-black line - the MCS section shown in Figure 2. Yellow star - OBS location shown in Figure 2. Red triangles - active and Neogene volcanoes. Dashed blue line - a submarine Sumba Ridge (SR). Dashed red line - the crest of the outer forearc high. Black lines - faults [after *Rutherford et al.*, 2001; *Audley-Charles*, 2004]. Relocated earthquakes in the region are shown by filled circles, color-coded with depth [after *Engdahl and Villaseñor*, 2002].

and hydrophones (OBH) [*Mueller et al.*, 2008] (Text S1 of the auxiliary material).[1]

[7] The seismic velocity model was constrained by joint refraction/reflection 2D tomographic inversion [*Korenaga et al.*, 2000]. Data from a total of 36 stations were used as input to the tomographic modeling. First, ~16,000 first arrival phases with offsets of up to 120 km were picked; subsequently, ~4,000 reflected phases were added to the dataset. We applied a "top to bottom" approach with a simple layered starting model, initially constraining the model only for the near offsets and then increasing the depth extent of the ray coverage to constrain the entire model space. The structure of the sediments and the upper crust was controlled by the MCS data (Figure 2), thus constraining the upper section of the profile in great detail. Calculated uncertainty of traveltimes for ~85% of the all picked phases lies within the picking error range of 50 ms.

[8] The resulting Vp seismic tomography model was extended 100 km to the north and south and to a depth of 75 km to be used in forward gravity modeling. Velocities were converted to densities [*Christensen and Mooney*, 1995; *Carlson and Herrick*, 1990] and the subducting slab extended to 75 km depth underneath the island arc, where the deep seismicity commences. A constant density of 3.35 g/cm^3 was assumed for the mantle (Figure 3c).

4. Results (South to North Along 121°E)

4.1. Scott Plateau: Australian Crust

[9] The 2 km thick sedimentary cover of the Java trench has average Vp seismic velocities of 2–3 km/s in the trench section. A facies transition from deep marine fine grained carbonates to Upper Cretaceous shallow marine clastic deposits [*Stagg and Exon*, 1979] recognized in the MCS data forms the décollement at ~5 km depth (Figure 2a). A mud diapir observed at CDP 12900 (Figure 2) may be related to high pore pressures in the lower unit, also a series of linear mud diapirs nearby have been reported by *Breen et al.* [1986]. At depths between 6 km and 10 km Vp below the reflection gradually change from 3.5 km/s to 5 km/s (Figure 3a). Upper crustal velocities are ~6.0 km/s and increase to 6.7–7.0 km/s in the lower crust (Figure 3a), as revealed by the Puc and Plc phases (Figure 2c). The transition from the upper to the lower crust is marked by a strong reflection well documented by Pic phases. The Moho is recovered by the PmP phases at a depth of 20 km and is apparently dipping northwards at an angle of ~1°. Thus, the thickness of the crystalline crust reaches 10 to 12 km only. Although a continental crust with an Australian affinity was proposed to exist further east [*Kaneko et al.*, 2007], these values are in contrast to the typical thickness of the continental crust in NW Australia [*Collins et al.*, 2003] and at other continental shelves [e.g., *Ritzmann and Faleide*, 2007].

4.2. Frontal Prism and the Neogene Accretionary Wedge

[10] Imbricate thrusting (Figure 2a) and relatively low seismic velocities of 2.5–3.5 km/s down to 6–7 km depth indicate the presence of a large, ~20 km wide, frontal prism arcward of the deformation front (51 km distance). The ~60 km wide Neogene accretionary prism, imaged in the MCS data and confirmed by Vp values <4.0 km/s, is located between 85–130 km profile distance and forms the middle prism, app. bounded by the 3 km/s isoline. It is characterized by a laterally inhomogeneous velocity field and thrust fault-

[1] Auxiliary materials are available in the HTML. doi:10.1029/2009GL037533.

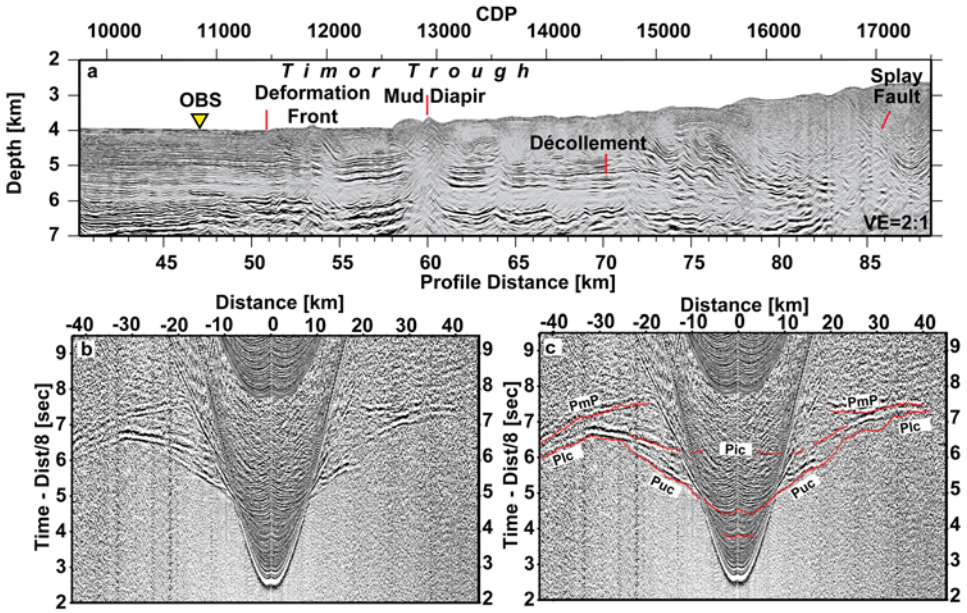

Figure 2. (a) MCS depth migrated section for the areas around Timor Trough (location shown in Figure 1). (b and c) example of the OBS data used in this study. Yellow triangle - the OBS position, shown in Figure 2b and 2c. Red dots show the computed travel-times of the seismic rays shot through the tomography model.

ing, observed in the MCS data. A system of splay faults that originate at the décollement and trend upwards at the angle of ~20° marks the transition to the middle prism (Figure 2a). The trench fill is composed of Mesozoic and Cenozoic sediments, eroded from the Australian continental shelf, with the lower part composed of clastic and volcano-clastic rocks, and the upper part composed of deep-water carbonates [*Breen et al.*, 1986]. The upper half of the sediments in the Timor trough is incorporated into the frontal prism. The lower 1000–1200 m of the clastic unit are currently bypassing the frontal prism (Figures 2a and 3a) and most likely underplate below the accretionary prism. The décollement is traced as a high-amplitude reflector for 30 km landward of the deformation front and extends to a depth of 6 km.

4.3. Paleo-accretionary Wedge

[11] The central section of the profile (140–210 km) suffers from limited energy penetration due to anomalous high attenuation and/or significant scattering. The opaque seismic character of the forearc high as observed both in the wide-angle and MCS data together with moderate Vp in the sedimentary cover (ranging from 2 km/s below the sea floor to 5 km/s at a depth of 10 km) (Figure 3a) suggests that the forearc high is composed of pre-Neogene accreted material that forms the paleo-accretionary complex. This material is probably derived from the stratigraphic units currently present on the Scott Plateau, which are composed of Jurassic sandstones overlain by Cretaceous marine shales [*Breen et al.*, 1986] and could have accumulated during the initial subduction of the passive Australian margin [*van der Werff et al.*, 1994] or during the subduction of Jurassic oceanic lithosphere of the Banda embayment (as shown by *Hall and Smyth* [2008]). Geologically the prism may be linked to the southern part of Timor, underlain by the outcropping Kolbano Complex, including Jurassic-Pliocene folded sediments of Australian origin, representing a segment of the accretionary complex [*Karig et al.*, 1987]. As suggested by numerical modeling of collisional margin settings [*Selzer et al.*, 2008], the opaque seismic character of the deeper portion may be caused by basally stacked packages of highly scattering rock fabric thus inhibiting deep energy penetration.

4.4. Sumba Ridge

[12] The crest of the Sumba ridge [*Silver et al.*, 1983] is located at 250 km profile distance; the basement top (app. corresponding to the 4 km/s isoline) is at a depth of 3 km below sea level at the crest and slopes down to 9 km depth in the south and to 6 km depth in the north (Figure 3a). A sharp velocity change in the upper crust at ~200 km distance marks the southern limit of the Sumba ridge. A vertical displacement of the basement occurs at 260 km underneath a small sedimentary basin and again at the northern edge of the ridge (at 310 km). The ridge is covered by sediments (presumably eroded from the Sumba, Savu and Timor islands) with a thickness of 0.5 km increasing to more than 2 km in thickness at its flanks. A crustal reflection observed below the entire northern portion of the profile at depths of 15–17 km probably corresponds to the transition between the upper and the lower crust (Figure 3a). Vp velocities vary from 5.5 km/s to 6.4–6.5 km/s in the upper crust, and from 6.7–6.8 km/s to 7.1 km/s in the lower crust and are typical of a mature arc massif or possibly of a fragment of a continental crust, which can be linked to the existence of a volcanic arc in the eastern Indonesia during the Paleogene, traces of which may be found in the highest nappes of Timor and other Banda islands [*Hall and Smyth*, 2008]. The PmP phases indicate the slightly southwards dipping Moho at a depth of ~26 km below the Sumba ridge. Available Pn phases indicate Vp ~ 8.0 km/s in the forearc mantle.

4.5. Savu Basin

[13] The transition from the Sumba ridge to the Savu basin (at 310 km) is marked by sea floor deepening and an increase in sedimentary thickness. The sedimentary fill eroded from

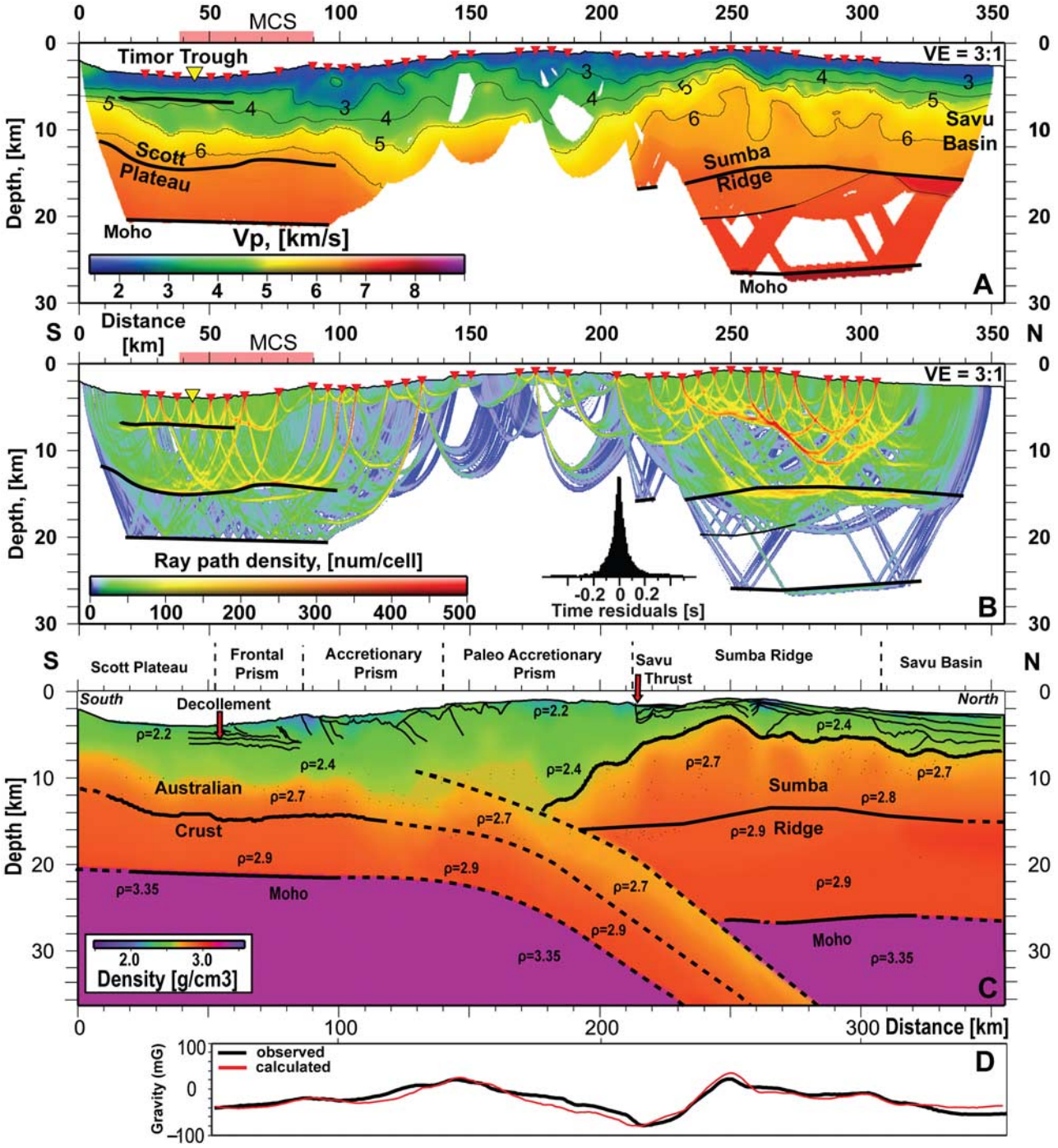

Figure 3. (a) Results of seismic tomography and gravity modeling a) Recovered tomography model, black lines - seismic reflectors. Red triangles - the OBS/OBH locations. Yellow triangle - OBS location (Figure 2). Pink line along the distance axis - MCS data shown in Figure 2. (b) Ray path coverage obtained during the tomographic inversion. Insert shows the time residuals distribution. (c) Combined model. Background color and numbers - density based the tomography and gravity results. Thin solid black lines - reflection horizons from the MCS data. Thick black lines - interfaces used in the gravity modeling. Interfaces not seismically resolved - dashed lines. (d) results of gravity modeling. Red line - observed data; black line - calculated gravity field.

the island arc [*Audley-Charles*, 2004] reaches a total thickness of 3 km with Vp velocities ranging from <2 km/s to 4 km/s (Figure 3a). The basement topography and sedimentary layering are consistent with earlier seismic reflection profiles in the Savu basin [*Karig et al.*, 1987; *Breen et al.*, 1986; *van der Werff et al.*, 1994]. Our wide-angle data for the first time document the Moho at a depth of 26 km.

4.6. Crustal Structure From Seismic Inversion and Gravity Modeling

[14] Figure 3c shows the tectonic model based on the results of the reflection seismic imaging, the wide-angle tomography, and gravity modeling. In the south, the crust of Australian affinity is dipping arcward at an angle of ~10–11°. The 10–12 km thick crystalline crust of the Scott plateau as a promontory of the Australian continent (described above) underthrusts the Banda forearcs.

[15] Between the Sumba ridge and the trough, the accretionary complex shows thrusting and represents a nascent orogeny, forced by post-Pliocene convergence and buoyant uplift associated with the transition from active oceanic subduction to continent-island arc collision. The complex is composed of a frontal prism, where active frontal accretion is documented, juxtaposed against a 130 km wide accretionary prism. The central section of the profile (140–210 km distance) consists of the paleo-accretionary prism bounded northwards by the Sumba ridge, which acted as backstop to the paleo-prism during the time of accretion. Most likely the paleo-prism was added to the Sumba ridge, during the SSW tectonic escape of Sumba Island, caused by the initial contact of Australia and the Banda arc [*Rutherford et al.*, 2001]. The Savu thrust marks the tectonic transition from the accretionary wedge to the tectonic units of the Sumba ridge. Vertical growth of the prism facilitated backthrusting over the Sumba ridge along the Savu thrust [*Silver and Reed*, 1988], however, motion along the Savu thrust must primarily be driven by high basal friction due to the low relief difference between the prism and the ridge. The crustal thickness of the Sumba ridge is ~23 km with crustal densities ranging from 2.65 g/cm^3 to 2.90 g/cm^3. Towards the island arc, the thickness of the crystalline crust is ~20 km below the Savu basin with the upper plate Moho at a depth of ~26–27 km, as also supported by gravity modeling. The crustal thickness is increased compared to the Lombok basin west of Sumba Island, which is underlain by 7 km thick crust (E. Lueschen et al., Structure, evolution and tectonic activity at the Eastern Sunda forearc, Indonesia, from marine seismic investigations, submitted to *Tectonophysics*, 2009).

5. Discussion

[16] Newly acquired seismic reflection/refraction and gravity data east and south of Sumba Island resolve the deep crustal structure at the Sunda-Banda arc transition (Figure 3c). The current system can be regarded as a precursor of a fold-and-thrust belt, which may develop in the forearc as the collision progresses. The wide-angle seismic data resolve the full crustal structure of the Sumba ridge and the Savu basin and for the first time provide the geophysical background for geodynamic models of nascent collisional systems. The observed variations in crustal structure along the profile may be typical for tectonic settings with continental margins approaching island arcs. The observed variations in the crustal structure along the profile are similar to the present structure around Taiwan, formed by the transition from subduction to collision of Eurasia and the Philippine Sea plate [*Huang et al.*, 2006; *Sibuet and Hsu*, 2004].

[17] **Acknowledgments.** We would like to thank Captain Meyer and the crew of R/V Sonne and the SINDBAD Working group for their enormous help in collecting and processing of the data. Authors express great gratitude to Jun Korenaga for the discussion on seismic tomography and Tomo2D code. We would like to thank the GRL editor Fabio Florindo and reviewers for their help in improving the manuscript. The SINDBAD project is funded by the German Federal Ministry of Education and Research (BMBF) (grants 03G0190A and 03G0190B).

References

Audley-Charles, M. G. (1975), The Sumba fracture: A major discontinuity between eastern and western Indonesia, *Tectonophysics*, *26*, 213–228.

Audley-Charles, M. G. (2004), Ocean trench blocked and obliterated by Banda forearc collision with Australian proximal continental slope, *Tectonophysics*, *389*, 65–79.

Breen, N. A., E. A. Silver, and D. M. Hussong (1986), Structural styles of an accretionary wedge south of the island of Sumba, Indonesia, revealed by SeaMARC II side scan sonar, *Geol. Soc. Am. Bull.*, *97*, 1250–1261.

Bock, Y., L. Prawirodirdjo, J. F. Genrich, C. W. Stevens, R. McCaffrey, C. Subarya, S. S. O. Puntodewo, and E. Calais (2003), Crustal motion in Indonesia from Global Positioning System measurements, *J. Geophys. Res.*, *108*(B8), 2367, doi:10.1029/2001JB000324.

Carlson, R. L., and C. N. Herrick (1990), Densities and porosities in the oceanic crust and their variations with depth and age, *J. Geophys. Res.*, *95*, 9153–9170.

Christensen, N. I., and W. D. Mooney (1995), Seismic velocity structure and composition of the continental crust: A global view, *J. Geophys. Res.*, *100*, 9761–9788.

Collins, C. D. N., B. J. Drummond, and M. G. Nicoll (2003), Crustal thickness patterns in the Australian continent, *Geol. Soc. Am. Spec. Pap.*, *372*, 121–128.

Curray, J. R. (1989), The Sunda arc: A model for oblique plate convergence, *Neth. J. Sea Res.*, *24*, 131–140.

Elburg, M. A., M. J. van Bergen, and J. D. Foden (2004), Subducted upper and lower continental crust contributes to magmatism in the collision sector of the Sunda-Banda arc, Indonesia, *Geology*, *32*, 41–44.

Engdahl, E. R., and A. Villaseñor (2002), Global seismicity: 1900–1999, in *International Handbook of Earthquake and Engineering Seismology*, pp. 665–690, Academic, San Diego, Calif.

Hall, R. (2002), Cenozoic geological and plate tectonic evolution of SE Asia and the SW Pacific: Computer-based reconstructions, model and animations, *J. Asian Earth Sci.*, *20*, 353–434.

Hall, R., and H. R. Smyth (2008), Cenozoic arc processes in Indonesia: Identification of the key influences on the stratigraphic record in active volcanic arcs, *Geol. Soc. Am. Spec. Pap.*, *436*, 27–54.

Hamilton, W. B. (1988), Plate tectonics and island arcs, *Geol. Soc. Am. Bull.*, *100*, 1503–1527.

Harris, R. A. (1991), Temporal distribution of strain in the active Banda orogen: A reconciliation of rival hypotheses, *J. Southeast Asian Earth Sci.*, *6*, 373–386.

Huang, C.-Y., P. B. Yuan, and S.-J. Tsao (2006), Temporal and spatial records of active arc-continent collision in Taiwan: A syntasis, *Geol. Soc. Am. Bull.*, *118*, 274–288.

Kaneko, Y., S. Maruyama, A. Kadarusman, T. Ota, M. Ishikawa, T. Tsujimori, A. Ishikawa, and K. Okamoto (2007), On-going orogeny in the outer-arc of the Timor-Tanimbar region, eastern Indonesia, *Gondwana Res.*, *11*, 218–233.

Karig, D., A. Barder, T. Charlton, S. Klemperer, and D. Hussong (1987), Nature and distribution of deformation across the Banda Arc: Australia collision zone at Timor, *Geol. Soc. Am. Bull.*, *98*, 18–32.

Katili, J. A. (1989), Review of past and present geotectonic concepts of eastern Indonesia, *Neth. J. Sea Res.*, *24*, 103–129.

Korenaga, J., et al. (2000), Crustal structure of the southeast Greenland margin from joint refraction and reflection seismic tomography, *J. Geophys. Res.*, *105*, 21,591–21,614.

Milsom, J. (2001), Subduction in eastern Indonesia: How many slabs?, *Tectonophysics*, *338*, 167–178.

Mueller, C., et al. (2008), From subduction to collision: The Sumba-Banda Arc transition, *Eos Trans. AGU*, *89*, 49–50.

Ritzmann, O., and J. I. Faleide (2007), Caledonian basement of the western Barents Sea, *Tectonics*, *26*, TC5014, doi:10.1029/2006TC002059.

Rutherford, E., K. Burke, and J. Lytwyn (2001), Tectonic history of Sumba Island, Indonesia, since the Late Cretaceous and its rapid escape into forearc in the Miocene, *J. Asian Earth Sci.*, *19*, 453–479.

Selzer, C., S. J. H. Buiter, and O. A. Pfiffner (2008), Numerical modeling of frontal and basal accretion at collisional margins, *Tectonics*, *27*, TC3001, doi:10.1029/2007TC002169.

Sibuet, J.-C., and S.-K. Hsu (2004), How was Taiwan created?, *Tectonophysics*, *379*, 159–181.

Silver, E. A., and D. L. Reed (1988), Backthrusting in accretionary wedges, *J. Geophys. Res.*, *93*, 3116–3126.

Silver, E. A., D. L. Reed, and R. McCaffrey (1983), Back arc thrusting in the eastern Sunda arc, Indonesia: A consequence of arc-continent collision, *J. Geophys. Res.*, *88*, 7429–7448.

Stagg, H. M. J., and N. F. Exon (1979), Western margin of Australia: Evolution of a rifted arch system—Discussion, *Geol. Soc. Am. Bull.*, *90*, 795–797.

van der Werff, W. (1995), The evolution of the Savu Forearc Basin, Indonesia (Forearc response to arc/continent collision), *J. Mar. Petrol. Geol.*, *12*, 247–262.

van der Werff, W., D. Kusnida, and H. Prasetyo (1994), On the origin of the Sumba forearc basement, *J. Mar. Petrol. Geol.*, *11*, 363–374.

Y. Djajadihardja, Agency for the Assessment and Application of Technology, Jl.M.H. Thamrin No. 8, Jakarta 10340, Indonesia.

M. Engels, E. Lueschen, and C. Mueller, Federal Institute for Geosciences and Natural Resources, Stilleweg 2, D-30655 Hannover, Germany.

E. R. Flueh, H. Kopp, A. Krabbenhoeft, L. Planert, and A. Shulgin, Leibniz Institute of Marine Sciences, IFM-GEOMAR, Wischhofstr. 1-3, D-24148 Kiel, Germany. (ashulgin@ifm-geomar.de)

Submarine landslides at the eastern Sunda margin: observations and tsunami impact assessment

Sascha Brune [1*], Stefan Ladage [2], Andrey Y. Babeyko [1], Christian Müller [2], Heidrun Kopp [3], Stephan V. Sobolev [1]

[1] Helmholtz Centre Potsdam GFZ German Research Centre for Geosciences, Potsdam, Telegrafenberg, 14473 Potsdam, Germany

[2] Federal Institute for Geosciences and Natural Resources (BGR), Stilleweg 2, 30655 Hannover, Germany

[3] Leibniz Institute of Marine Sciences at the Christian-Albrechts University of Kiel (IFM-GEOMAR), Wischhofstr. 1-3, 24148 Kiel, Germany

[*] Corresponding author. e-mail: brune@gfz-potsdam.de, phone: 0049/331/288-1928, fax: 0049/331/288-1938

Abstract

Our analysis of new bathymetric data reveals six submarine landslides at the eastern Sunda margin between central Java and Sumba Island, Indonesia. Their volumes range between 4 km³ in the Java fore-arc basin up to 95 km³ at the trench off Sumba and Sumbawa. We estimate the potential hazard of each event by modeling the corresponding tsunami and its run-up on nearby coasts. Four slides are situated remarkably close to the epicenter of the 1977 tsunamigenic Sumba M_w=8.3 earthquake. However, comparison of documented tsunami run-up heights with our modeling results neither allows us to confirm nor to decline the hypothesis that the earthquake triggered these submarine landslides. Finally, we investigate whether a slope failure at the trench off Bali could cause a dangerous tsunami at the highly populated coasts of Bali and Lombok.

Keywords: Submarine landslide; Tsunami; Numerical modeling; Indonesia; Padang; Hazard assessment

2.1 Introduction

Tsunamis pose a major threat to population and structures in many coastal areas around the world. Although most tsunamis are generated by submarine earthquakes, underwater slope failures can be responsible for local tsunamis as well. Landslide-generated tsunamis comprise at least 8 % of all documented historical events worldwide (ITDB catalogue 2007). That makes the investigation of submarine landslides a necessary step for future tsunami hazard assessment. One of the best studied historical events took place in Papua New Guinea, 1998, where a 4 km³ submarine slump was triggered by a comparatively small earthquake (Tappin et al. 1999; Sweet and Silver 2003). The generated tsunami inundated nearby coasts, leading to maximal run-up heights of 15 m (Lynett et al. 2003). Whether a submarine mass movement generates significant inundation, depends on slide volume, tsunami propagation distance and local bathymetry. If the tsunami propagation distance is of the order of a few kilometers, even small landslides (0.0024 km³ slide at Fatu Hiva, French Polynesia, 1999 (Hébert et al. 2002)) can cause significant damages to coastal communities. Very large events like the 200 km³ 1929 Grand Banks slide (Fine et al. 2005) or the 2400 km³ pre-historic Storegga slide (Bondevik et al. 2005) were capable of generating large run-up even at locations in several hundred kilometers distance.

Indonesia is especially endangered by tsunamis, due to its proximity to the Sunda subduction zone stretching over 5000 km from the Andaman Islands and Sumatra to Java, and the Lesser Sunda Islands. The subduction of the Indo-Australian plate beneath the Sunda shelf creates tectonic stresses which upon sudden release cause earthquakes of major magnitudes that potentially generate large tsunamis (Hamzah et al. 2000). The M_w=9.3 Sumatra-Andaman earthquake in December, 2004 rupured over 1000 km (Krüger and Ohrnberger 2005) and induced a catastrophic ocean-wide tsunami. Run-up heights reached more than 30 m in Aceh, Indonesia (Borrero et al. 2006) and nearly 20 m in Thailand (Tsuji et al. 2006). Off Java and the Lesser Sunda Islands, devastating tsunamis were induced by the M_w=8.3 Sumba earthquake of 1977, the eastern Java earthquake (M_w=7.8) of 1994 and the M_w=7.7 Pangandaran earthquake in 2006 (ITDB catalogue 2007). Maximum run-up values of respectively 8 m (Kato and Tsuji 1995), 14

m (Tsuji et al. 1995a) and 20 m (Lavigne et al. 2007; Fritz et al. 2007) have been identified.

By triggering submarine mass failures, however, even moderate earthquakes can induce dangerous tsunamis. Large local run-up during the 1979 tsunami at Lomblen Island and in 1992 at the northern coast of Flores Island has been explained by underwater mass failures (Tsuji et al. 1995b; Rynn 2002). Whether the above mentioned 20 m run-up during the 2006 Central Java tsunami was caused by a landslide, is currently discussed (Matsumoto et al. 2007). Submarine debris avalanches have been identified west of Sumatra (Tappin et al. 2007), at the toe of the accretionary prism. The overall slide volume of the largest event is with 1 km³ (Moran and Tappin 2006) comparably small which excludes it as a significant tsunami source (Tappin et al. 2007).

Our present study is based on new bathymetric data collected onboard the RV "Sonne" during the MERAMEX (2004) and SINDBAD (2006) surveys. The multibeam bathymetry data has a resolution of 2° (corresponding to 200 m at ocean depths of 6000 m). The cruises have been conducted by two German institutions: IFM-GEOMAR, Kiel, and the Federal Institute for Geosciences and Natural Resources (BGR), Hannover. Our study area comprises the eastern Sunda margin off Indonesia, between central Java and Sumba (Figure 1). Detailed analysis of the bathymetry data revealed evidences of six landslide events. We start with a short geological background of the studied area and proceed with detailed slide descriptions and numerical models of the tsunamis generated during these events.

2.2 Geological setting

The over 5000 km long Sunda margin extends from the Andaman Sea in the north to Sumba Island in the east. It is characterized by the subduction of oceanic lithosphere of the Indo-Australian plate beneath the Indonesian Archipelago. East of Sumba Island a transition to the Banda Arc and the collision with continental Australian crust takes place. Subduction initiated in the late to middle Tertiary (Hall 1997) and has formed a mature

convergent margin with a well developed accretionary prism, an outer fore-arc high and fore-arc basins (Schlueter et al. 2002; Kopp and Kukowski 2003).

The eastern Sunda Arc sector from East Java to just west of Sumba Island resembles a unique segment of this subduction zone. Here, the oldest oceanic crust along the entire Sunda Arc of Late Jurassic age (155-145 Ma; Heine et al. 2004; Müller et al. 2008) subducts at a rate of up to 70 mm per year in nearly trench normal direction (Simons et al. 2007). With water depths reaching more than 7000 m, this is also the deepest segment of the Java trench. Off eastern Java the sediment thickness on the incoming plate and in the trench is less than 1 km (Kopp et al. 2003). Further east the oceanic crust and trench are largely devoid of sediments, except for a thin hemipelagic sediment cover. The accretionary wedge in the eastern segment is between 70-100 km wide and forms a discontinuous outer fore-arc high with maximal water depths exceeding 2000 m. Internally, the accretionary wedge is built up of a series of landward dipping imbricate thrust sheets of accreted and deformed rocks (Lueschen et al., submitted; van der Werff 1995).

Off eastern Java the Roo Rise, elevated about 1500 m above surrounding sea floor, is recently subducting and causing frontal erosion of the accretionary wedge (Kopp et al. 2006). Further east the Java trench morphology is rugged and controlled by normal faulting of the oceanic crust with horst and graben structures along the outer trench wall. The faults are more than 60 km long and have a throw of 500 m. They strike slightly oblique to the trench and can be imaged deep beneath the slope toe. Subduction of these faults and horst and grabens contributes to local oversteepening of the slope toe with slumping (van der Werff 1995; Müller et al. 2008; Lueschen et al., submitted). The distribution and focal mechanisms of shallow seismicity along the Java trench clearly shows recent activity of these faults (Eva et al. 1988; Spence 1986).

2.3 Slide descriptions

We analyzed the bathymetric data searching for head scarp walls and associated landslide deposits. Six major subrecent landslides have been identified within the studied area. In

the following, they will be designated alphabetically from A to F (Figure 1). Slide A is located within the Java fore-arc basin, 120 km off coast. Slide B was found at the accretionary wedge 240 km off Lombok and slides C to F near the trench, at a distance of 130 to 200 km to Sumba Island.

The deposition lobes of slides A and F are clearly visible (Figure 2). Their shape and proximity to the failure area suggest rotational slumping as probable failure mechanism. In the cases B, C, D, and E, the depositional area is barely observable. We analyzed backscatter data, 3.5 kHz sub-bottom - and multichannel-reflection seismic profiles. Landslide head scarps were identified, however associated landslide sediment deposits were not detectable.
The position of the slides and their geometrical parameters are deduced from the bathymetric maps and listed in Table 1. Slide dimensions perpendicular and parallel to the slope, denoted as width and length, respectively, range between 4 and 25 km. The travel distance which corresponds to the center of mass translation, is obvious only for the cases A and F, as they exhibit typical deposit lobes. Travel distances estimated for the other four slides comprise rather high uncertainties. We evaluate the slide heights by comparing the slope profile inside the slide zone and besides it. This yields values between 100 m for slide D and up to 300 m for slide E and F. Slide volumes of slides A to F (13 km^3, 15 km^3, 60 km^3, 4 km^3, 60 km^3, and 95 km^3, respectively) are estimated under the assumption of a parabolic slide shape.

It is very difficult to date underwater mass movements based on bathymetric images only. As submarine diffusion rates are notably smaller than on land, landscapes evolve much slower. So, even a “fresh” looking slide can be thousands of years old (McAdoo and Simpson 2005). Dating techniques involving the steepness of the head wall are only applicable if at least one additional independent failure date is provided by a secondary method (Kukowski et al. 2008). In this region, this has not been done so far. However, in section 2.5 we investigate the possibility that slides C to F have been triggered by the 1977 Sumba earthquake (M_w=8.3). If confirmed, this would also imply the age of the slumps.

Most submarine slope failures are caused by interplay of several factors like oversteepening of slopes and ground shaking due to an earthquake (Masson et al. 2006). At the position of slide A, basin slopes have been possibly steepened due to the subduction of a seamount located on the oceanic plate (Masson et al. 1990; Kopp et al. 2006). Concerning the other five events at the slope toe in the trench, oversteepening can be attributed to tectonic erosion (Kopp et al. 2006). For slopes close to failure, even a comparatively small earthquake is sufficient to induce a landslide.

2.4 Modeling of induced tsunamis

2.4.1 Methods

Our tsunami model consists of three distinct stages: generation, propagation and run-up. We describe tsunami generation using the technique of Watts et al. (2005) and Grilli et al. (2005). It provides a set of semi-empirical equations that are based on physical arguments and wave tank experiments. The initial tsunami wave height η_{2HD}, the wave length λ and the characteristic time t_0 (Table 2) are estimated based on landslide geometry parameters length, width, height, depth and travel distance as well as the mean local slope angle (Table 1).

Following Watts et al. (2003), an initial wave distribution can be used to approximate the sea surface deformation provoked by the mass movement. It is argued that during the acceleration phase of a slide, most of the tsunami energy is invested in potential energy. Only after the characteristic time t_0, when the slide does not accelerate any longer, the transformation of potential energy into kinetic energy takes place. The initial sea surface was constructed according to Watts et al. (2005) and Synolakis et al. (2002): Along slide direction, two Gaussian curves of different sign approximate the wave profile. Their heights correspond to η_{2HD} and the widths are defined by λ. Perpendicular to the slide direction, a solitary-like extrapolation proportional to $\mathrm{sech}^2(3 \cdot y/(w+\lambda))$ is used, where w is the slump width and y the corresponding coordinate. The semi-empirical equations are applicable as long as wave breaking can be excluded. To ensure this, the ratio of slide length to initial submergence depth must be smaller than 17 (Watts et al. 2005). The

corresponding values of slide A to F (4, 1.3, 1.5, 0.7, 0.8 and 2, respectively) clearly satisfy this condition.

Alternative formulations include a dynamic slide movement that continuously influences the surface wave, like the shallow water approach of Harbitz (1992) or the Boussinesq model of Lynett and Liu (2002). These models allow for a more detailed slide description, however, they are only valid if the ratio of slide length to submergence depth is bigger than 30 for shallow water models or 7 for Boussinesq simulations (Lynett and Liu 2002). In our case, with length to depth ratios between 0.7 and 4, these formulations cannot be used.

The tsunami propagation is modeled with the finite difference, nonlinear shallow water code TUNAMI-N2 (Imamura et al. 1997). The shallow water approximation is fulfilled, as all wave lengths are much larger than the water depth. Tsunami calculations are performed on a 3200×2200 grid using a spatial step size of 10 arc seconds (~309 m) and a time step of 0.5 s. Bathymetry is based on interpolated GEBCO data (IOC, IHO and BODC 2003).

Run-up heights are estimated using the formula of Chesley and Ward (2006): $R = A(d)^{4/5} \cdot d^{1/5}$, where A is the wave amplitude, measured at water depth d. This formula is based on the conservation of wave energy flux and can be used for both breaking and non-breaking waves (Ward and Asphaug 2003). In this paper we use virtual gauges at depths of approximately 20 m. In section 2.8, we address the influence of the choice of water depth d on the run-up value R.

2.4.2 Results

Figure 3 presents distributions of the maximum tsunami heights for the slides A to F. Although events A, B and D involve significant slide volumes (13 km³, 15 km³, 4 km³, respectively) they do not generate significant tsunamis (run-up heights generally do not exceed 1 m). This is interesting, as the Papua New Guinea slump with a comparative volume of 4 km³ was far more efficient in tsunami excitation. The difference lies in slide

geometry. While the Papua New Guinea slump had a thickness of 600 m and a length of 4000 m (Synolakis et al. 2002), our slides A, B and D exhibit heights of 100 to 200 m with lengths between 4000 and 8000 m. We investigate the influence of the slide thickness by a parameter study. We double the slide heights of events A, B and D, while correspondingly decreasing their lateral dimensions to keep the volumes constant. According to Watt's formula, the resulting initial tsunami wave height increases by a factor of approximately 7. Hence, a compact slump with larger thickness generates a much higher tsunami, than a broad slump of the same volume.

The volumes of slides C, E, and F (60 km^3, 60 km^3, 95 km^3) are considerably larger than those mentioned before. Generated tsunamis feature initial wave heights of 6 to 7 m. As the tsunami propagates, it is influenced by the regional bathymetry (Satake 1988). So, the central part of the wave front is diffracted eastward by the underwater onset of the Sumba strait (Figure 3, slides C and E). Similarly, off-shore seafloor elevations focus the wave energy, as can be seen for Sumbawa (Slide C and E) and Sumba (Slide E). Computed run-up heights for each event are shown in Figure 3 by blue bars. Maximum run-up heights of nearly 6 m are computed on Sumbawa for slide C and E. A run-up of 7 m is reached in Ubuoleta on Sumba for slide F.

Tsunami arrival times vary between 20 and 30 minutes for all areas exposed to large wave heights (here arrival time corresponds to the first 1 cm sea surface anomaly). Arrival times for slide D are only shown at locations experiencing water elevations of more than 1 cm (Figure 3).

While slide width and length can be estimated from bathymetric data quite accurately, both height and travel distance are subjected to a higher uncertainty. If projected up to the coast, this uncertainty can be responsible for about 50 % run-up variation.

2.5 Triggering of landslides by the 1977 Sumba M_w=8.3 earthquake?

The 1977 Sumba earthquake (M_w=8.3; Lynnes and Lay 1988) was the biggest event in our study area during the 20th century (ITDB catalogue 2007), and one of the largest

normal fault earthquakes ever recorded. Its epicenter (11° 8’ S, 118° 14’ E; CMT catalogue) is located about 200 km southwest of Sumba Island. The earthquake generated a tsunami which inundated the coasts of Sumba, Sumbawa, Lombok, and Bali resulting in 440 damaged houses and 161 casualties or missing (Kato and Tsuji 1995). In Figure 4, we mapped the epicenter location, the seven-days aftershock distribution and the assumed fault plane. Interestingly, slides C to F are located directly above the fault plane. Especially, the location of slide F coincides with an area of high aftershock intensity. This raises the question, if one or more slides might have been triggered by the earthquake. As our knowledge about the slumps is based on remote sensing only, we cannot determine the age of the events and whether they failed during the earthquake. However, an ITIC survey team and Indonesian investigators visited the tsunami affected areas and measured run-up heights (ITIC 1977). That gives us the opportunity to compare results of an earthquake tsunami model to real run-up data. Thereby, we can test if possible discrepancies might be explained by an additional landslide source.

The survey accessed eight locations on Bali and Lombok. Due to difficult accessibility, only two places on Sumbawa and three on Sumba have been visited, whereof two are situated on the far side of the island. Survey locations are mapped in Figure 4. Measured run-up values are given with respect to the sea level at time of measurements (ITIC 1977). For our study, we use run-up data that was corrected for astronomical tides (Kato and Tsuji 1995). These run-up values are shown in Figure 5a. If more than one run-up is given for the same location, minimal and maximal values are marked in deep and light blue, respectively.

Based on the aftershock distribution (Figure 4), we assess the following earthquake parameters: centroid location 118.5°E, 11.2°S, rupture extension 195 km, fault plane width 65 km and strike 70°. The fault plane is slightly wider as if one had used the empirical scaling relations of Wells and Coppersmith (1994). All other parameters are taken from the Global CMT Catalog: magnitude M_w 8.3, scalar moment $3.59 \cdot 10^{21}$ Nm, dip angle 67°, slip angle -98° and depth 23.3 km. In contrast to Kato and Tsuji (1995), we use the steeper of the two possible fault plane solutions which dips southward. In their

paper, Kato and Tsuji (1995) assumed the Sumba event to be of the same type as the 1933 Great Sanriku earthquake and decided in favor of the shallow, northward dipping fault plane solution. However, a conjugate set of steeply northward and southward dipping normal faults dominate the morphology of the oceanic crust in the eastern Java trench (Müller et al. 2008; van der Werff 1995). The resemblance in strike and dip angle with the CMT fault mechanism of the 1977 Sumba earthquake clearly favors the southward dipping focal mechanism solution. Assuming a rigidity modulus of 30 GPa, we assess the co-seismic slip to be 9.5 m. Initial sea surface deformation is calculated according to Okada (1985), using the software AVI-NAMI v1.2 (Pelinovsky et al. 2006). We compute maximal subsidence of -3.3 m towards southeast and maximal uplift of 1.1 m in the opposite direction. Calculated run-up heights at surveyed locations are shown in Figure 5b. They exhibit only minor discrepancies to measured values (compare with Figure 5a).

Interestingly, modeled results for the second, perpendicular fault plane solution of the CMT catalog are quite similar. The initial maximal depression amounts to -3.6 m and the maximum elevation is 0.9, the distribution appears to be shifted slightly southward, but the overall shape is likewise. This explains why the tsunami model calculated by Kato and Tsuji (1995) exhibited similarly good correspondence with measured run-up values.

To test whether the presented landslides were triggered by the Sumba earthquake, we also calculate tsunami run-up heights for slides C, E, and F at the survey locations. As slide D induces only a negligible tsunami (maximum run-up is 40 cm), it will not be discussed. Results are depicted in Figure 5c, d and e, respectively. The run-up distribution due to slide C exhibits a similar pattern as the earthquake. The same is true for slide E, but with somewhat smaller amplitudes. If one of these slides were triggered by the earthquake, the corresponding wave fields would superpose at each time step. This does not mean that the maximum run-up values have to be added at each location. They rather depend on the exact timing of the slide failure with respect to the earthquake's main shock. If the largest slide-induced wave arrives several minutes after the highest wave of the earthquake tsunami, it might not contribute to the run-up distribution. As the earthquake tsunami

simulation corresponds well with the surveyed run-up values, we can only conclude, that no such superposition can be evidently observed at the given locations.

Slide F however, shows a different picture. In this case, run-up at Ubuoleta exceeds the measured value by about 2 m. One could deduce that this slide was not induced by the 1977 earthquake. However, this conclusion would be based on one data point only and, regarding the intrinsic error range of the model (section 2.4.2), appears to be premature.

2.6 Hypothetical slide event in the Bali/Lombok region

In present day bathymetry, no landslide evidences could be found off Bali or Lombok. As both islands feature high population densities, we investigate the possible impact of a slope failure south of Bali. Assuming that sediment properties are similar, we model an event that resembles slide F in volume and geometry, but is located 250 km south of Bali, at the seaward slope of the accretionary wedge (115.25° E, 11.12° S). Slide F constitutes the largest event in our study region (95 km^3), so this test event can be considered as a worst case scenario.

As mapped in Figure 6b, the first wave arrives at Bali and Lombok after almost 30 minutes. Offshore wave heights reach 2 m off Bali, 1.5 m off Lombok and decrease rapidly when entering the straits between the islands. Calculated run-up heights (Figure 6a) reach nearly 4 m in Benoa, 2 m at Sanur beach and only 1 m in Kuta, which appears to be sheltered by the Bukit peninsula. Run-up on the southern coast of Lombok ranges around 4 m. These values somewhat depend on the assumed failure location. Moving the slide 70 km westward increases the run-up in Benoa up to 5 m while decreasing it in Lombok down to 2 m. Alternatively, moving the event 70 km eastward yields 3 m for Bali and 5 m for Lombok. Depending on current tidal conditions, these run-up values could be modified by ±1 m (UHSLC).

In a recent publication (Brune et al., submitted), we address the possibility of real-time submarine landslide detection by means of coastal tiltmeters. This technique relies on the fact that a displacement of several cubic kilometers of sediments leads to considerable

and measurable land surface inclination inside some predicted radius. We apply this technique to check if a motion of our hypothetical slide could be tracked by tiltmeters on Bali or Lombok Island. Unfortunately, the distance to the coast appears to be so large, that even most accurate land-based tiltmeters cannot detect the event.

2.7 Conclusions

We identified six submarine landslides in new, high-resolution bathymetry data along the eastern Sunda trench. Three small events which involved between 4 and 15 km³ of sediments are located off Java, Lombok and Sumbawa. The remaining three landslides of significantly larger volumes (between 60 and 95 km³) are found at the margin toe off Sumba and Sumbawa.

Numerical modeling of landslide-generated tsunamis suggest that the largest events might have generated run-up heights of 7 m at Sumba, more than 5 m on Sumbawa and 3 m at Lombok Island. Maximum run-up on Bali and Java did not exceed 2 m.

As four slides are located directly above the assumed fault plane of the 1977 Sumba M_w=8.3 earthquake, we investigated if evidences for seismic landslide triggering could be revealed with the help of numerical modeling. Comparison of the measured run-up heights to our tsunami simulations show that the earthquake tsunami model alone adequately explains the observations. This fact cannot, however, exclude co-seismic landslide triggering: the potential landslide tsunami might have propagated shortly after the earthquake tsunami so that the waves did not measurably superpose at the survey point. Hence, based on the available data, we can neither support, nor decline the hypothesis of seismic triggering by the 1977 Sumba earthquake.

As the largest landslides are located off Sumba, the resulting run-up at the highly populated islands of Bali and Lombok was comparatively small. To estimate the potential impact of a large-size slope failure near Bali and Lombok, we modeled an event similar to slide F (95 km³) but located 250 km off Bali. Despite the large distance to the coast,

this landslide could generate a tsunami with run-up heights of about 4 m at both islands, thus posing a significant hazard to the population and industry centers.

Acknowledgements

This is publication 25 of the GITEWS project (German Indonesian Tsunami Early Warning System). The project is carried out through a large group of scientists and engineers from GeoForschungsZentrum Potsdam (GFZ) and its partners from DLR, AWI, GKSS, IFM-GEOMAR, UNU, BGR, GTZ, as well as from Indonesian and other international partner institutions. Funding is provided by the German Federal Ministry for Education and Research (BMBF), grants 03TSU01 (GITEWS) and 03G0190 (SINDBAD).

References

Bondevik S, F Løvholt, C Harbitz, J Mangerud, A Dawson, JI Svendsen (2005) The Storegga Slide tsunami - comparing field observations with numerical simulations. Mar Pet Geol. 22:195–208

Borrero JC, Synolakis, CE, and Fritz, H (2006) Northern Sumatra field survey after the December 2004 Great Sumatra earthquake and Indian Ocean tsunami, Great Sumatra Earthquakes and Indian Ocean Tsunamis of December 26, 2004 and March 28, 2005. Earthq Spectra. 22

Chesley SR, SN Ward (2006) A Quantitative Assessment of the Human and Economic Hazard from Impact-generated Tsunami. Nat Hazards. 38:355–374

Eva C, M Cattaneo, F Merlanti (1988) Seismotectonics of the central segment of the Indonesian Arc. Tectonophys. 146:241-259

Fine IV, AB Rabinovich, BD Bornhold, RE Thomson, EA Kulikov (2005) The Grand Banks landslide-generated tsunami of November 18, 1929: preliminary analysis and numerical modeling. Mar Geol. 215:45-57

Fritz H, W Kongko, A Moore, B McAdoo, J Goff, C Harbitz, B Uslu, N Kaligeris, V Titov, CE Synolakis (2007) Extreme run-up from the 17 July 2006 Java tsunami. Geophys Res Abstr. 9, 10765

Grilli ST, M ASCE, Watts, P (2005) Tsunami generation by submarine mass failure Part I: Modeling, Experimental Validation, and Sensitivity Analyses. J Waterway Port Coastal and Ocean Eng. 131(6):283-297

Hall R (1997) Cenozoic plate tectonic reconstructions of SE Asia. Geological Society Special Publications 126:11-23

Hamzah L, NT Puspito, F Imamura (2000) Tsunami Catalog and Zones in Indonesia. J Nat Disaster Sci. 22(1):25-43

Harbitz CB (1992) Model simulations of tsunamis generated by the Storegga slides. Mar Geol. 105:1-21

Hébert H, A Piatanesi, P Heinrich, and F Schindelé (2002) Numerical modeling of the September 13, 1999 landslide and tsunami on Fatu Hiva Island (French Polynesia). Geophys Res Lett. 29(10):1484

Heine C, RD Müller and C Gaina (2004), Reconstructing the lost Thethys Ocean basin: Convergence history of the SE Asian margin and marine gateways. In: P Clift, P Wang, W Kuhnt and D Hayes (eds) Geophysical Monograph Series Vol 149: Continent-Ocean interactions within East Asian marginal seas, AGU, Washington DC, pp 37-54

IOC, IHO and BODC (2003) Centenary Edition of the GEBCO Digital Atlas, British Oceanographic Data Centre, Liverpool

ITDB/WLD (2007) Integrated Tsunami Database for the World Ocean, Version 6.51 of February 20, 2007. CD-ROM, Tsunami Laboratory, ICMMG SD RAS, Novosibirsk, Russia

ITIC (International Tsunami Information Center), Tsunami reports No. 1977-12

Imamura F, N Shuto, C Goto, Y Ogawa, (1997) IUGG/IOC Time Project IOC Manuals and Guides No.35, (UNESCO)

Kato K, Y Tsuji (1995) Tsunami of the Sumba earthquake of August 19, 1977. J Nat Disaster Sci. 17(2):87-100

Kopp H, N Kukowski (2003) Backstop geometry and accretionary mechanics of the Sunda margin. Tectonics 22(6):1072.

Kopp H, ER Flueh, CJ Petersen, W Weinrebe, A Wittwer, Meramex Scientists (2006) The Java margin revisited: Evidence for subduction erosion off Java. Earth Planet Sci Lett. 242:130–142

Kukowski N, A Hampel, S Hoth, J Bialas (2008) Morphotectonic and morphometric analysis of the Nazca plate and the adjacent offshore Peruvian continental slope - Implications for submarine landscape evolution. Mar Geol. 254:107-120

Lavigne F, C Gomez, M Giffo, P Wassmer, C Hoebreck, D Mardiatno, J Prioyono, R Paris (2007) Field observations of the 17 July 2006 Tsunami in Java. Nat Hazards Earth Syst Sci. 7:177–183

Lynett P, PLF Liu (2002) A numerical study of submarine-landslide-generated waves and run-up. Proc R Soc A. 458:2885

Lynett PJ, JC Borerro, PLF Liu, and CE Synolakis (2003) Field Survey and Numerical Simulations: A Review of the 1998 Papua New Guinea Tsunami. Pure Appl Geophys. 160:2119–2146

Lynnes CS, T Lay (1988) Source Process of the Great 1977 Sumba Earthquake. J Geophys Res. 93(Bll):13,407-13,420

Masson DG, LM Parson, J Milsom, G Nichols, N Sikumbang, B Dwiyanto, H Kallagher (1990) Subduction of seamounts at the Java Trench: a view with long-range sidescan sonar. Tectonophys. 185:51– 65

Masson DG, CB Harbitz, RB Wynn, G Pedersen, F Løvholt (2006) Submarine landslides: processes, triggers and hazard prediction. Phil. Trans R Soc A. 364:2009-2039

Matsumoto T (2007) An underwater landslide or slump on an active submarine fault - A possible source of a devastating tsunami? Eos Trans AGU. 88(52), Fall Meet. Suppl., Abstract S53A-1018

McAdoo B, G Simpson (2005) Morphometric dating of submarine landslide scarps. Geophys Res Abstr. 7, Abstract 00629

Moran K, D Tappin (2006) SEATOS 2005 Cruise Report: Sumatra Earthquake and Tsunami Off shore Survey (SEATOS). 92 pp. (Online) available at http://ocean.oce.uri.edu/seatos.

Müller C, H Kopp, YS Djajadihardja, U Barckhausen, Ehrhardt A, Engels M, Flueh ER, Gaedicke C, Keppler H, Lutz R, Lüschen E, Neben S, Seeber L, Dzulkarnaen DPS (2008)

From subduction to collision; The Sunda-Banda Arc transition. Eos, Transactions, American Geophysical Union 89:49-50

Okada Y (1985) Surface deformation due to shear and tensile faults in a half-space. Bull Seism Soc Am. 75(4):1135-1154

Pelinovsky E, Kurkin A, Zaytsev A, Yalciner A, Imamura F (2006) AVI-NAMI Version 1.2

Rynn J (2002) A preliminary assessment of tsunami hazard and risk in the Indonesian region. Sci Tsunami Hazard. 20(4):193

Satake K (1988) Effects of Bathymetry on Tsunami Propagation: Application of Ray Tracing to Tsunamis. Pure Appl Geophys. 126(1):27-36

Schlueter HU, C Gaedicke, HA Roeser, B Schreckenberger, H Meyer, C Reichert, Y Djajadihardja, A Prexl (2002) Tectonic features of the southern Sumatra-western Java forearc of Indonesia. Tectonics. 21(5):15

Simons WJF, A Socquet, C Vigny, BAC Ambrosius, S Haji Abu, C Promthong, C Subarya, DA Sarsito, S Matheussen, P Morgan, W Spakman (2007) A decade of GPS in Southeast Asia: Resolving Sundaland motion and boundaries. J Geophys Res. 112

Spence W (1986) The 1977 Sumba Earthquake Series: Evidence for Slab Pull Force Acting at a Subduction Zone. J Geophys Res. 91:7225-7239.

Sweet S, and EA Silver (2003) Tectonics and Slumping in the Source Region of the 1998 Papua New Guinea Tsunami from Seismic Reflection Images. Pure Appl Geophys. 160:1945–1968

Synolakis CE, JP Bardet, JC Borrero, HL Davies, EA Okal, EA Silver, S Sweet and DR Tappin (2002) The slump origin of the 1998 Papua New Guinea Tsunami. Proc R Soc Lond A. 458:763–789

Tappin DR, T Matsumoto, P Watts, K Satake, GM McMurtry, M Matsuyama, Y Lafoy, and Y Tsuji (1999) Sediment slump likely caused 1998 Papua New Guinea tsunami. Eos Trans AGU. 80(30):329

Tappin DR, LC McNeil, T Henstock, D Mosher (2007) Mass wasting processes - offshore Sumatra. In: V Lykousis, D Sakellariou, J Locat (eds) Advances in Natural and Technological Hazards Research Vol 27: Submarine Mass Movements and Their Consequences, Springer, Dordrecht, pp 327-336

Tsuji Y, F Imamura, H Matsutomi, CE Synolakis (1995a) Field Survey of the East Java Earthquake and Tsunami of June 3, 1994. Pure Appl Geophys. 144(3/4):839

Tsuji Y, H Matsutomi, F Imamura, M Takeo (1995b) Damage to Coastal Villages due to the 1992 Flores Island Earthquake Tsunami. Pure Appl Geophys. 144(3/4):481

Tsuji Y, Y Namegaya, H Matsumoto, SI Iwasaki, W Kanbua, M Sriwichai, V Meesuk (2006) The 2004 Indian tsunami in Thailand: Surveyed runup heights and tide gauge records. Earth Planet Space. 58:223-232

UHSLC (University of Hawai, Sea Level Center) 2008 http://ilikai.soest.hawaii.edu/

van der Werff W (1995) Structure and morphotectonics of the accretionary prism along the Eastern Sunda-Western Banda Arc. J Southeast Asian Earth Sci. 11:309-322.

Ward SN, E Asphaug (2003) Asteroid impact tsunami of 16 March, 2880. Geophys J Int. 153:F6–F10

Watts P, ST Grilli, JT Kirby, GJ Fryer, and DR Tappin (2003) Landslide tsunami case studies using a Boussinesq model and a fully nonlinear tsunami generation model. Nat Hazards Earth Sys Sci. 3:391-402

Watts P, ST Grilli, DR Tappin, GJ Fryer (2005) Tsunami Generation by Submarine Mass Failure. I: Modeling, Experimental Validation, and Sensitivity Analyses. J Wtrwy Port Coast Oc Eng. 131:283

Wells DL, KJ Coppersmith (1994) New Empirical Relationships among Magnitude, Rupture Length, Rupture Width, Rupture Area, and Surface Displacement. Bull Seism Soc Am. 84(4):974-1002

Figures and tables

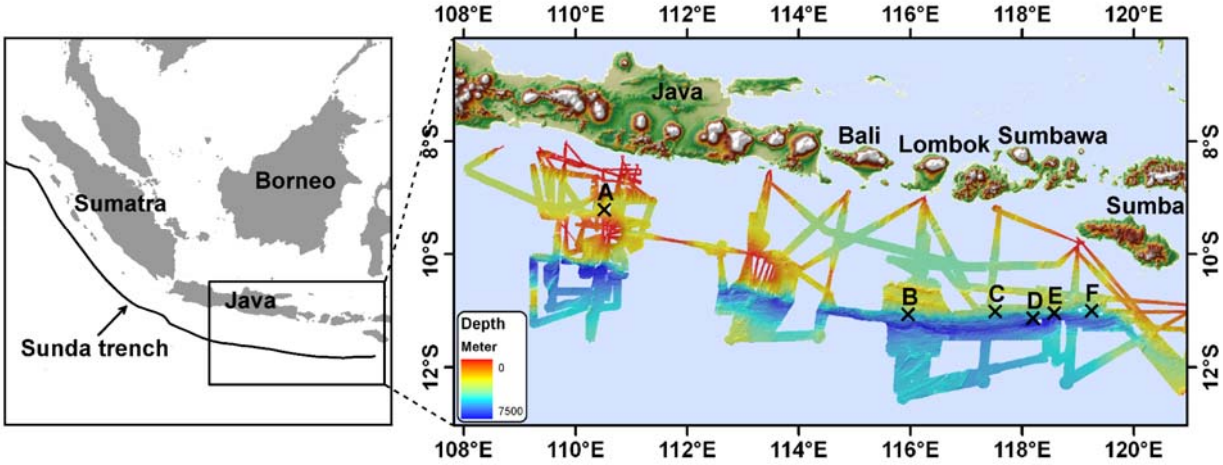

Figure 1 *Overview map showing bathymetric coverage and locations of slides A to F.*

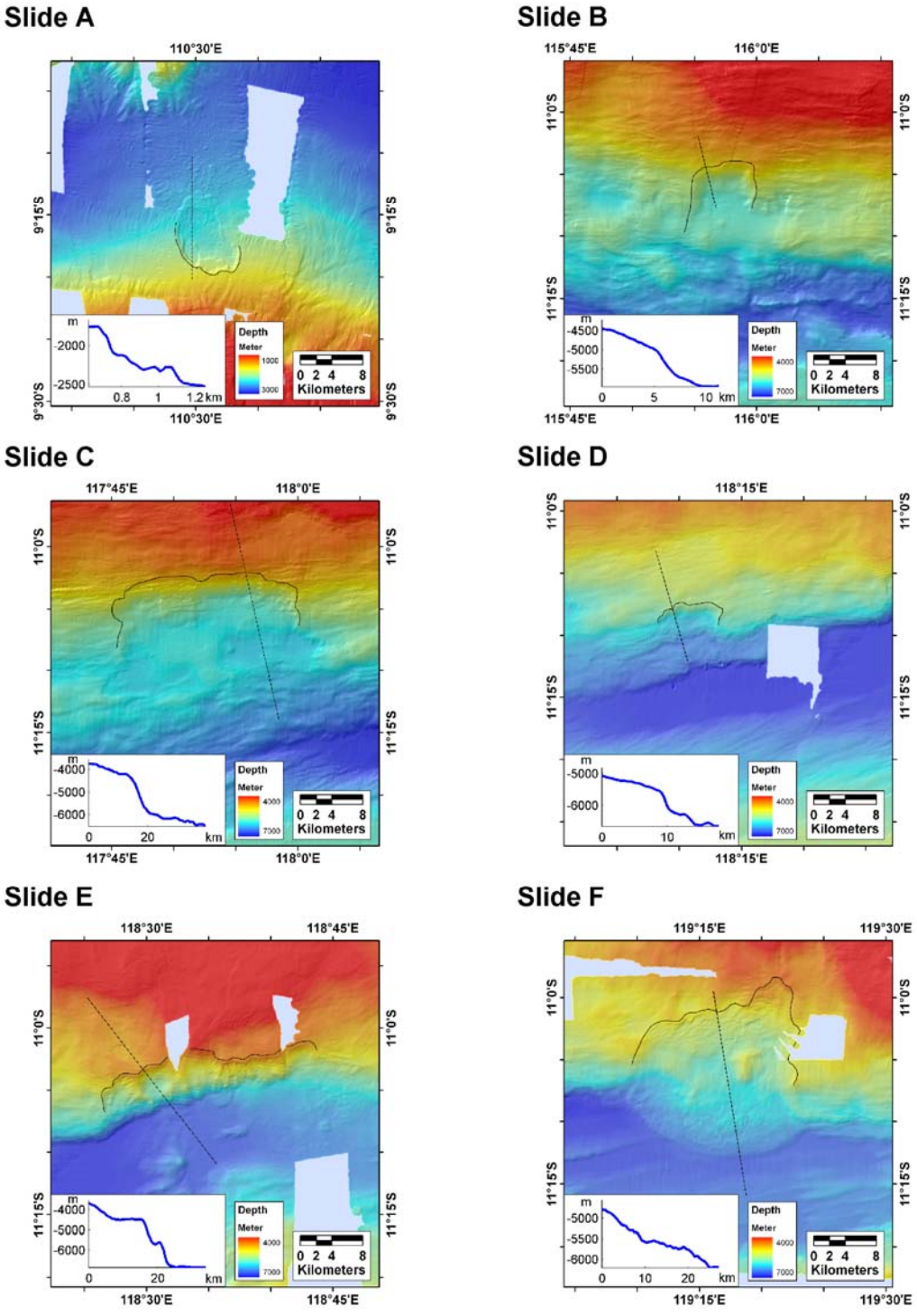

Figure 2 *Bathymetry maps, interpretations of the escarpments (solid lines) and locations of cross sections (dashed lines). Corresponding profiles are shown in white inlets. Note the different depth scale for slide A. Slide locations are mapped in Figure 1.*

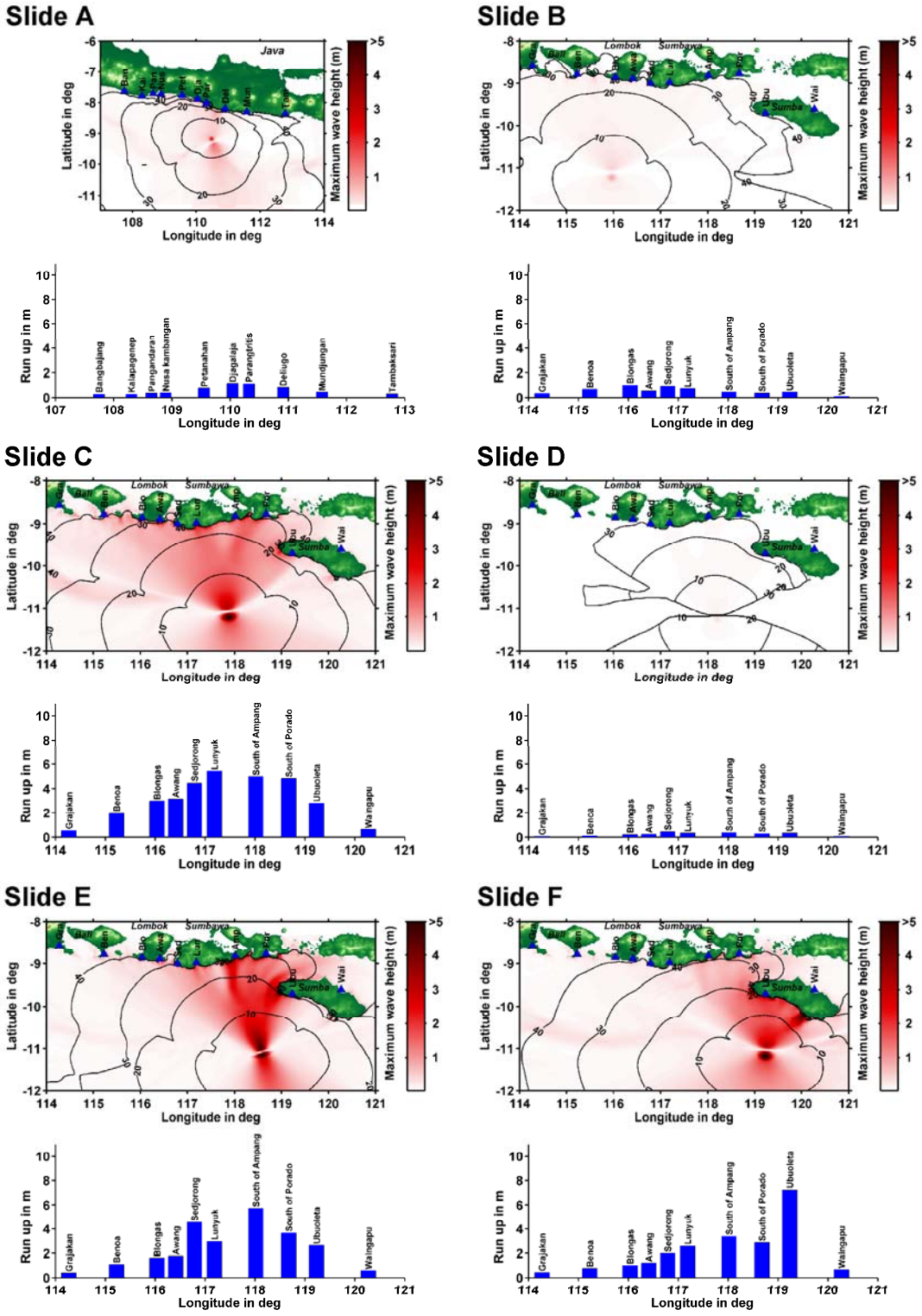

Figure 3 *Maximum wave height distributions after 4 hours, arrival times in minutes as well as corresponding run-up heights along the coast projected onto the longitude (bar*

plots). Locations of virtual gauge stations are mapped as blue triangles with abbreviated names.

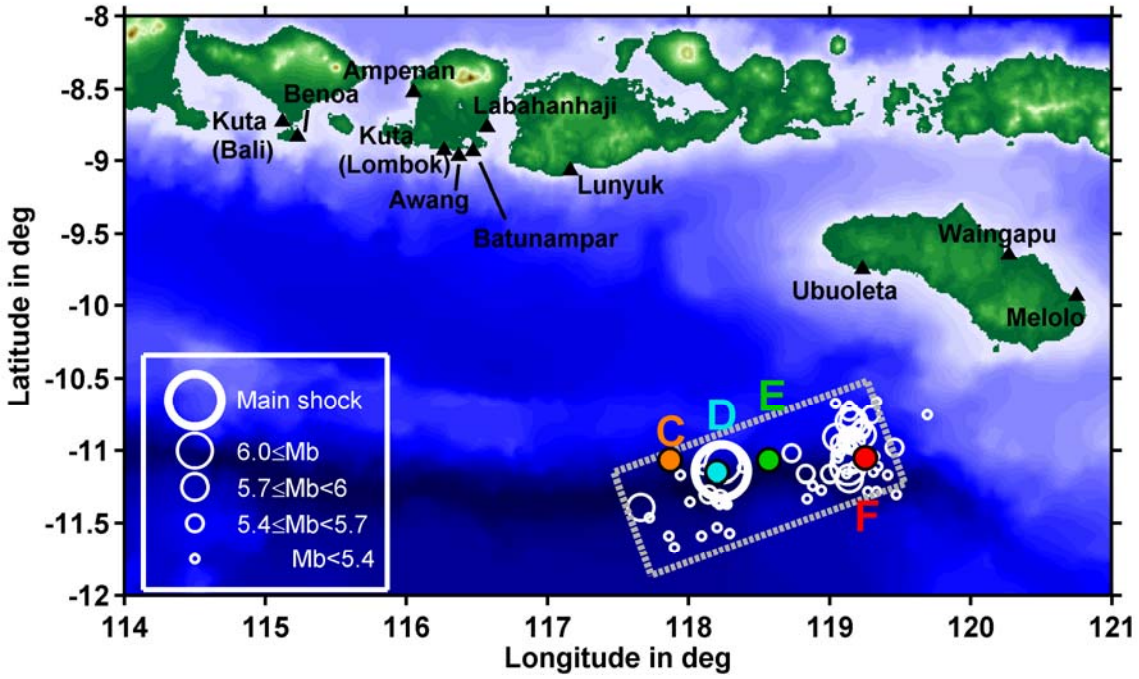

Figure 4 *1977 Sumba earthquake: Main shock location, seven-days aftershock distribution and assumed fault plane (dotted rectangle). Also designated are positions of slides C to F as well as locations of the measured run-up (black triangles).*

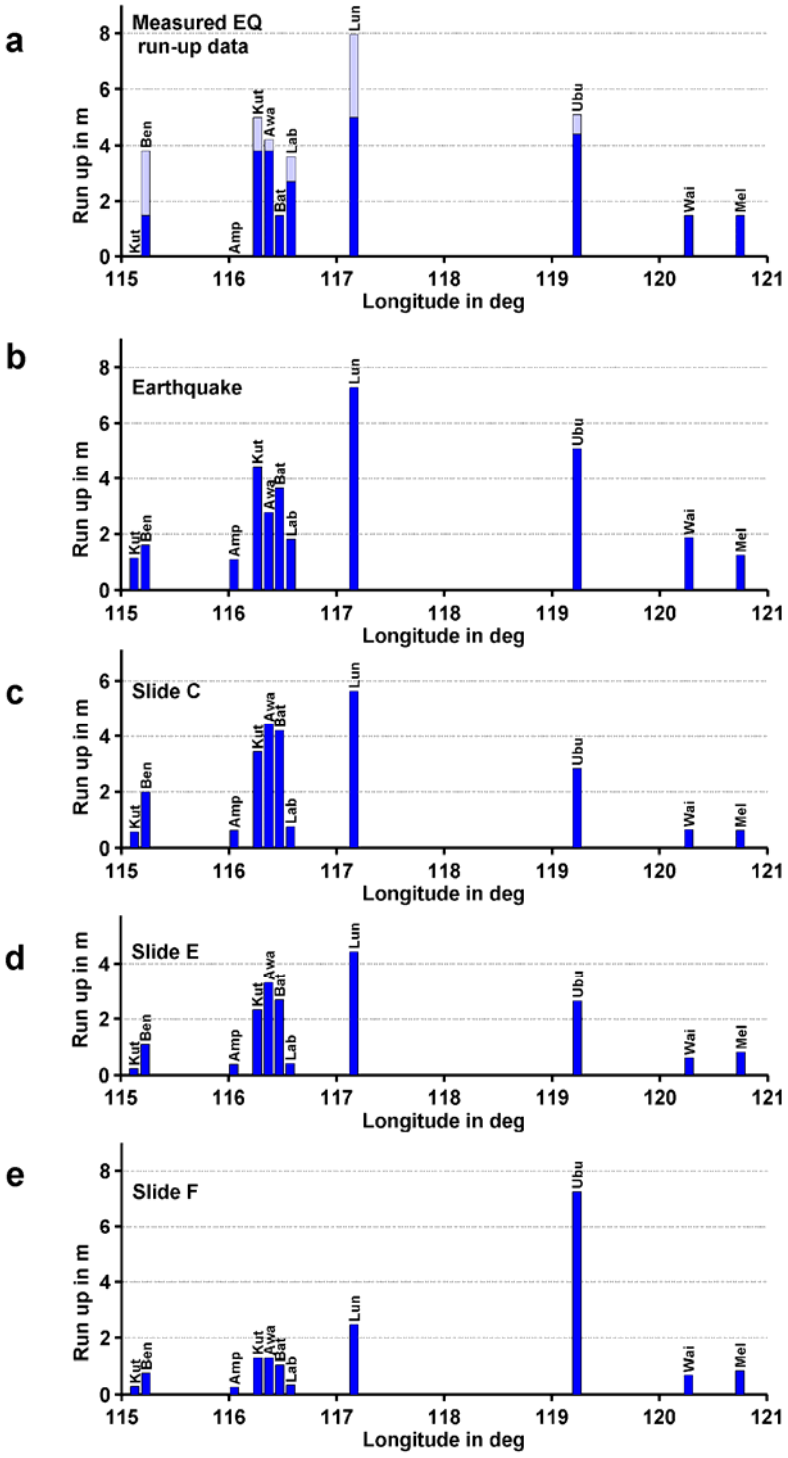

Figure 5 *Run-up distributions.* ***(a)*** *Measured run-up of the 1977 Sumba earthquake. If more than one value was measured at a location, light blue bars show the maximum run-up, while dark blue bars correspond to the minimum run-up.* ***(b)*** *Computed run-up*

caused by the 1977 Sumba earthquake. ***(c,d,e)*** *Modeled landslide-generated run-up heights for slides C, E and F, respectively. Measurement locations are mapped in Figure 4.*

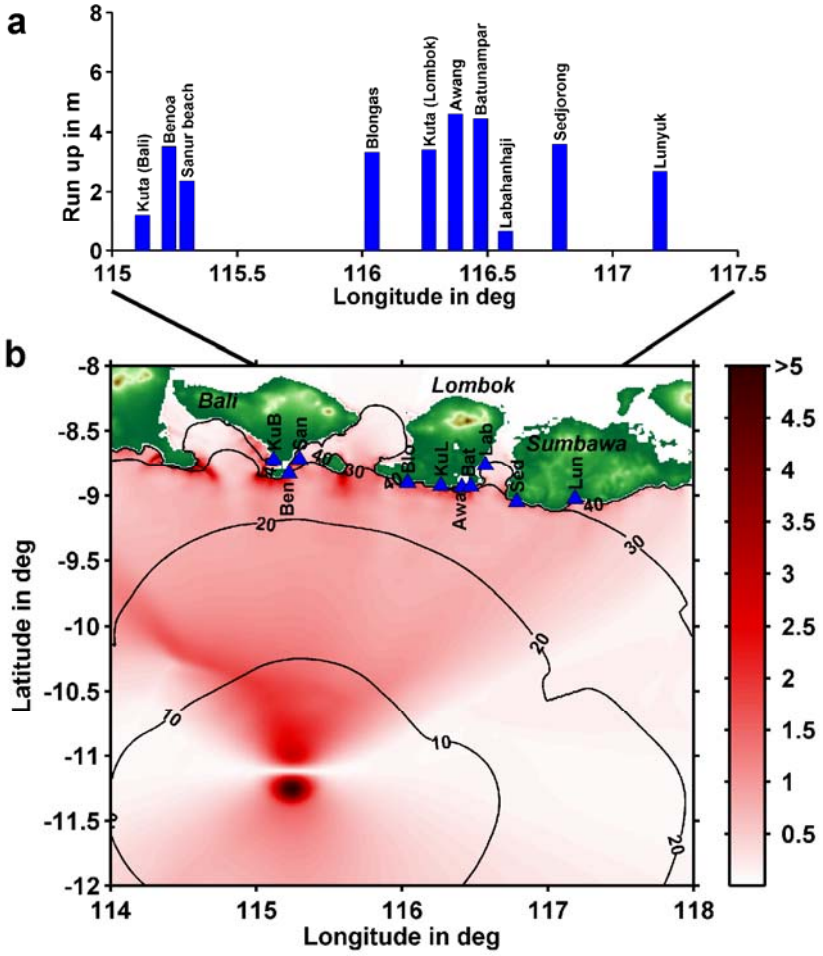

Figure 6 *Maximum wave heights, arrival times and run-up distribution for a hypothetical 95 km³ event off Bali. Calculation time was 4 hours. Virtual gauge locations are marked with blue triangles and abbreviated names.*

	Slide A	Slide B	Slide C	Slide D	Slide E	Slide F
Longitude	110°31'E	115°57'E	117°52'E	118°12'E	118°34'E	119°15'E
Latitude	9°18'S	11°6'S	11°'4S	11°9'S	11°4'S	11°3'S
Width (km)	7	7	23	7	25	18
Length (km)	8	7	8	4	5	10
Height (m)	150	200	200	100	300	300
Volume (km^3)	13	15	60	4	60	95
Depth (m)	2000	5300	5300	6000	6100	5000
Travel Distance (km)	6	4	12	4	5	10
Mean local slope angle (°)	4	15	10	8	15	5

Table 1 *Slide parameters. Longitude and latitude designate the estimated initial center of mass location. Width is measured perpendicular, and length parallel to the slope. Volume is inferred by parabolic shape approximation. Travel distance denotes the estimated movement of the slide's center of mass. Mean local slope angles are inferred from bathymetry cross-sections of slide areas.*

	Slide A	Slide B	Slide C	Slide D	Slide E	Slide F
Initial wave height η_{2HD} (m)	2.9	1.0	6.4	0.4	8.8	7.0
Characteristic wave length λ (km)	19	23	27	20	15	27
Characteristic time t_0 (s)	130	100	120	80	60	120

Table 2 *Hotstart parameters defining the initial sea surface for the tsunami propagation model. Their calculation follows the technique of Watts et al. (2005).*

Structure, Evolution and Tectonic Activity at the Eastern Sunda Forearc, Indonesia, from Marine Seismic Investigations

Lüschen, E.[1], Müller, C.[1], Engels, M.[1], Kopp, H.[2], Planert, L.[2], Shulgin, A.[2], Djajadihardja, Y.S.[3]

[1] Federal Institute for Geosciences and Natural Resources (BGR), Stilleweg 2, 30655 Hannover, Germany, email: Ewald.Lueschen@bgr.de

[2] Leibniz-Institute of Marine Sciences (IFM-GEOMAR), Wischhofstr. 1-3, 24148 Kiel, Germany

[3] Agency for the Assessment and Application of Technology (BPPT), Jl.M.H. Thamrin No. 8, Jakarta 10340, Indonesia

Abstract

At the eastern Sunda arc, between east Java and Sumba Island, old Indo-Australian oceanic crust of late Jurassic age with a thin sedimentary cover (less than 600 m) is subducting at a high subduction rate of around 76 mm/yr since the late Oligocene. The incoming plate in this are is subdivided into two pronounced provinces, i) the Roo Rise with rough topography subducting off eastern Java to Bali with elevations reaching heights up to 1.5-2 km above the smooth oceanic Argo Abyssal Plain, subducting off Lombok to Sumba Island. This unique combination of key parameters characterizing the subducting plate results in unique characteristics of forearc structures in the overriding plate, which we decipher from new high-resolution reflection seismic imaging. Frontal accretion to a broad outer arc high, subdivided into a landward static backstop and a seaward dynamic backstop is the main mode of outer arc high growth further to the West along the Sunda Arc. However, in our study area we observe continuous tectonic activity of the entire outer arc high: active out-of-sequence thrust faults connecting upper/lower plate interface and seafloor, slope basins showing tilted sedimentary sequences on the outer arc high, vertical displacement of young seafloor sediments, and tilted sedimentary sequences in the Lombok forearc basin. While frontal accretion is a minor process, the growth of the outer arc high is mainly attributed to underplating. The incoming oceanic crust is dissected by normal faulting into 5-10 km wide

blocks within a 50-70 km wide belt seaward of the deep sea trench. These blocks determine geometry and evolution of duplexes attached to the base of the overriding plate landward of the trench. The Lombok forearc basin has a sediment thickness up to 4 km, which is less than in other forearc basins along the Sunda Arc. The seismic stratigraphy of the Lombok basin shows indications for strong subsidence reflecting the evolution of the forearc until recent times. In the Lombok basin we image mud diapirs, fed from deep sediments which may have been mobilized by fluids. A wrench fault system in the eastern Lombok forearc basin decouples the subduction regime of the Sunda Arc from the continent-island arc collision regime of the western Banda Arc. Thus, the observed tectonic activity of the entire forearc system reflects a high earthquake and tsunami hazard, similar to the western part of the Sunda Arc.

1 Introduction

The 7000 km long Sunda Arc has long been considered as a classical convergent margin system where the Indo-oceanic plate is underthrust beneath the South-East Asian continent, active since the upper Oligocene (Hamilton, 1977, 1988). This type of orogenic arc has produced a subduction complex landward of the deep sea trench, consisting of an accretionary wedge and a pronounced outer arc high, deep forearc sedimentary basins and a volcanic arc (Dickinson, 1977). The evolution of such subduction zones results in a high along-strike variability of tectonics and geologic structures. These structures evolve in response to a number of key parameters, such as the subducting plates age, composition and structure of the subducting plate, convergence rate and direction, and the thickness and origin of the incoming sediments (e.g. Van der Werff, 1996; and references therein). Mass transfer, backstop and accretionary mechanics of this ‘subduction factory’ offshore Sumatra and Java, ranging from accretionary to erosive styles, have recently been studied by Kopp and Kukowski (2003) and Kopp et al. (2001, 2006). At the eastern end of the Sunda arc the convergent system changes from oceanic subduction to continent-island arc collision of the Scott Plateau, as part of the Australian continent, colliding with the Banda island arc and Sumba Island, which origin is still debated, in between (Rutherford et al., 2001; and references therein).

The Sunda Arc is known as an active convergence zone of tremendous earthquakes, tsunamis and volcanic hazards. The M_w 9.3 Indian Ocean earthquake and tsunami of

December 26, 2004, killed more than 250,000 people. Numerous investigations have been commissioned near the epicentre offshore northern Sumatra to evaluate future earthquake and tsunami hazards. These projects have mapped seafloor morphology and imaged deep structures and faults in order to better understand the origin of megathrust earthquakes and tsunamis in the western portion of the Sunda Arc subduction system (e.g. Henstock et al., 2006; Ladage et al., 2006; Franke et al., 2008). Many of these projects, and also the one presented here, provide input data to the installation of the German-Indonesian Tsunami Early Warning System GITEWS (http://www.gitews.de). Relatively little attention concerning tectonics, structural geology and risk analysis has been paid to the eastern part of the Sunda arc, south of eastern Java, the islands of Bali, Lombok, Sumbawa and Flores, so far. This area is in the focus of the SINDBAD project (Seismic and Geoacustic Investigations Along the Sunda-Banda Arc Transition), a joint German-Indonesian project that carried out the marine survey cruise SO190 with R/V SONNE end of 2006 in two consecutive legs (Fig. 1).

The main goal of the SINDBAD project is (i) to image and characterise the interaction between the subducting and the overriding plate, (ii) to investigate the structure and evolution of the subduction complex and the Lombok Forearc basin in response to the variation in age and structure of the incoming oceanic plate (Roo Rise and Argo Abyssal Plain) and (iii) to characterise the transition from ocean-island arc subduction in the eastern Sunda arc to continent-island arc collision in the western Banda arc. In this article we focus on the first two points (i and ii). The data comprise 4933 km of multichannel reflection seismic (MCS) profiling, combined with magnetic and gravimetric measurements, sediment echo sounding and swath bathymetry, as well as refraction/wide-angle seismic measurements with ocean bottom seismometers (OBS) for velocity modelling on four corridors coincident with N-S running MCS profiles (Fig. 1). Preliminary images were presented by Müller et al. (2008) highlighting the structure of the incoming normal-faulted oceanic crust, the accretionary wedge and the outer arc high as the oldest part of the wedge with pronounced thrust sheets and piggy-back basins, the Lombok forearc basin and duplex structures between the subducting and overriding plates.

2 Regional Tectonic Setting

The subduction of the Indo-Australian Plate along the Java Trench has been going on continuously since the late Oligocene (e.g. Hamilton, 1988). The overriding plate is continental including Sumatra and Java (Kopp et al., 2001) and the basement below the forearc basin offshore Bali and Lombok is probably rifted crust of continental character in transition to oceanic character at Sumbawa and further east (Banda Sea) (Van der Werff, 1996). The convergence rate increased from 5 cm/a to 7 cm/a during the last 10 Ma (7.6 cm/a today according to the global velocity model NUVEL-1A, DeMets et al., 1994) and is almost perpendicular to the Java Trench, in contrast to oblique convergence offshore Sumatra, where plate motion is partitioned into thrust and strike-slip movements. The volcanism of the island arc was initiated during the Pliocene and shows a transition from intermediate to mafic composition between East Java and Sumbawa, which documents a transition from a continental to an oceanic overriding upper plate (Hamilton, 1988). The present-day configuration of plate boundaries in the southeastern Asian region shows a quite complex history of interaction of the Pacific, the Indo-Australian and the Eurasian plate. Reconstructions and modelling by Hall (2002, with a comprehensive literature list) show major plate reorganisations at 45, 25 and 5 Ma. Seismological mantle tomography reveals seismic velocity anomalies to at least 1500 km depth describing the subducted lithospheric slab, which is probably continuous below Java but discontinuous below Sumatra (Widiyantoro and v.d. Hilst, 1997). Seismicity is present in clusters following the Wadati-Benioff zone from the outer-trench bulge of the subducting oceanic plate to maximum 300 km depth beneath Sumatra and even 600 km depth beneath the eastern Sunda arc (e.g. Widiyantore and v.d. Hilst, 1997; Spicák et al., 2007).

The subducting Indo-Australian plate in the study area (Fig. 1) is oceanic offshore Java to Sumbawa and can be subdivided into two distinct provinces: The Roo Rise is characterized by a rough morphology. It rises to more than 1500 m above the surrounding seafloor level. The subduction of seamounts with their irregular relief is obviously the main reason for subduction erosion and for the block structure of the outer arc high (Kopp et al., 2006). The trench here is less deep in comparison to adjacent regions, 5600 m to 6000 m versus 7000 m, respectively (Masson et al., 1990). The Argo Abyssal Plain (Fig. 1) is smooth at water depths of 5000-5500 m and has a pelagic sediment cover of about 600 m, which was sampled in DSDP site 261 (e.g. Heirtzler et al., 1974; Van der Werff, 1995). The oceanic crust including the Roo Rise and the Argo Abyssal Plain dates from the late Jurassic (M25 = 155 Ma) to early Cretaceous (M0 = 125 Ma, Fig. 1) and is, particularly the Argo Abyssal Plain, regarded as

remnant of the Tethys ocean (e.g. Heine et al., 2004). In contrast, the Scott Plateau as the eastern part of the Indo-Australian plate in the study area is of continental character and in collision with Eurasia since the late Miocene (e.g. Harris, 1991; Van der Werff, 1995). This collision controls the uplift of the Sumba ridge and the development of the Savu basin. The origin of Sumba Island is still debated. It could be part of Australia, alternatively of Sundaland or of an island arc which rifted to its present position during Miocene times (Rutherford et al., 2001, and references therein).

The structure of the subduction complex (accretionary wedge, outer arc high) and the forearc basins has been studied by Hamilton (e.g., 1977, 1988), v.d. Werff (1995, 1996) and v.d. Werff et al. (1994) using single-channel seismic recordings of relatively low resolution and depth penetration, and, in parts, using multi-channel seismic profiling provided by industrial companies and other institutions in the 1980ies. These data have shown that the accretionary wedge consists of imbricated thrust sheets consisting of a melange of masses offscrapped from the subducting plate. Forearc basins are fed from the rising volcanic arc and the outer arc high as the oldest part of the accretionary prism. In the context of large megathrust earthquakes and ruptures, the subduction complex shows abrupt uplift of several meters, the forearc basin subsidence is in the same order of magnitude (Briggs et al., 2006). The youngest thrust faults in the accretionary wedge sole out at a pronounced décollement between upper and lower plate. The structure and stratigraphy of forearc subductions systems with subduction complexes (accretionary wedge, outer arc ridge) and forearc basins have been described in general terms by Dickinson and Seely (1979) and Dickinson (1995). The thickness and width of the subduction complex decrease from the western Sunda arc to the eastern Sunda arc in response to the decreasing thickness of seafloor sediments on the incoming plate (4 km offshore Sumatra, 1.3 km offshore western Java, less than 1 km in our study area) entering the trench from the northwest. The sediment thickness reflects southward progradation of immense submarine fans down the Bay of Bengal from sources in the Himalayan collision belt (Dickinson, 1995). Modern MCS data of the western and central Sunda arc are presented by Schlüter et al. (2002), Kopp and Kukowski (2003), Kopp et al. (2006) and Franke et al. (2008). Mass transfer variations have been in the focus of these investigations of the Sunda arc to the West of our study area. Whereas mass accretion from the lower to the upper plate dominates in the western and central Sunda arc, erosional processes at the base of the upper plate are facilitated by seafloor roughness of the Roo Rise, low sediment supply and higher convergence rate further east (Kopp et al., 2006).

The Lombok basin is one of the largest (600 x 120 km) and deepest (4 km water depth) of the forearc basins which are located between the subduction complex and the magmatic arc (Fig. 1), divided by transverse ridges some 1000-1500 Meters higher and covered with less sediments. To the East, the Lombok basin is controlled by the collision of the Scott Plateau with Sumba and the Banda arc, resulting in an uplift of the eastern part of the basin. The basement of the Lombok basin is of unknown nature, but has been interpreted variously as anomalously thick oceanic crust, rifted continental crust or as metamorphosed accretionary prism (Dickinson, 1995). Five relatively undeformed seismostratigraphic units have been interpreted in the Lombok basin based on early seismic measurements and analogies to well data from the Bali basin in the backarc area north of Bali (v.d. Werff et al., 1994). Horst and graben structures in the basement have also been recognized. The sediment thickness amounts up to around 4.5 km. Underlying units have been interpreted as carbonate platforms from the Eocene. This implies that the basement subsided from the surface by nearly 10 km.

Even though some information and images have been gained on the subduction system in the study area in the past – much of it is adopted from the Sunda arc further west – we produced clearer images of the incoming material, the accretionary wedge, the outer arc high and the forearc basins for better knowledge of their structure and tectonic activity. Special focus was laid on the variability of the structure of the interface between upper and lower plate. These images may be used also to calculate the mass balance of the subduction system and the hydrocarbon potential of the forearc basins. In this paper we are presenting an overview on a great wealth of new seismic images.

3 Methods, Data Acquisition and Processing

During Leg 1 of cruise SO190 with RV SONNE from 9th October to 9th November 2006, a total of 4933 line kilometres of multichannel seismic reflection (MCS) data were acquired (Fig. 1), accompanied by swath bathymetry, echosounder, gravity and geomagnetic measurements. Seismic source was a tuned G-Gun array comprising 16 airguns with a total volume of 50.8 l, working pressure of 145 bar, array length of 15.5 m and a towing depth of 6 m. Shot intervals were 18 s, corresponding to 50 m at a speed of about 5 kn. Data were acquired with a 240 channel streamer of 3 km length (group interval: 12.5 m, offset to near

group: 150 m, maximum offset: 3137.5 m). Record length was 14 s at a sampling interval of 2 ms. Nominal coverage was 30-fold.

Processing of the twenty MCS lines produced Kirchhoff poststack time and depth sections as a standard and Kirchhoff prestack depth migrations on the six North-South running lines and some of the intersecting lines (Fig. 1). Prestack time processing included geometry setup, geometrical spreading correction based on stacking velocities, predictive deconvolution and time-variant bandpass filtering. For seabottom multiple attenuation various approaches were tested, among them parabolic Radon filter with inner trace mutes, f-k-filter and wave equation based prediction. However, because of varying success along a seismic line, the filter attenuated successfully the multiples, but also deep reflections, e.g. from the interface between upper and lower plates, we decided to use only a prestack time-variant bandpass filter (e.g. passband 4-26 Hz in the lower part of the recordings where multiples prevail). A frequency range of 4-120 Hz proved to be profitable, at least in the upper sedimentary part of the sections. Interactive velocity analysis was done at dense intervals, depending on brute-stack inspections. Smoothed stacking velocities were used for poststack time migrations. After conversion to interval-depth velocities, these models served as initial models for the migration velocity analysis (MVA) using Kirchhoff prestack depth migration (PSDM). The upper, sedimentary part of the velocity models was iteratively improved from top to bottom using the focussing technique. Because of the limited offset range, this approach was not sensitive enough for the deeper ranges. Therefore, the upper, sedimentary part was fixed and then extended towards greater depth using the tomography approach of the refraction/wide-angle modelling (see below). Because of computing time considerations, the frequency range was limited to 4-60 Hz for prestack depth migration. The resulting velocity-depth model could then be used for poststack time (with subsequent time to depth conversion) and depth migrations with the full frequency and resolution range.

Leg 2 of cruise SO190 from 11th November to 22nd December 2006 was dedicated to refraction/wide-angle seismic observations with ocean-bottom-seismographs (OBS). A cluster of 8 G-guns with a total volume of 64 l was used as seismic source. Average spacing between shots was 100/150 m and average OBS spacing was 6 km. 28 instruments were used on 239 sites. Four corridors were covered, including some cross-lines (Fig.1), resulting in approximately 1900 line-km. These measurements were accompanied by swath bathymetry, geomagnetic profiling and methane sensing. The main data processing steps of the OBS-

recorded refraction/wide-angle seismic data involved conversion to SEG-Y-format, geometry implementation, editing, time and offset-dependent bandpass filter, predictive deconvolution and linear moveout correction (reduction velocity 8 km/s). After picking of the first arrivals and the PmP (Moho) phases, the dataset for seismic tomography consisted of 16,000 refracted and 4,000 reflected picks, with offsets up to 120 km for several stations. Seismic tomography inversion for the Vp velocity distribution was performed by running a joint refraction/reflection inversion (Korenaga et al., 2000), complemented by forward modelling. Starting from a simple layered model, a 'top-to-bottom' approach was applied, constraining the model first for the near offsets and then increasing the depth extent of the rays, finally adding the reflecting phases. The structure of the sediments and the upper crust was controlled by the MCS-data.

Swath bathymetry was acquired by the shipboard 12-kHz SIMRAD EM 120 system. The data from the two legs were edited (for outliers) and merged to provide a consistent map over the area, extending the maps compiled by Ladage et al. (2006) and Franke et al. (2008) towards East.

Echosounding was performed by the shipboard PARASOUND system which works as a low-frequency sediment echosounder and as a high-frequency narrow beam sounder to determine the water depth with a hull-mounted transducer array. It utilizes the parametric effect which produces additional frequencies through non-linear interactions of acoustic waves of similar frequencies, 18 kHz and 22 kHz, which produce a resulting frequency of 4 kHz. The emission angle is only 4^{o} and the footprint size is 7 % of the water depth. On the other hand, the maximum slope of the seafloor cannot be more than $2\text{-}3^{o}$ in order to receive a useful reflected signal. Depth penetration in flat sedimentary sections is often of the order 100-150 m. The analogue traces of 250 ms around the seafloor are digitized onboard and transformed into the seismic SEG-Y format with the time delay and GPS-based coordinates in their headers. Processing is done with a seismic processing system (see above) involving resampling, dc-removal, time-variant scaling, delay correction, bandbass filtering, noise rejection and conversion to envelopes or perigrams for display.

We recorded magnetic data using a towed magnetometer array consisting of two total field sensors (Overhauser type) and one oriented vector magnetometer (fluxgate type). The two total field sensors operated 700 m and 850 m astern of the vessel in gradiometer mode

removing temporal variations, while the fluxgate sensor embedded in-between resolved component data. One additional fluxgate sensor recorded simultaneously shipboard data. Gravity data were obtained by the gyro-stabilized Askania type sea gravimeter KSS31M. Details of potential field data acquisition and processing are described in the cruise report (BGR, 2006).

4 Major Structural Units

In Fig. 2 a compilation of the six N-S running 250-380 km long profiles is shown. They range from the Indo-Australian oceanic/continental plate over the deep sea trench, the accretionary prism, the outer arc high, the forearc basin to the slope of the island arc. These sections were obtained with the Kirchhoff prestack depth migration approach (PSDM). Velocity control is shown for the line P31 (coincident with MCS line BGR06-313) as a sample. In the following we discuss the sections from South to North first based on Fig. 2, then in more detail from West to East in the following figures.

Indo-Australian crust: The subducting/colliding crust is characterized by only a few hundred Meters thick sedimentary layer, except several kilometres of sediments of the Australian crust (Scott Plateau) just south of the main deformation front (Fig. 2, easternmost section). The water depth ranges from about 3500 m in the westernmost profile (Roo Rise) to 5000 m (Argo Abyssal Plain) and again to 3500 m at the Scott Plateau on the easternmost profile. A pronounced outer bulge is not observed even on the longest profile BGR06-313. Instead, a stepwise downbuckling over a distance ranging between 30 km and 70 km, decreasing from West to East, is observed before reaching the deep sea trench and the deformation front. This is indication of an old non-elastic lithosphere under rigid deformation. The steps or vertical displacements are related to normal faulting within the oceanic crust as response to the downbending. Crustal and mantle velocities are remarkably decreasing when approaching the deep sea trench, probably caused by intruding seawater (normal faults as pathways) and subsequent serpentinization. On profiles BGR06-311 and -317, were the sea floor is particularly smooth, continuous reflections from the crust-mantle boundary are observed, indicating a 7-9 km thick crystalline oceanic crust.

Subduction complex: Landward of the deep sea trench, which is marked by only slightly increased sediment thickness, a pronounced interface of complex shape between upper and lower plate is observed over a distance of 50-70 km from the trench on most of the profiles. Further imaging of the plate interface is prevented most likely due to the increasing subduction angle. The 70-120 km wide, widest opposite to the Roo Rise, subduction complex on top is up to 12 km thick with sediment-type velocities. Van der Werff (1995) postulated that the decreasing width of the complex towards the East may be due to the younger age of the subduction system. The accretionary wedge and its older part, the outer arc high, has long been suggested as being trench-fill turbidites, pelagic sediments and oceanic crust scraped from the descending oceanic plate by the leading edge of the overriding plate to which they become accreted (Karig and Sharman, 1975). Our sections show that the entire subduction complex is characterized by a northward dipping system of imbricate thrust sheets with major thrust faults of listric shape connecting seafloor and plate interface. These faults are associated with pronounced breaks in morphology at the seafloor. Small piggy-back sedimentary basins are observed between the morphologic kinks, particularly seaward of the Lombok forearc basin.

Forearc basin: The Lombok forearc basin located between the outer arc high and the volcanic island arc is up to 120 km wide with up to 4500 m of sediment thickness and water depth of about 4000 m. It has been imaged on the three lines BGR06-303, -313 and -311 (from West to East). The basement is characterized by a central high or horst. Several unconformities are visible within the sedimentary layer. The basin is underlain by anomalously low mantle velocities at relatively shallow depths of about 15 km, which might be due to an alteration from dehydration processes by rising fluids within the subducting oceanic plate. Seismostratigraphic analysis of the basin fill based upon early seismic profiling in the context of hydroncarbon exploration has been carried out by Van der Werff et al. (1994). On the westernmost profile BGR06-305, only a small amount of sediments cover the elevated basement, which forms a basement high or ridge there. The easternmost profiles BGR06-317 and -319 are characterized by the collision of the oceanic/continental Indo-Australian plate with the block of Sumba Island. Underthrusting of the Scott Plateau beneath a large accretionary prism and the Sumba block is observed, which produces uplift there and a large bivergent structure. The Savu basin with up to 4 km sediment thickness is shown at the northern end of the easternmost profile.

5 Results and Discussion

In the following chapters we discuss the main structural units, the Roo Rise and the Argo Abyssal Plain with their counterparts in the overriding plate, the Lombok forearc basin and the transition zone between the subduction regime in the West and the collision regime in the East in further detail.

5.1 Roo Rise and Forearc

On profile BGR06-305, the westernmost part (Fig. 3), we zoom into the coupling zone of upper and lower plate with the accretionary wedge on top. Landward of the Roo Rise the seabottom is about 1-2 km higher than in the other profiles. The downbending oceanic crust is segmented by steep normal faults which become reversed due to compression when approaching the main subduction front. Exceptionally, sediments gradually accumulate in the trench up to 2 km thickness over a distance of 30 km in front of the trench. This is probably due to reverse backthrusting and folding induced by the toe of the accretionary wedge. Turbiditic slumps from the inner-trench slope (3-4^{o}) may contribute to this thickness. The boundary between upper and lower plate, which is imaged over 70 km length, is of irregular shape with km-wide vertical displacements obviously imprinted by the complex shape of the subducting oceanic basement. This may be interpreted as duplex building with most of the oceanic sediments beneath and in front of the accretionary wedge. Landward dipping reflections at the toe of the accretionary wedge indicate that sediment sheets are underplated beneath the toe. The wedge is relatively opaque over a distance of about 20 km. However, at the pronounced slope break, a series of steep landward dipping reflections, obviously thrust sheets, connect to the plate interface. Here, the interface changes its dip and shape abruptly. We speculate that a major block of the Roo Rise or perhaps even the onset of the Roo Rise, has arrived here and produced compression-related uplift during the last 500,000 years. The splay faults of the thrust sheets, which originate here, and the pronounce slope break indicate recent movements which produce the ridge between adjacent forearc basins. This uplift is also confirmed on profile BGR06-302 by the pronounced unconformities of a sedimentary wedge at the western part of the Lombok forearc basin (Fig. 4).

The pattern of deformation within the subduction zone and forearc is directly seen on all of the N-S running profiles, however, most prominently, on profile BGR06-303 (Fig. 5). Normal faulting dissecting the oceanic crust with vertical steps of 0.5 km and block widths of 5-10 km is observed on the outer-trench slope. Most of the oceanic sediments are subducted and underplated beneath the acrretionary wedge to form there a several Kilometre thick reflection pattern including duplex structures. A single decóllement is not observed. Instead, the roof thrusts of the duplexes connect listrically with landward dipping thrust sheets inside the subduction complex to pronounced breaks in seafloor morphology. The length of the duplexes seems to be controlled by the length of the dissected blocks of the oceanic crust. If we imagine that a sudden major slip occurs between upper and lower plate, perhaps causing also a greater earthquake, it will appear that this slip is partitioned into several branches (see arrows in Fig. 5). The slip may be deviated at the edges of the dissected oceanic blocks, which might act as bulldozers against the bottom of the upper plate, towards the seabottom where they cause horses with breaks in the morphology. From there the sediments are moved towards the trench where they are recycled, while others fill the piggy-back basins. At the toe of the accretionary wedge slump activity can be recognized by the echosounder recordings (Fig. 5). Therefore, the subducted sediments may be partly incorporated into a cycle, first being underplated beneath the outer arc high, then thrusted upward and slumped down into the trench again. This cycle is ongoing, and first of all, recently active over the complete subduction complex, not only at the acrretionary wedge, and is responsible for forming out-of-sequence splay faults. This is convincingly demonstrated by the structure of several small piggy-back basins (Fig. 6). They are entirely seaward tilted by thrust activity of the outer arc high basement. In one case, a vertical displacement of about 100 m, particularly seen in the echosounder recordings, indicates recently active movements.

5.2 Argo Abyssal Plain and Forearc

The piggy-back basins are located between major breaks in seafloor morphology. These breaks and corresponding basins can be correlated in E-W direction over more than 300 km (Fig. 7). Given this length, plus the water depth of 1-2 km, it means that this forearc area is characterized by a tremendous tsunami hazard in case of a sudden displacement of several Meters related to a megathrust earthquake. The E-W extension of the piggy-back basins and their confining breaks in seabottom morphology correlate with the extension of the Lombok

forearc basin, and furthermore, roughly with the E-W extension of the Argo Abyssal Plain. Therefore, a genetic relationship between these major structural units of the subduction system might be suspected. The high perpendicular convergence rate of 76 mm/yr in combination with the old oceanic crust, which is therefore relatively cold and brittle, may be responsible for growth and deformation of the entire forearc system, despite of relatively low sedimentary input as compared to the arc further west.

Duplex formation at different scales and modes is the prevailing process at the interface upper/lower plate instead of a simple decollèment. A 1-2 km thick duplex structure is visible beneath the toe of the accretionary wedge in profile BGR06-313 (Fig. 8). The upper/lower plate interface consists of a series of branching thrusts building multiple imbricates. These imbricate sheets are composed of a melange of oceanic sediments and crystalline crust as well as sediments of the upper plate wedge. The geometry of the glide planes is concave upward and continues generally into the landward dipping thrusts of the outer arc high. However, since the preexisting oceanic spreading structures and blocks, of which fracturing of the oceanic crust is initiated, strike obliquely to the profile direction, there is no direct connection obvious in Fig. 8. Crosscutting features in the upper/lower plate interface are also indicative for this 3-D effect. In principle, younger parts of the oceanic plate underthrust the already subducted parts, which are continuously compressed and steepened. Since about 1500 km of oceanic plate have been subducted already, a continued process as described may have formed the basement of the outer arc high, the forearc basin as well as the basement of the island arc east of Java, composed of ophiolite sheets and nappes as described e.g. by Nicolas (1989). Relatively low seismic velocities (see Fig. 2) of the upper plate basement confirm this interpretation. At this point we predict that the basement of the forearc basin exhibits a heavily broken geometry because of steeply dipping ophiolitic sheets (compare Fig. 13).

A similar, but more drastic situation concerning the upper/lower plate interface is observed on profile BGR06-311 (Fig. 9). Normal faulting affects the oceanic sediments and their basement over a distance of 40 km. The bathymetry shows that this corresponds to a belt of ripples striking obliquely to the trench and parallel to magnetic lineations. In contrast to the former N-S running profiles, the plate interface is relatively smooth over long distances. Only small signs of duplex formation are present there. The great difference occurs beneath the toe of the accretionary wedge, where a prominent break is visible. This break seems to be mirrored at the base of the oceanic crust. The crust-mantle boundary is imaged on this profile

nearly continuously as a discrete reflection band at 7-8 km beneath the seabottom. The crystalline part of the oceanic crust is relatively transparent or shows scattered events. The displacements in plate interface and crust-mantle boundary may be interpreted as the initial stage of underthrusting of the seaward part of the entire oceanic crust beneath the subducted crust, or in other words, the initial stage of a large duplex formation. Such duplexes with horses dipping to the Hinterland (island arc) may have been building the basement of the forearc structure. Duplexes or imbricate thrust structures at the upper/lower plate interface occur at different sequences and dimensions and may have mixed character: piggyback imbricate thrust structures in which the faults develop from Hinterland (forearc) to Foreland (ocean) or overstep imbricate thrust structure in which the faults develop from Foreland to Hinterland. The dimension of the imbricate slices is determined by the length of oceanic blocks after fracturing and normal faulting in the outer trench swell. We argue that this duplex formation may be the principal cause for building the outer arc high.

Earthquake focal mechanisms confirm the mechanism described above (Fig. 10). A belt of extensional mechanism is located in front of the trench. Compressional mechanism may correspond to disrupting and duplex building of the oceanic crust. Magnetic lineations correlate roughly with elongated ripples in the oceanic seafloor indicating that extensional faulting occurs at preexisting oceanic structures produced at the former seafloor spreading centre. These preexisting oceanic spreading structures, since they strike at an oblique angle to the trench, together with transform faults, may be responsible for segmentation of the subducting plate leading to the variety of plate interface geometries from West to East. A dramatic segmentation in North-South direction is visible on profile BGR06-317 (Fig. 11). The oceanic crust is segmented into 5-7 km wide blocks which show vertical displacements of about 1 km against each other. The blocks are rotated as they approach the main deformation front. Thick sediment wedges have been formed within the basement traps. We speculate that there is also a block rotation in E-W direction. These structures may be seen as initial piggyback imbricate thrust sheets, obviously driven by the enhanced compression between the oceanic plate and the thick upper plate, which is thickened here because of the collision of the continental Scott Plateau and Sumba Island little further east.

5.3 Lombok Forearc Basin

Recent deformation with prominent vertical components is not only confined to the outer arc high as demonstrated by out-of-sequence splay faults and tilted and disrupted piggy-back basins (Fig. 5) but also affect the formation of the Lombok forearc basin. A major unconformity (Fig. 12 top, horizon B) and a pronounced land- and seaward movement of the depocentre of sedimentation are expression of vertical deformation during basin development. This can be demonstrated by a simple restoration through flattening of selected horizons. As there are no severe time constraints, we adopted our time scaling to that of a seismic stratigraphy done by Van der Werff et al. (1994, and references therein) based on early single-channel and multi-channel reflection profiles obtained until end of the 80ties. At the beginning there is the situation of a passive margin until the Late Eocene with a continuously thickening sedimentary shelf basin (Fig. 12, A). The basement shows signs of a rifted continental margin by horst and graben structures. However, as discussed earlier, the basement could also consist of stacked ophiolitic nappes. The nature of the basement has long been in debate (e.g. Dickinson, 1995). We speculate, that the basement is gradually changing from continental character beneath Sumatra and Java (Sundaland) to intermediate or mixed character further east below the present island arc.

The insets in Fig. 12 show the development of the forearc basin as response of the initiation of subduction corresponding directly to the seismic stratigraphy. At about Late Oligocene the onset of oceanic subduction occurs pulling the southern part of the basin downward. The Early Oligocene horizon (Figs. 12, B) is observed as unconformity where sediment wedges onlap until Late Oligocene (Figs. 12, C) derived from a raising first accretionary wedge at the southern margin of the basin. While the accretionary wedge grows towards the ocean, rebound forces lift the southern part of the basin upward, now showing downlapping strata on the unconformity (Figs. 12, D). The depocentre of sedimentation moves to the centre of the basin which is fed by sediments from North and South. The outer arc high grows by stacking and the forearc basin continuously thickens while its depocentre moves slightly northward (Figs. 12, E). The individual strata show different wedge shapes, indicating that the depocentre moves back- and forward. Sedimentation until the Early Oligocene unconformity differs in reflection strength from the younger strata. This might be due to a change from terrestrial input to clay-rich marine input. Most of the characteristic features observed on profile BGR06-303 can be correlated along the E-W axis of the Lombok forearc basin. The ridge-like western termination of the basin (compare Fig. 4) is very likely due to the incorporation of seamounts of the Roo Rise into the forearc as argued by Kopp et

al. (2006). The eastern termination is characterized by elevated compressional structures in transition from subduction to collision tectonics (compare Fig. 15).

The basement of the Lombok forearc basin exhibits a rather irregular geometry, as mentioned earlier (Fig. 13). This is obvious particularly in E-W direction, but also in N-S direction, where a mid-basin ridge is seen on most of the N-S profiles (Fig. 2). The reason might be that it is formed by a stretched continental margin with horsts and grabens in the West and/or a melange or stack of ophiolitic nappes. Local magnetic anomalies of several hundred nT may be attributed to these structures. Sediment thickness varies strongly between 500 m and 4000 m in E-W direction along the axis of the basin (Fig. 13). Only smooth signs of deformation inside the sediments are visible, mostly attributable to differential compaction. A particular feature of interest is a relatively blank zone above the basement (Fig. 14). Such zones are typically interpreted as carbonate buildups, which have certain implications for hydrocarbon exploration because of their porosity. However, when searching for typical seismic signatures (Vail et al., 1977), no roof reflections nor velocity anomalies against adjoining layers could be found (Fig. 14). Instead, a pinnacle-like feature penetrates the seafloor, particularly seen in the echosounding profile (Fig. 14, top) and deforms the adjoining layers upward. This is clear evidence for diaprism of a mud volcano, driven by a density contrast of the blank zone (lower density) against the adjoining sediments. The density contrast is probably caused by an enhanced fluid content which also lowers the viscosity of the involved sedimentary layers, probably clay-rich, and mobilizes the stratified sediments driven by overpressure at depth. Their strata are still visible by weak reflections. These blank zones just above the basement are a widespread phenomenon. The involved fluids may originate from dewatering of subducted oceanic sediments pervading the basin basement.. In this case it seems to be a continuing process, instead of a cyclic one as observed frequently in the Barbados accretionary prism (Deville et al., 2006). An analogue case is known as the catastrophic East Java mud volcano (Davies et al., 2008). Since most of the oceanic sediments of the Argo Abyssal Plain is subducted (and partly recycled within the outer arc high), the amount of subducted seawater must be relatively high.

So far the basins between an outer arc high and the volcanic arc are seldom considered as an important petroleum province, despite of some industrial seismic surveying. The sediment thickness of the Lombok forearc basin is with about 3 s TWT much less than in other forearc basins further west. The Simulue basin with a sediment burial of 5 s TWT

offshore Sumatra has been shown by 3-D basin modelling to bear enough hydrocarbon potential in its depocentre, if the heatflow is high enough (Lutz et al., 2008). Heatflow values between 40 and 60 mW/m^2 have been deduced from the presence of BSRs (bottom simulating reflectors) which indicate the base of the gas hydrate stability zone. Gas hydrates require relatively low temperatures. BSRs are a widespread phenomenon in the western and central Sunda arc (Kopp, 2002; Lutz et al., 2008). However, in the present study area they are not observed. The reason might be that enough organic rich sediment input is missing or that the heatflow is considerably higher than in the western forearc basins. Further indication for higher temperatures is the observation of a submarine volcano offshore Bali at the western boundary of the Lombok basin, shown as a 500 m high cone-like edifice with a crater on top in bathymetry and by free-air gravity and magnetic anomalies. Echo-sounding signals reveal a very hard bottom in the western Lombok basin, probably caused by an ash layer. Therefore, inspite of relatively low sediment thickness, the hydrocarbon potential might be enhanced due to higher temperatures.

5.4 Transition From Subduction to Collision

The block rotation of oceanic crust (Fig. 11) is probably related to the transition between the subduction regime in the West to the collision regime in the East. We might expect related structures further north-northwest, located at the eastern boundary of the Lombok forearc basin. In the sections of BGR06-308 and BGR06-310 (Fig. 15) prominent basement highs of similar geometry can be correlated in north-northwestern direction showing signs of flower structures due to compression and uplift. We interpret these features as belonging to a broad complex system of right-lateral wrench faults which decouple the subduction regime in the West from the collision regime in the East. The long E-W profile BGR06-315, which is located on top of the outer arc high, is difficult to interpret in this respect, however it shows a very rough topography with horsts and sediment-filled grabens. We further speculate that the wrench fault system continues to the Southeast into the Scott Plateau. From 24-channel seismic measurements during the cruise VA-16 Hinz et al. (1978) suggested to interpret a NW trending fault system at the western margin of the Scott Plateau as a transform fault system and called it ‘Wilson Spur’. They also suggested that this system separates thrust-faulted continental crust to the East from oceanic crust to the West. In the section of BGR06-316 there is only sparse indication of this presumed fault zone within the oceanic crust (Fig. 15).

However, its strike direction is in continuation of the wrench fault system at the eastern end of the Lombok forearc basin. Therefore, a relationship cannot be excluded.

….

…..

6 Conclusions

Seismic images of unprecedented resolution and depth penetration have been collected during cruise SO190 in the eastern Sunda forearc at the transition from an oceanic-island arc subduction regime to a continental-island arc collision regime in the western Banda arc. Six long N-S traverses cover the entire subduction system, from the oceanic crust, accretionary wedges, outer arc high, forearc basin to the slope of the volcanic arc. The interface between the subducting oceanic plate and the forearc structures of the upper plate is imaged in great detail and variability in terms of dip, segmentation, subducted sediments, tectonic melange and duplex structures.

The following main conclusions can be drawn:

1) The oceanic crust is dissected by normal faulting into 5-10 km wide blocks within a 50-70 km wide belt seaward of the deep sea trench. These blocks determine geometry and evolution of duplexes at the base of the upper plate.
2) Duplexes of various modes and geometries are observed at the interface between upper and lower plate. These duplexes are combined with landward dipping splay faults which penetrate the entire outer arc high. Here, these thrust faults cause prominent breaks in seabottom morphology as well as rotation and vertical displacements of piggy-back basins.
3) Major volumes of oceanic sediments are subducted and incorporated into a thrust and erosion cycle in the outer arc high. The outer arc high is characterized by deep-reaching, recently active thrust faults and vertical displacements, which constitute a considerable tsunami hazard.
4) The 3.5-4 km sediment thickness of the Lombok forearc basin is less than in other forearc basis of the Sunda arc and contains therefore less hydrocarbon potential, depending on the thermal regime. Bottom simulating reflectors are not observed, in contrast to the Sunda arc further west.

5) The seismic stratigraphy of the Lombok basin shows vertical movements responding to the evolution of the forearc until recent times.
6) Mud diapirs of deep sediments mobilized by fluids are observed. Some of these relatively opaque sediment formations at the bottom of the forearc basins may be erroneously interpreted as carbonate build-ups.
7) The western termination of the Lombok forearc basin is determined by an inter-basin ridge which is caused by increased compression by the arrival of elevated features of the Roo Rise.
8) A wrench fault system at the eastern boundary of the Lombok forearc basin decouples the subduction regime of the Sunda arc in the West from the continent-island arc collision regime of the Banda arc in the East.

Acknowledgements

Cruise SO190 and project is funded by the Federal Ministry of Education and Research (BMBF) under grants 03G0190A and03G0190B. We thank Captain Oliver Meyer and his crew from RV SONNE for their professional assistance. Special thanks go the SINDBAD scientific crew members and working group. We thank E.R. Engdahl who provided us with new data of focal mechanisms. We are grateful to the Indonesian government for allowing us to work in its territorial seas.

References

BGR, 2006. Research Cruise SO190 Leg 1, SINDBAD. Cruise Report and Preliminary Results. Federal Institute For Geosciences And Natural Resources, Hannover, 2006.

Briggs, R.W., Sieh, K., Meltzner, A.J., Natawidjaja, D., Galetzka, J., Suwargadi, B., Hsu, Y., Simons, M., Hananto, N., Suprihanto, I., Prayudi, D., Avouac, J.-P., Prawirodirdjo, L., Bock, Y., 2006. Deformation and slip along the Sunda Megathrust in the great 2005 Nias-Simeulue earthquake. Science 311, doi: 10.1126/science.1122602.

Davies, R.J., Brumm, M., Manga, M., Rubiandini, R., Swarbrick, R., Tingay, M., 2008. The East Java mud vulcano (2006 to present): An earthquake or drilling trigger? Earth and Planetary Science Letters 272, 627-638.

Deville, E., Guerlais, S-H., Callec, Y., Griboulard, R., Huyghe, P., Lallemant, S., Mascle, A., Noble, M., Schmitz, J., the collaboration of the Caramba working group, 2006. Liquefied vs stratified sediment mobilization processes: Insight from the South of the Barbados accretionary prism. Tectonophysics 428, 33-47, doi: 10.1016/j.tecto.2006.08.011.

DeMets, C., Gordon, R.G., Argus, D.F., Stein, S., 1994. Effect of recent revisions to the geomagnetic reversal time scale on estimates of current plate motions. Geophys. Res. Lett. 21, 2191-2194.

Dickinson, W.R., 1977. Tectono-stratigraphic evolution of subduction-controlled sedimentary assemblages. In: Talwani, M. and Pitmann III, W.C. (Eds.), Island Arcs, Deep Sea Trenches and Back-Arc Basins. Maurice Ewing Series 1, pp.33-40, American Geophysical Union, Washington D.C.

Dickinson, W.R., Seely, D.R., 1979. Structure and stratigraphy of forearc regions. American Association of Petroleum Geologists Bulletin 63, 2-31.

Dickinson, W.R., 1995. Forearc basins, In: Busby, C.J. and Ingersoll, R.V. (Eds.), Tectonics of Sedimentary Basins. Blackwell Science, pp.221-261.

Franke, D., Schnabel, M., Ladage, S., Tappin, D.R., Neben, S., Djajadihardja, Y.S., Müller, C., Kopp, H., Gaedicke, C., 2008. The great Sumatra-Andaman earthquakes – Imaging the boundary between the ruptures of the great 2004 and 2005 earthquakes. Earth and Planetary Science Letters 269, 118-130.

Hall, R., 2002. Cenozoic geological and plate tectonic evolution of SE Asia and the SW Pacific: computer-based reconstructions, model and animations. Journal of Asian Earth Sciences 20, 353-431.

Hamilton, W., 1977. Subduction in the Indonesian region. In: Talwani, M. and Pitmann III, W.C. (Eds.), Island Arcs, Deep Sea Trenches and Back-Arc Basins. Maurice Ewing Series 1, pp.15-31, American Geophysical Union, Washington D.C.

Hamilton, W.B., 1988. Plate tectonics and island arcs. Geol. Soc. Am. Bull. 100, 1503-1527.

Hamzah, L., Puspito, N.T., Imamura, F., 2000. Tsunami Catalog and Zones in Indonesia. Journal of Natural Disaster Science 22, 1, 25-43.

Harris, R.A., 1991. Temporal distribution of strain in the active Banda orogen: a reconciliation of rival hypotheses. Journal of Southeast Asian Earth Sciences 6, 373-386.

Heine, C., Müller, R.D., Gaina, C., 2004. Reconstructing the lost Tethys Ocean basin: Convergence history of the SE Asian margin and marine gateways. In: Clift, P. et al. (Eds.), Continent-Ocean Interactions Within East Asian Marginal Seas. Geophys. Monogr. Ser., Vol. 149, pp. 37-54, American Geophysical Union, Washington D.C.

Heirtzler, J.R., Cameron, P., Cook, P.J., Powell, T., Roeser, H.A., Sukardi, S., Veevers, J.J., 1974. The Argo Abyssal Plain. Earth Plan. Sci. Lett. 41, 21-31.

Henstock, T.J., McNeill, L.C., Tappin, D.R., 2006. Seafloor morphology of the Sumatran subduction zone: Surface rupture during megathrust earthquakes? Geology 34, 485-488.

Hinschberger, F., Malod, J.-A., Réhault, J.-P., Villeneuve, M., Royer, J.-Y., Burhannuddin, S., 2005. Late Cenozoic geodynamic evolution of eastern Indonesia. Tectonophysics 404, 91-118.

Hinz, K., Beiersdorf, H., Exon, N.F., Roeser, A., Stagg, H.M.J., v. Stackelberg, U., 1978. Geoscientific investigations from the Scott Plateau off northwest Australia to the Java Trench. BMR Journal of Australian Geology & Geophysics 3, 319-340.

Karig,, D.E., Sharman, G.F., 1975. Subduction and accretion in trenches. Bull. Geol. Soc. Am. 86, 377-389.

Kopp, H., 2002. BSR occurrence along the Sunda margin: evidence from seismic data. Earth and Planetary Science Letters 197, 225-235.

Kopp, H., Kukowski, N., 2003. Backstop geometry and accretionary mechanics of the Sunda margin. Tectonics 22, doi: 10.1029/2002TC001420.

Kopp, H., Flueh, E.R., Klaeschen, D., Bialas, J., Reichert, C., 2001. Crustal structure of the central Sunda margin at the onset of oblique subduction. Geophys. J. Int. 147, 449-474.

Kopp, H., Flueh, E.R., Petersen, C.J., Weinrebe, W., Wittwer, A., Meramex Scientists, 2006. The Java margin revisited: Evidence for subduction erosion off Java. Earth and Planetary Science Letters 242, 130-142.

Korenaga, J., Holbrook, W.S., Kent, G.M., Kelemen, P.B., Detrick, R.S., Larsen, H.-C., Hopper, J.R., Dahl-Jensen, T., 2000. Crustal structure of the southeast Greenland margin from joint refraction and reflection seismic tomography. J. Geophys. Res. 105, 21591-21614.

Ladage, S., Gaedicke, C., Barckhausen, U., Heyde, I., Weinrebe, W., Flueh, E.R., Krabbenhoeft, A., Kopp, H., Fajar, S., Djajadihardja, Y., 2006. Bathymetric survey images structure off Sumatra. EOS Trans. AGU 87 (17), 165.

Lutz, R., Gaedicke, C., Berglar, K., Schlömer, S., Franke, D., Djajadihardja, Y.S., 2008. Petroleum systems of the Simeulue forearc basin off Sumatra, Indonesia. AAPG Bulletin, submitted.

Masson, D.G., Parson, L.M., Milsom, J., Nichols, G., Sikumbang, N., Dwiyanto, B., Kallagher, H., 1990. Subduction of seamounts at the Java Trench: a view with long-range sidescan sonar. Tectonophysics 185, 51-65.

Müller, C., Kopp, H., Djajadihardja, Y.S., Barckhausen, U., Ehrhardt, A., Engels, M., Flueh, E.R., Gaedicke, C., Keppler, H., Lutz, R., Lüschen, E., Neben, S., Seeber, L., Dzulkarnaen, D.P.S., 2008. From subduction to collision: The Sunda-Banda arc transition. EOS, Transactions, American Geophysical Union, 89, No.6, 49-60.

Nicolcas, A., 1989. Structures of Ophiolites and Dynamics of Oceanic Lithosphere. Kluwer Academic Publishers, Dordrecht, 367 pp.

Rutherford, E., Burke, K., Lytwyn, J., 2001. Tectonic history of Sumba Island, Indonesia, since the Late Cretaceous and its rapid escape into forearc in the Miocene. Journal of Asian Earch Sciences 19, 453-479.

Sandwell, D.T., Smith, W.H.F., 1997. Marine gravity data from GEOSAT and ERS-1 altimetry. J. Geophys. Res. 102, 10039-10054.

Spicák, A., Hanus, V., Vanek, J., 2007. Earthquake occurrence along the Java trench in front of the onset of the Wadati-Benioff zone: Beginning of a new subduction cycle? Tectonics 26, doi: 10.1029/2005TC001867.

Vail, P.R., Mitchum Jr., R.M., Todd, R.G., Widmier, J.M., Thompson III, S., Sangree, J.B., Bubb, J.N., Hatlelid, W.G., 1977. Seismic stratigraphy and global changes of sea level. In: Payton C. E. (Ed.), Seismic Stratigraphy – Application to Hydrocarbon Exploration, The American Association of Petroleum Geologists, Tulsa, p. 49-212.

Van der Werff, W., 1995. Structure and morphotectonics of the accretionary prism along the Eastern Sunda - Western Banda Arc. Journal of Southeast Asian Earth Sciences 11, 309-322.

Van der Werff, W., 1996. Variation in forearc basin development along the Sunda Arc, Indonesia. Journal of Southeast Asian Earth Sciences 14, 331-349.

Van der Werff, W., Prasetyo, H., Kusnida, D., van Weering, T.C.E., 1994. Seismic stratigraphy and Cenozoic evolution of the Lombok Forearc Basin, Eastern Sunda Arc. Marine Geology 117, 119-134.

Widiyantoro, S, v.d.Hilst, R., 1997. Mantle structure beneath Indonesia inferred from high-resolution tomographic imaging. Geophys. J. Int. 130, 167-182.

Figure Captions

Fig. 1: Location map and inset (upper right) of the SINDBAD survey SO190 with 4933 kilometers of multichannel reflection seismic (MCS) profiling (red lines) and 4 corridors of wide-angle/refraction seismic measurements with ocean bottom seismometers (OBS, red/white dotted lines). Yellow lines are magnetic lineations of reinterpreted anomalies based on studies of Heine et al. (2004) and SO190 measurements. Age of the oceanic plate ranges from early Cretaceous (M0) to late Jurassic (M25). Convergence rates (inset, upper right) of 76 mm/yr in the study area are according to the global velocity model NUVEL-1A (DeMets et al., 1994). Bathymetry from Sandwell and Smith (1997) is based mainly on satellite gravity data. Lines discussed in the text: North-South: 1 = BGR06-305, 2 =BGR06-303, 3 = BGR06-313, 4 = BGR06-311, 5 = BGR06-317, 6 = BGR06-319; East-West: 7 = BGR06-302, 8 = BGR06-307, 9 = BGR06-308, 10 = BGR06-310, 11 = BGR06-316.

Fig. 2: Compilation of six North-South running profiles from West (top) to East (bottom) traversing oceanic crust, deep sea trench, subduction system and forearc basin (see Fig. 1 for location) according to Kirchhoff prestack depth migration and frequency range 4-60 Hz. As a sample, for profile BGR06-313 a velocity-depth model is shown according to refraction/wide-angle seismic tomography on coincident profile P31. Triangles indicate positions of ocean-bottom seismographs.

Fig. 3: Details of profile BGR06-305. For location see inset. Note the prominent interface between lower (oceanic, Roo Rise) and upper plate, and thrust sheets and splay faults within the subduction complex.

Fig. 4: Details of profile BGR06-302. See inset for location. The sedimentary wedge above the red line has been tilted due to the relative uplift of the subduction complex (outer arc high) in the Southwest. The reason for this uplift may be the collision of the upper plate with the northern limit of the Roo Rise. Compare with Fig. 3. The transparent layer above a basement high in the center of the line may be interpreted as a carbonate platform.

Fig. 5: Details of profile BGR06-303. See inset for location. Arrows mark relative movements, normal faulting in the outer trench swell, thrust faulting within the subduction complex. Note that arrows for opposite relative movements are omitted for clarity. Frame (a) marks position of lower left section. Frame. Echosounder (b) detail marks slump activity from the inner trench slope. Frame (c) in the upper right corner points to Fig. 6.

Fig. 6: Pattern of three piggy-back basins on top of the outer arc high. Arrows indicate proposed thrust activity within the outer arc high basement, which is responsible for tilting the small basins. This post-stack time-migrated (4-120 Hz) section corresponds to frame (c) in Fig 5. The vertical displacement of 100 m in the centre of the section marks recent activity.

Fig. 7: Bathymetry showing the seafloor morphology in the area of the three profiles BGR06-303, -313 and -311 as view from West (top) and as map view (bottom). Note that pronounced breaks (dashed lines) in seafloor morphology of the outer arc high and related piggy-back basins correlate over more than 300 km in E-W direction.

Fig. 8: Details of profile BGR06-313 in the Argo Abyssal Plain area. See inset for location. Note the wave-form interface upper/lower plate. Uppermost morphologic breaks of the outer arc high with the piggy-back basin in between correlate with similar features of the profile further west.

Fig. 9: Details of profile BGR06-311 in the Argo Abyssal Plain area. Arrows mark relative movements with normal faulting in the outer trench swell. The upper/lower plate interface beneath the outer arc high is relatively smooth, in contrast to other profiles. However, beneath the toe of the accretionary wedge a prominent break is visible, which is mirrored also at the base of the oceanic crust. Large arrows indicate interpreted thrust movements affecting the whole oceanic crust. Note that the dashed line indicating the oceanic crust-mantle boundary has been shifted a little to greater depth in order to do not obscure the boundary. Bathymetry (upper left) shows rippled seafloor south of the trench, corresponding to the belt of normal faulting.

Fig. 10: Focal mechanism (Engdahl, pers. comm., 2008) of normal faulting type (upper left) and thrust type (upper right) in the study area. Normal faulting southward of the trench is characterized by an extensional regime (upper left). Compressional mechanismn (upper right)

may correspond to disrupting and duplex building of the subducted oceanic crust. Bathymetry with interpreted magnetic lineations is overlain (bottom). Black bar marks position of seismic section of Fig. 9. Plate convergence is in North-South direction. Age of subducting oceanic plate varies from Cretaceous (Roo Rise) to Jurassic (Argo Abyssal Plain) from West to East.

Fig. 11: Details of profile BGR06-317. See inset for location. Note the heavily broken oceanic crust while subducting beneath the upper plate.

Fig. 12: Simplified restoration of the Lombok forearc basin development on profile BGR06-303. Present situation is shown on top with marked horizons A, B, C, D and E. Note the unconformity of horizon C, onlapping on horizon B. Vertical restoration is done by flattening the marked horizons step by step. Situation E shows the present seafloor flattened. Time appointment from Eocene (A) to Early-Mid Miocene is adopted from Van der Werff et al. (1994). Insets show cartoons of the basin development according to seismic sections A to D. Initial stage (A) is that of a passive margin before subduction commenced, including a shelf basin with sediments derived from the continent (or a fossil island arc). Continued sediment loading depresses the shelf (B) until subduction creates first accretionary wedges and seaward moving of the depocentre of the basin (C). Further subduction leads to landward moving of the depocentre and, when the oceanic plate has reached a depth of the order of 100 km, to island arc magmatism (D). Horizontal bars denote the length of the seismic sections.

Fig. 13: Profile BGR06-307 at full length (top). Zoom (middle) corresponds to frame above. Same zoom without any vertical exaggeration at bottom. See inset for location. Note the irregular geometry of the top of basement of the Lombok forearc basin. Several 60^{o} dipping faults in the basin are probably caused by differential compaction.

Fig. 14: Detail of profile BGR06-307, eastern end, post-stack Kirchhoff time migration, 8-120 Hz (compare Fig. 13). Note the relatively transparent zone above the basement. High-resolution echosounder section is shown on top of the profile. Clear evidence for diapirism of a mud volcano is discernable as well as a small ramp at the bottom of the mud volcano. Velocity-depth section of part of the profile (bottom) indicates that there is no sharp velocity contrast between the transparent zone and the surrounding sediments.

Fig. 15: Details of profiles BGR06-310 (top), BGR06-308 (middle) and BGR06-316 (bottom) in the presumed transition zone between the subduction regime in the West and the collision regime in the East. Sections are presented in post-stack time-migrated version (4-120 Hz). See inset (lower right) for location. Arrows in the middle section mark an abrupt termination of the Lombok forearc basin, with relative uplift in the East and subsidence in the basin. Basement highs between the upper two sections correlate and may be interpreted as a wrench fault system (dashed line in location map). A continuation to the 'Wilson Spur' on the Scott Plateau may be suspected (see text). Focal mechanisms (Engdahl, pers. comm., 2008; lower left) show dominant right-lateral strike-slip movements in the transition area west of Sumba Island.

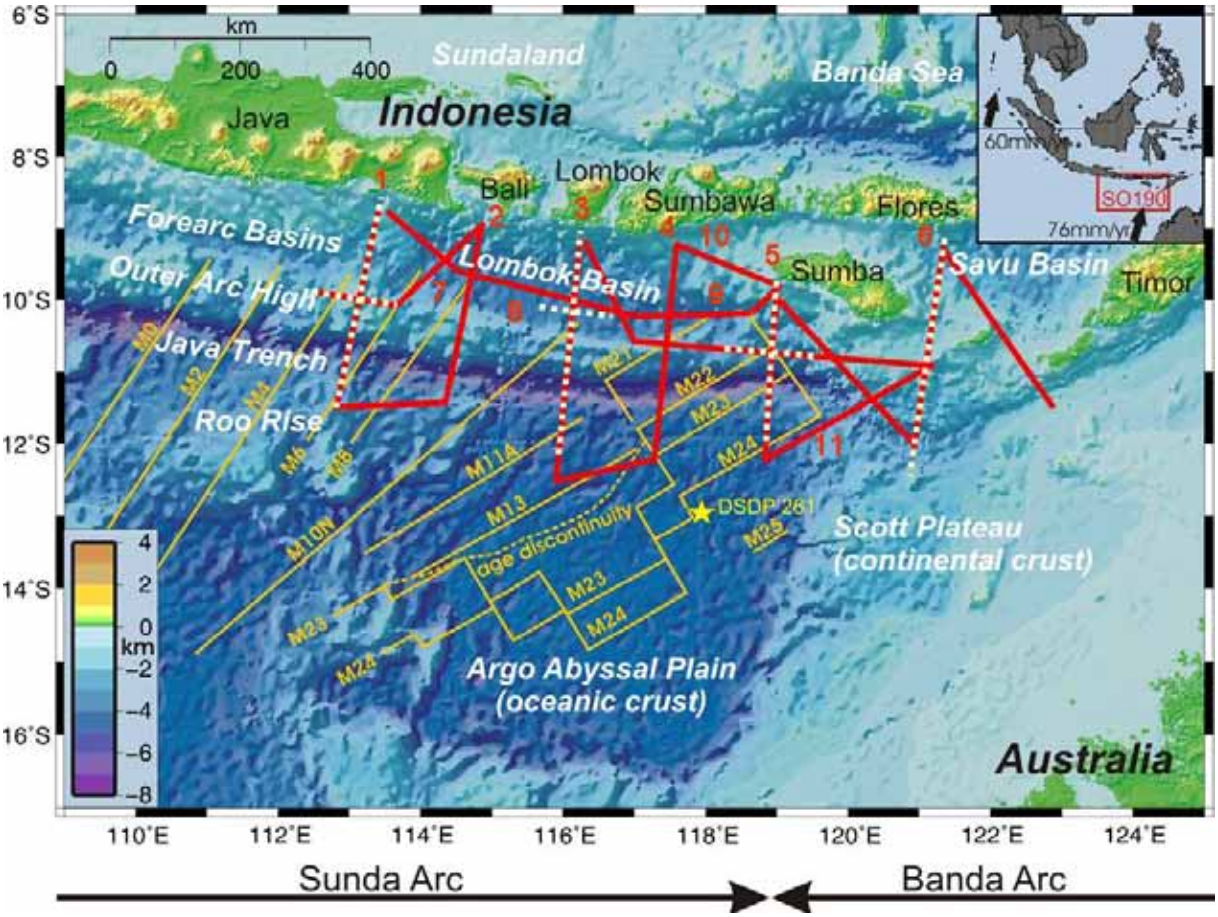

Fig. 1: Location map and inset (upper right) of the SINDBAD survey SO190 with 4933 kilometers of multichannel reflection seismic (MCS) profiling (red lines) and 4 corridors of wide-angle/refraction seismic measurements with ocean bottom seismometers (OBS, red/white dotted lines). Yellow lines are magnetic lineations of reinterpreted anomalies based on studies of Heine et al. (2004) and SO190 measurements. Age of the oceanic plate ranges from early Cretaceous (M0) to late Jurassic (M25). Convergence rates (inset, upper right) of 76 mm/yr in the study area are according to the global velocity model NUVEL-1A (DeMets et al., 1994). Bathymetry from Sandwell and Smith (1997) is based mainly on satellite gravity data. Lines discussed in the text: North-South: 1 = BGR06-305, 2 =BGR06-303, 3 = BGR06-313, 4 = BGR06-311, 5 = BGR06-317, 6 = BGR06-319; East-West: 7 = BGR06-302, 8 = BGR06-307, 9 = BGR06-308, 10 = BGR06-310, 11 = BGR06-316.

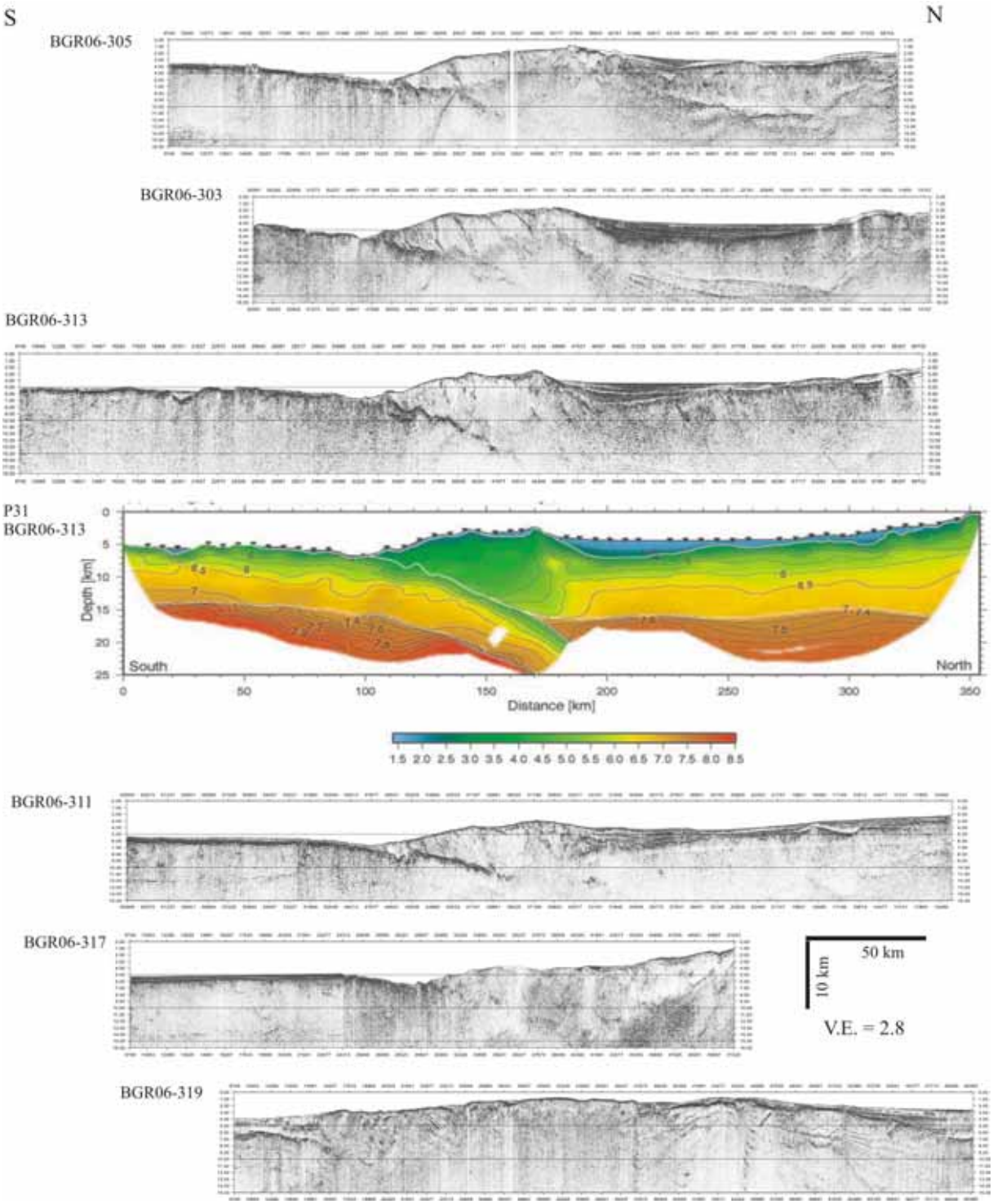

Fig. 2: Compilation of six North-South running profiles from West (top) to East (bottom) traversing oceanic crust, deep sea trench, subduction system and forearc basin (see Fig. 1 for location) according to Kirchhoff prestack depth migration and frequency range 4-60 Hz. As a sample, for profile BGR06-313 a velocity-depth model is shown according to refraction/wide-angle seismic tomography on coincident profile P31. Triangles indicate positions of ocean-bottom seismographs.

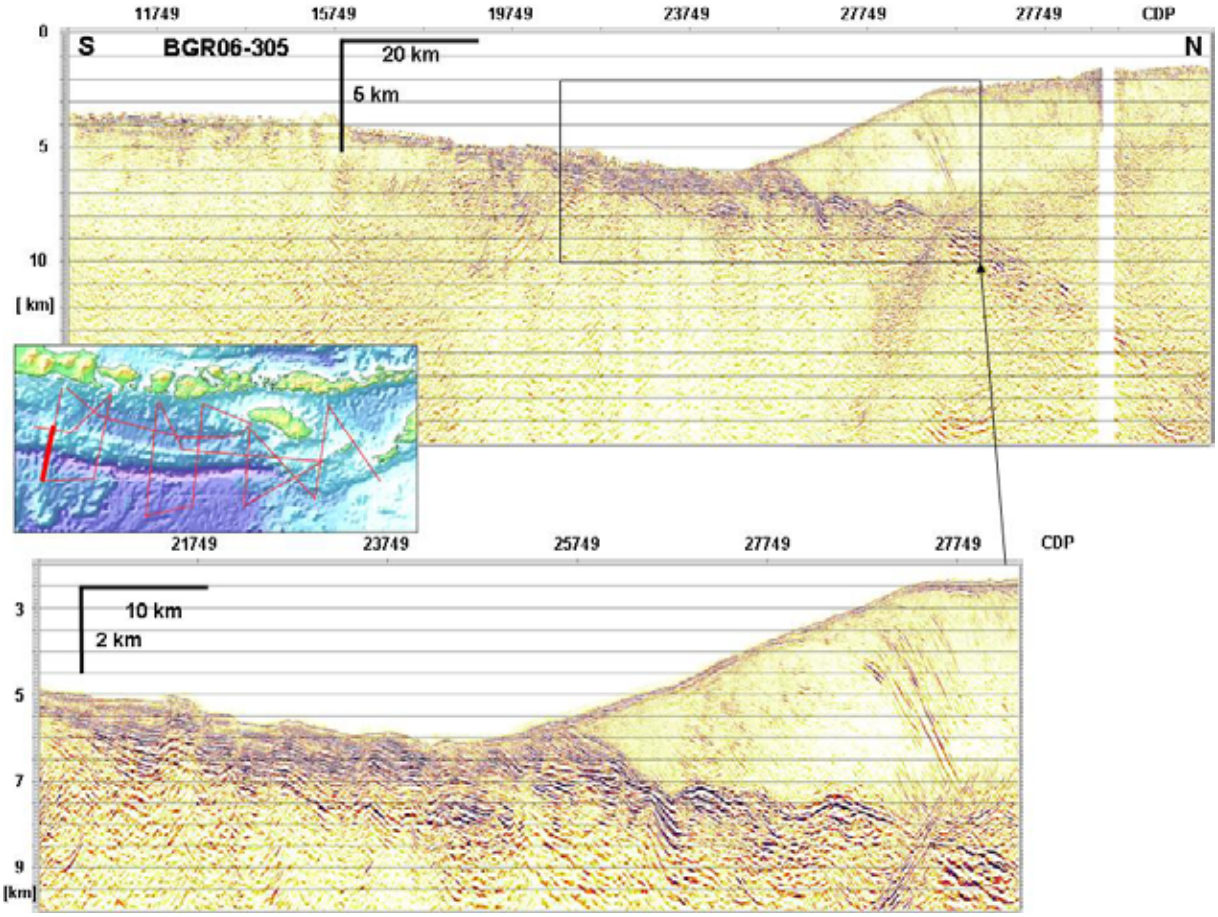

Fig. 3: Details of profile BGR06-305. For location see inset. Note the prominent interface between lower (oceanic, Roo Rise) and upper plate, and thrust sheets and splay faults within the subduction complex.

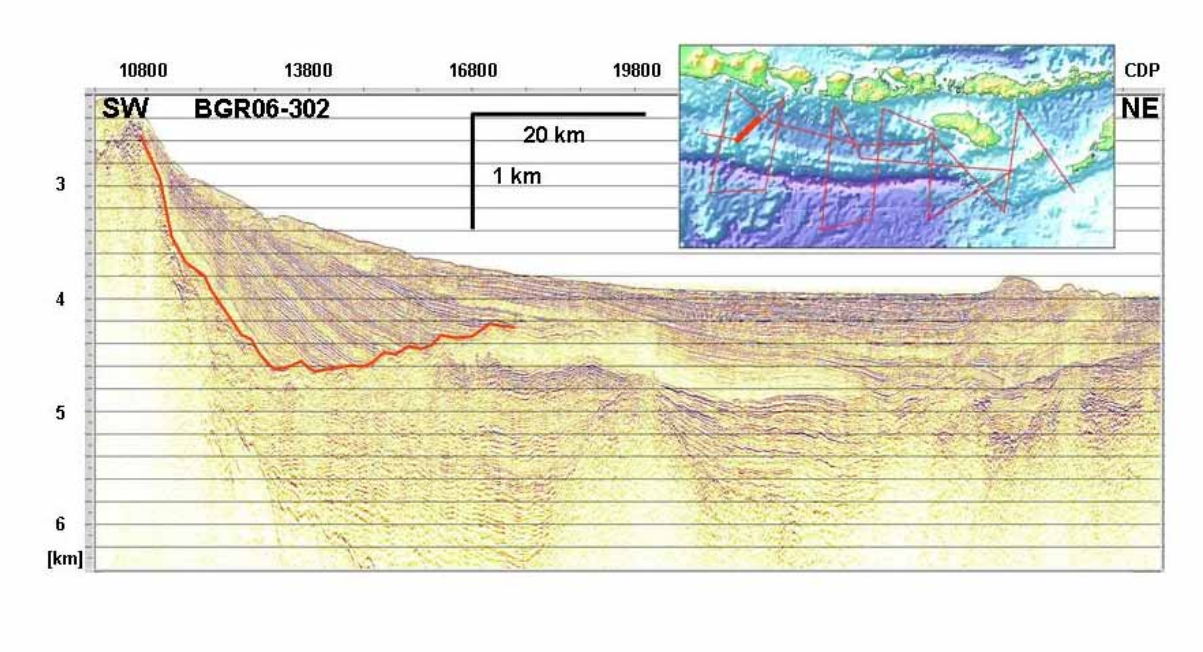

Fig. 4: Details of profile BGR06-302. See inset for location. The sedimentary wedge above the red line has been tilted due to the relative uplift of the subduction complex (outer arc high) in the Southwest. The reason for this uplift may be the collision of the upper plate with the northern limit of the Roo Rise. Compare with Fig. 3. The transparent layer above a basement high in the center of the line may be interpreted as a carbonate platform.

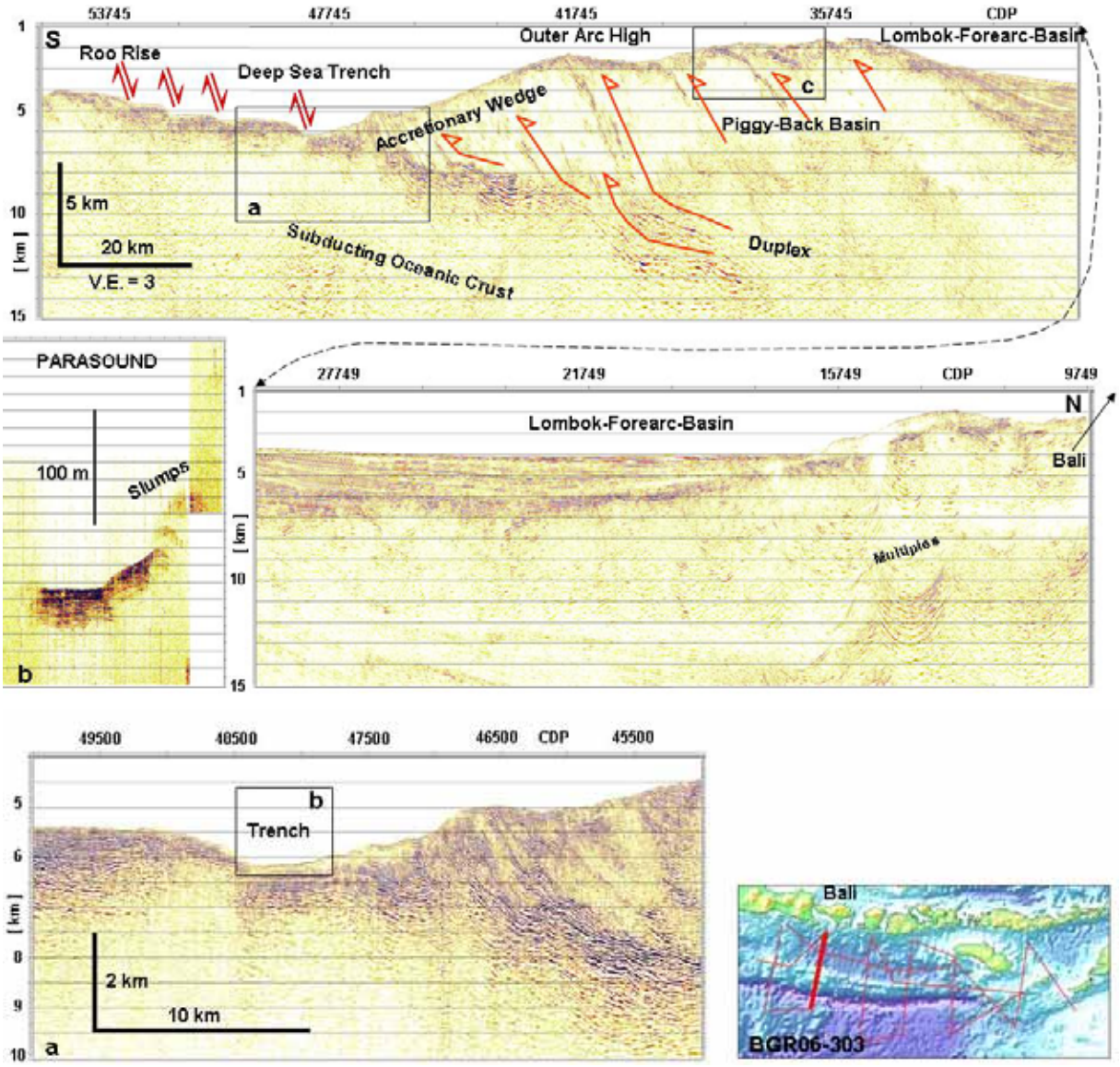

Fig. 5: Details of profile BGR06-303. See inset for location. Arrows mark relative movements, normal faulting in the outer trench swell, thrust faulting within the subduction complex. Note that arrows for opposite relative movements are omitted for clarity. Frame (a) marks position of lower left section. Frame. Echosounder (b) detail marks slump activity from the inner trench slope. Frame (c) in the upper right corner points to Fig. 6.

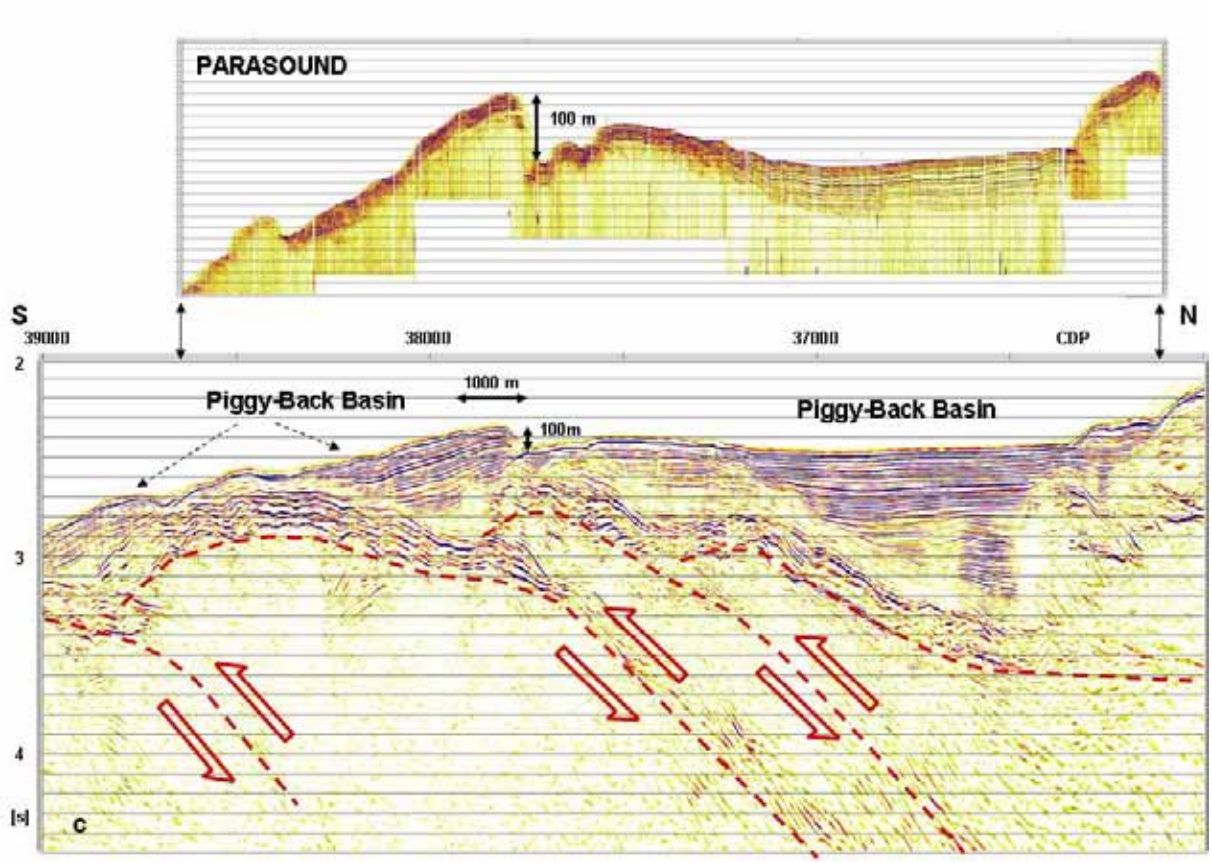

Fig. 6: Pattern of three piggy-back basins on top of the outer arc high. Arrows indicate proposed thrust activity within the outer arc high basement, which is responsible for tilting the small basins. This post-stack time-migrated (4-120 Hz) section corresponds to frame (c) in Fig 5. The vertical displacement of 100 m in the centre of the section marks recent activity.

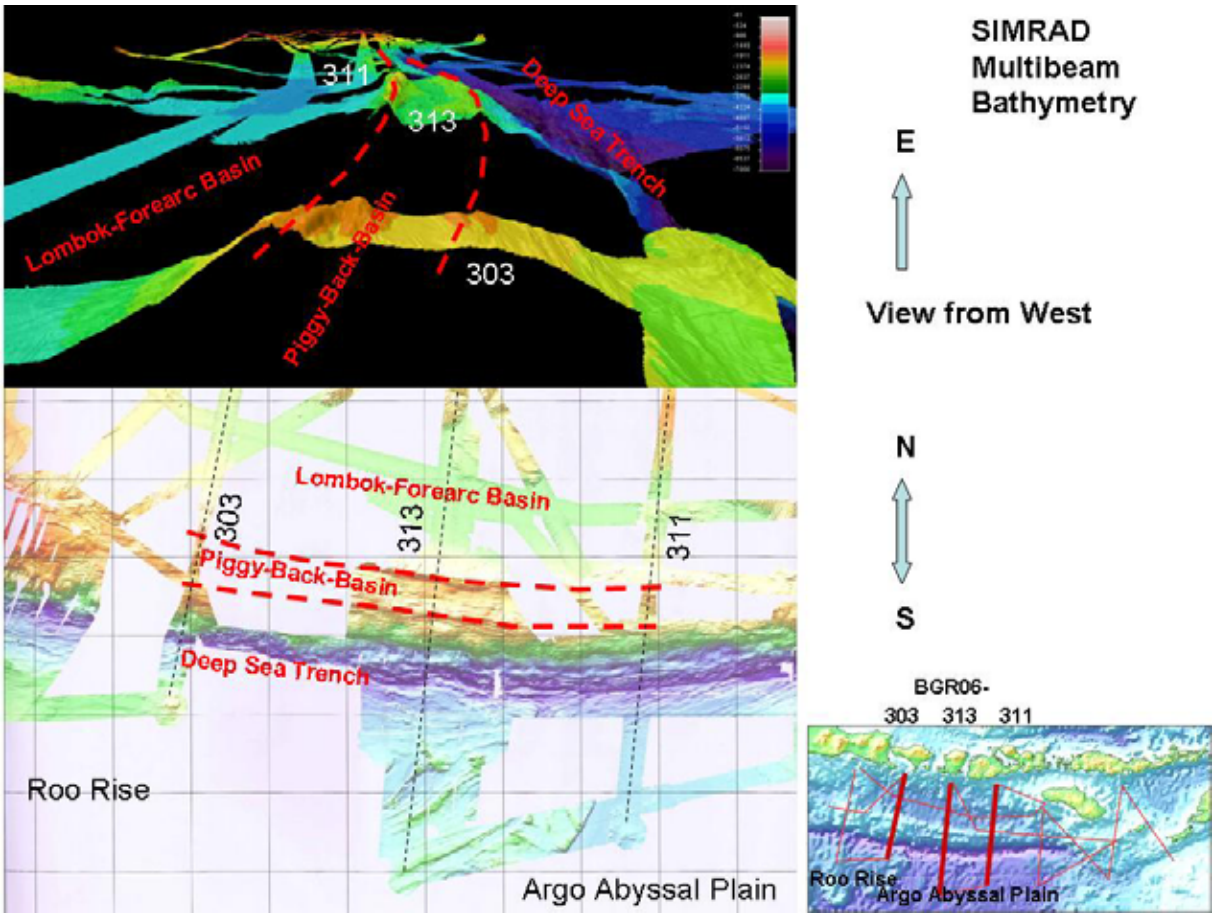

Fig. 7: Bathymetry showing the seafloor morphology in the area of the three profiles BGR06-303, -313 and -311 as view from West (top) and as map view (bottom). Note that pronounced breaks (dashed lines) in seafloor morphology of the outer arc high and related piggy-back basins correlate over more than 300 km in E-W direction.

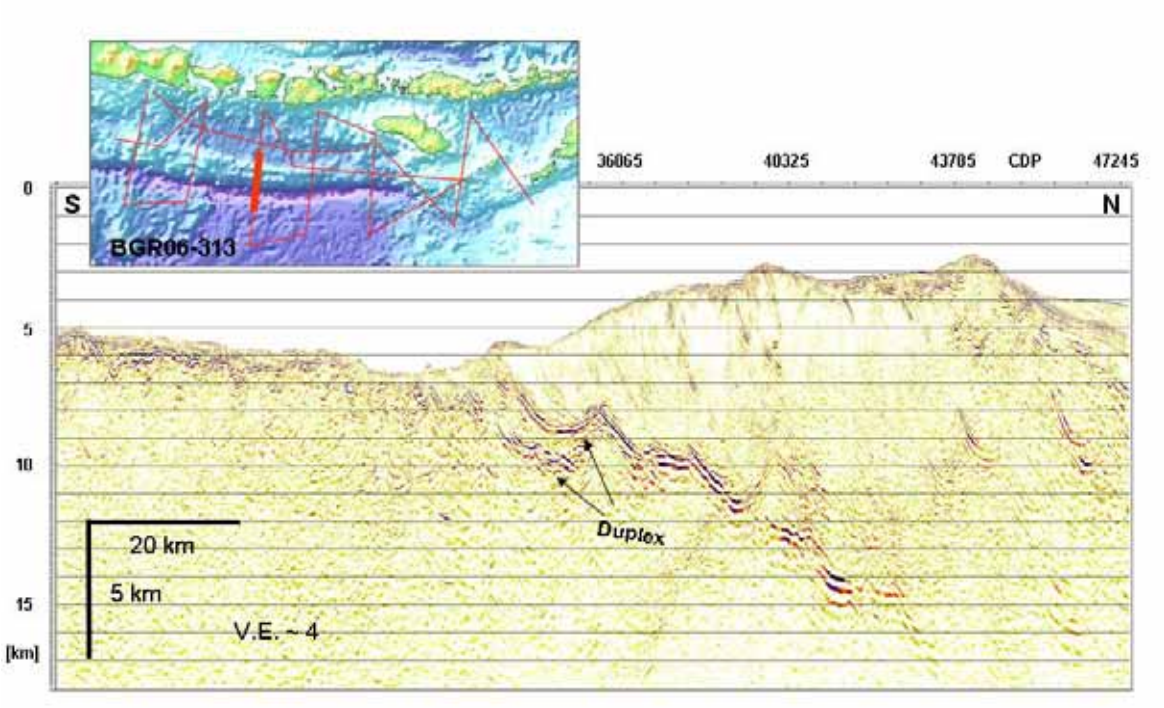

Fig. 8: Details of profile BGR06-313 in the Argo Abyssal Plain area. See inset for location. Note the wave-form interface upper/lower plate. Uppermost morphologic breaks of the outer arc high with the piggy-back basin in between correlate with similar features of the profile further west.

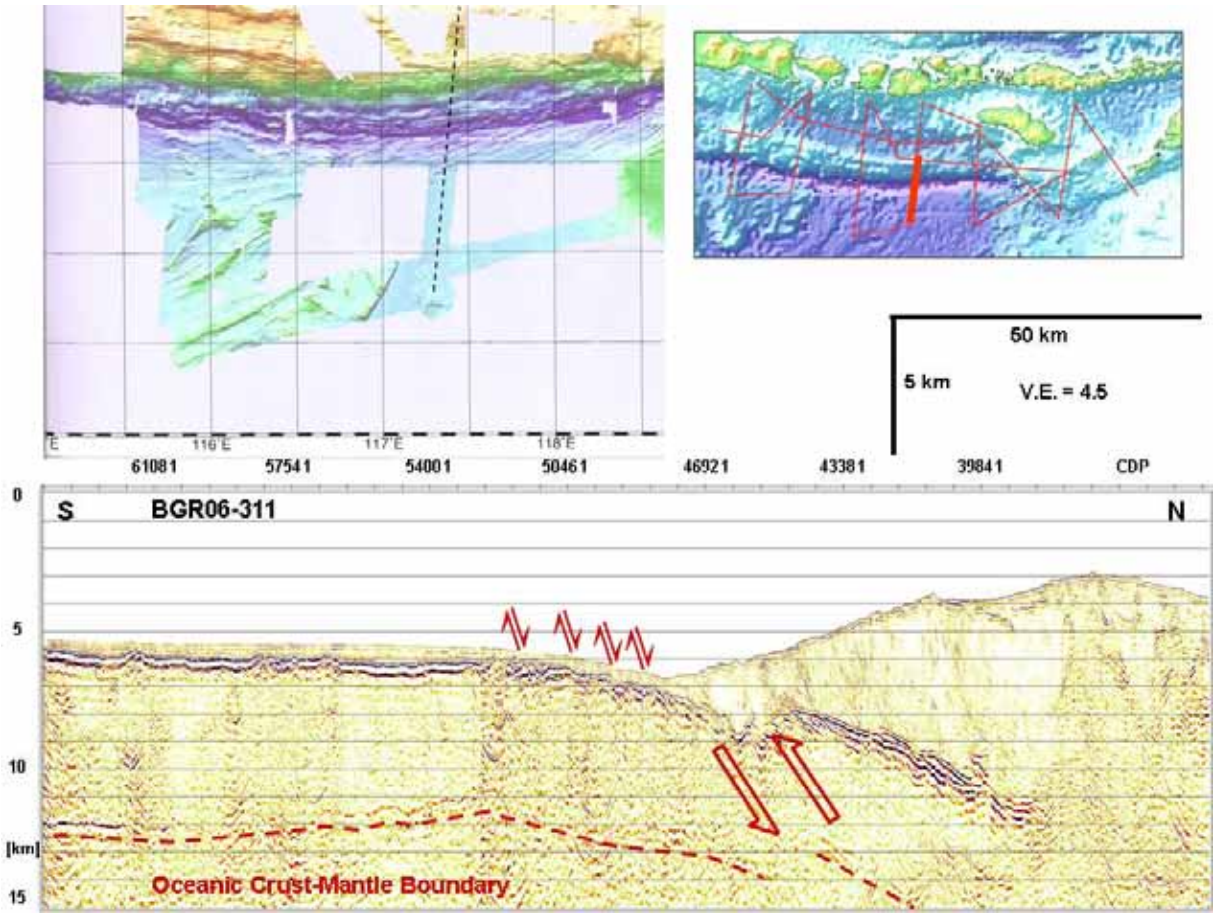

Fig. 9: Details of profile BGR06-311 in the Argo Abyssal Plain area. Arrows mark relative movements with normal faulting in the outer trench swell. The upper/lower plate interface beneath the outer arc high is relatively smooth, in contrast to other profiles. However, beneath the toe of the accretionary wedge a prominent break is visible, which is mirrored also at the base of the oceanic crust. Large arrows indicate interpreted thrust movements affecting the whole oceanic crust. Note that the dashed line indicating the oceanic crust-mantle boundary has been shifted a little to greater depth in order to do not obscure the boundary. Bathymetry (upper left) shows rippled seafloor south of the trench, corresponding to the belt of normal faulting.

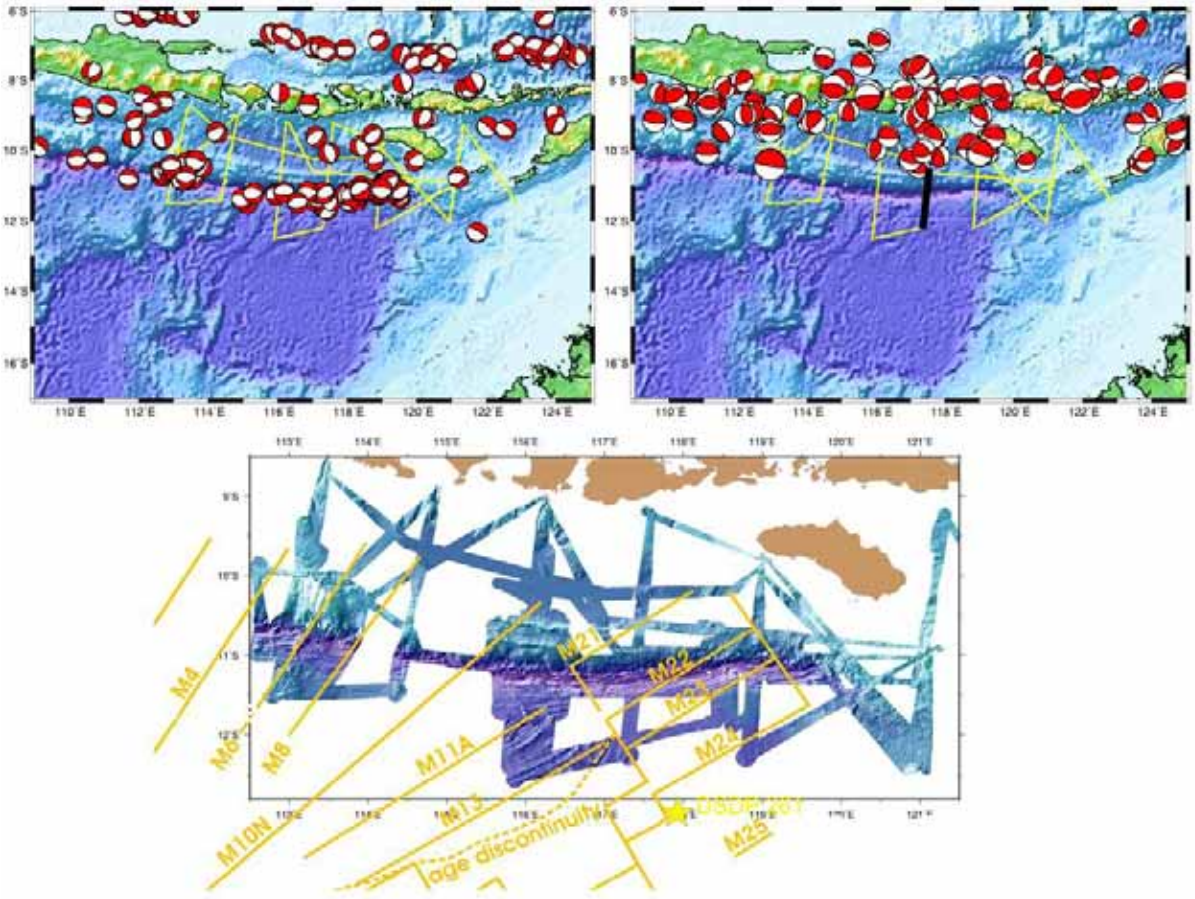

Fig. 10: Focal mechanism (Engdahl, pers. comm., 2008) of normal faulting type (upper left) and thrust type (upper right) in the study area. Bathymetry with interpreted magnetic lineations are overlain (bottom). Black bar marks position of seismic section of Fig. 9. Plate convergence is in North-South direction. Age of subducting oceanic plate varies from Cretaceous (Roo Rise) to Jurassic (Argo Abyssal Plain) from West to East.

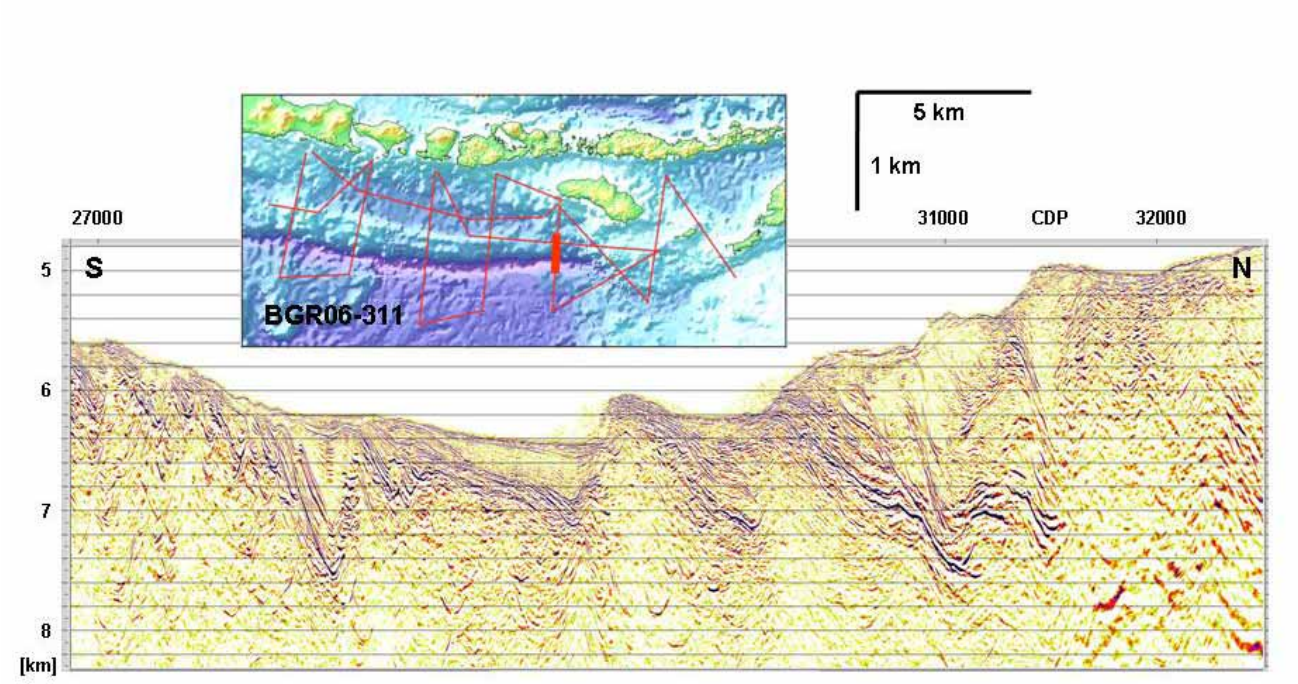

Fig. 11: Details of profile BGR06-317. See inset for location. Note the heavily broken oceanic crust while subducting beneath the upper plate.

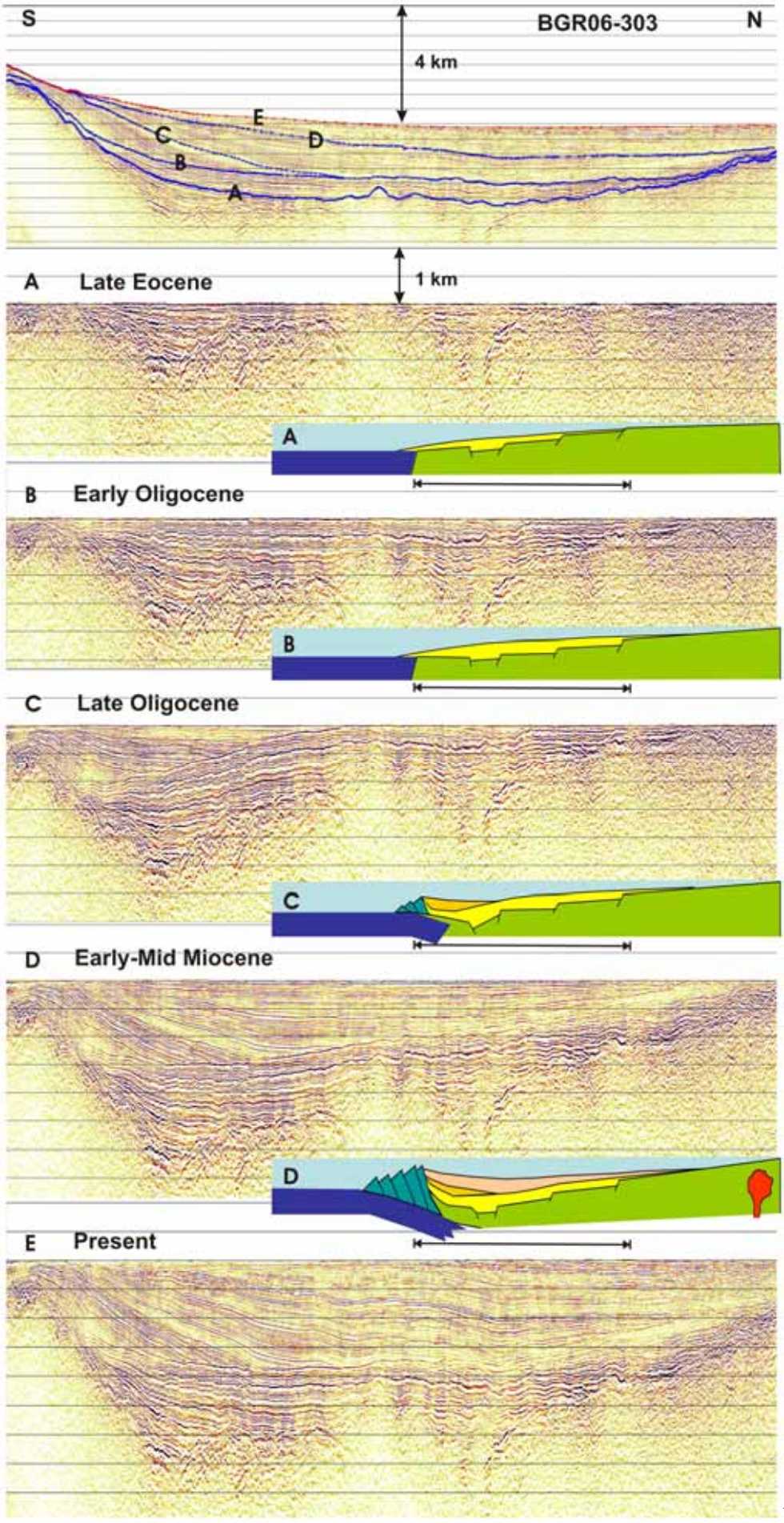
S
BGR06-303
N
4 km
E
C
D
B
A
1 km
A Late Eocene
A
B Early Oligocene
B
C Late Oligocene
C
D Early-Mid Miocene
D
E Present

Fig.12

Fig. 12: Simplified restoration of the Lombok forearc basin development on profile BGR06-303. Present situation is shown on top with marked horizons A, B, C, D and E. Note the unconformity of horizon C, onlapping on horizon B. Vertical restoration is done by flattening the marked horizons step by step. Situation E shows the present seafloor flattened. Time appointment from Eocene (A) to Early-Mid Miocene is adopted from Van der Werff et al. (1994). Insets show cartoons of the basin development according to seismic sections A to D. Initial stage (A) is that of a passive margin before subduction commenced, including a shelf basin with sediments derived from the continent (or a fossil island arc). Continued sediment loading depresses the shelf (B) until subduction creates first accretionary wedges and seaward moving of the depocentre of the basin (C). Further subduction leads to landward moving of the depocentre and, when the oceanic plate has reached a depth of the order of 100 km, to island arc magmatism (D). Horizontal bars denote the length of the seismic sections.

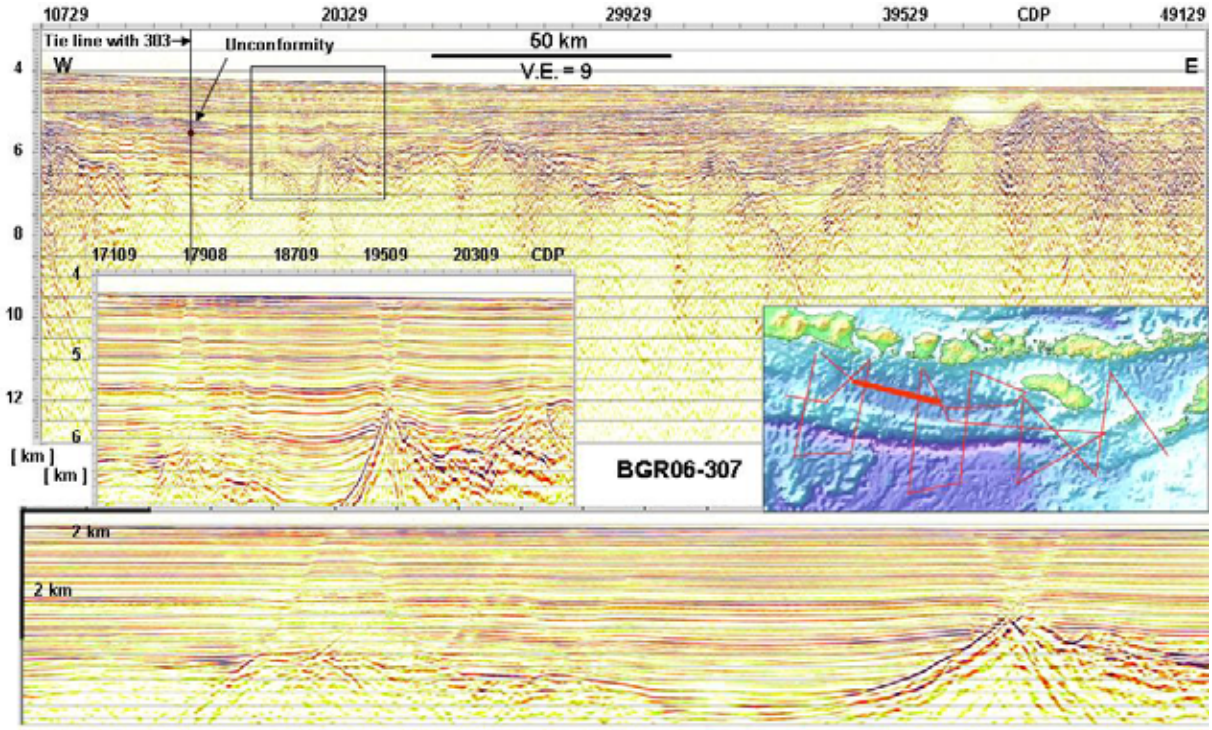

Fig. 13: Profile BGR06-307 at full length (top). Zoom (middle) corresponds to frame above. Same zoom without any vertical exaggeration at bottom. See inset for location. Note the irregular geometry of the top of basement of the Lombok forearc basin. Several 60^{o} dipping faults in the basin are probably caused by differential compaction.

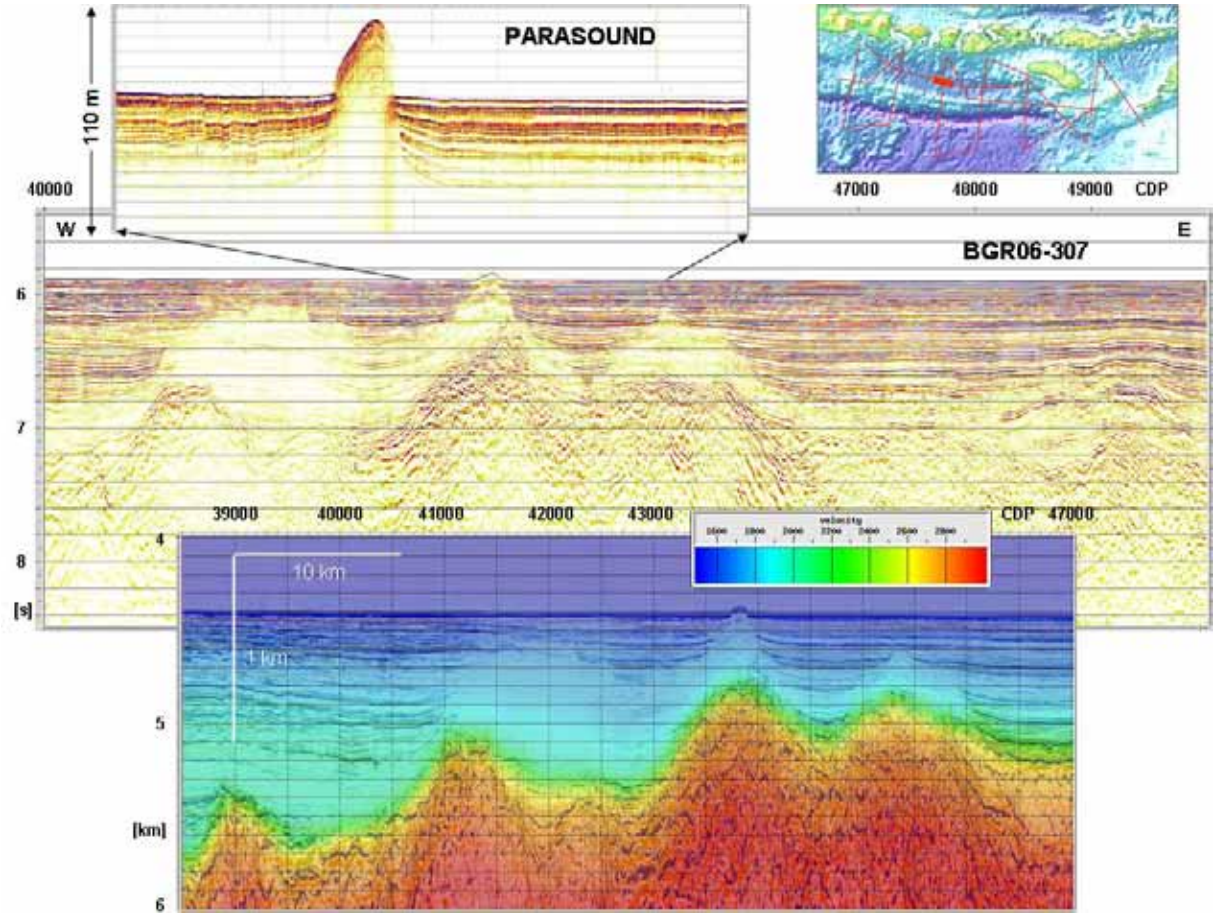

Fig. 14: Detail of profile BGR06-307, eastern end, post-stack Kirchhoff time migration, 8-120 Hz (compare Fig. 13). Note the relatively transparent zone above the basement. High-resolution echosounder section is shown on top of the profile. Clear evidence for diapirism of a mud volcano is discernable as well as a small ramp at the bottom of the mud volcano. Velocity-depth section of part of the profile (bottom) indicates that there is no sharp velocity contrast between the transparent zone and the surrounding sediments.

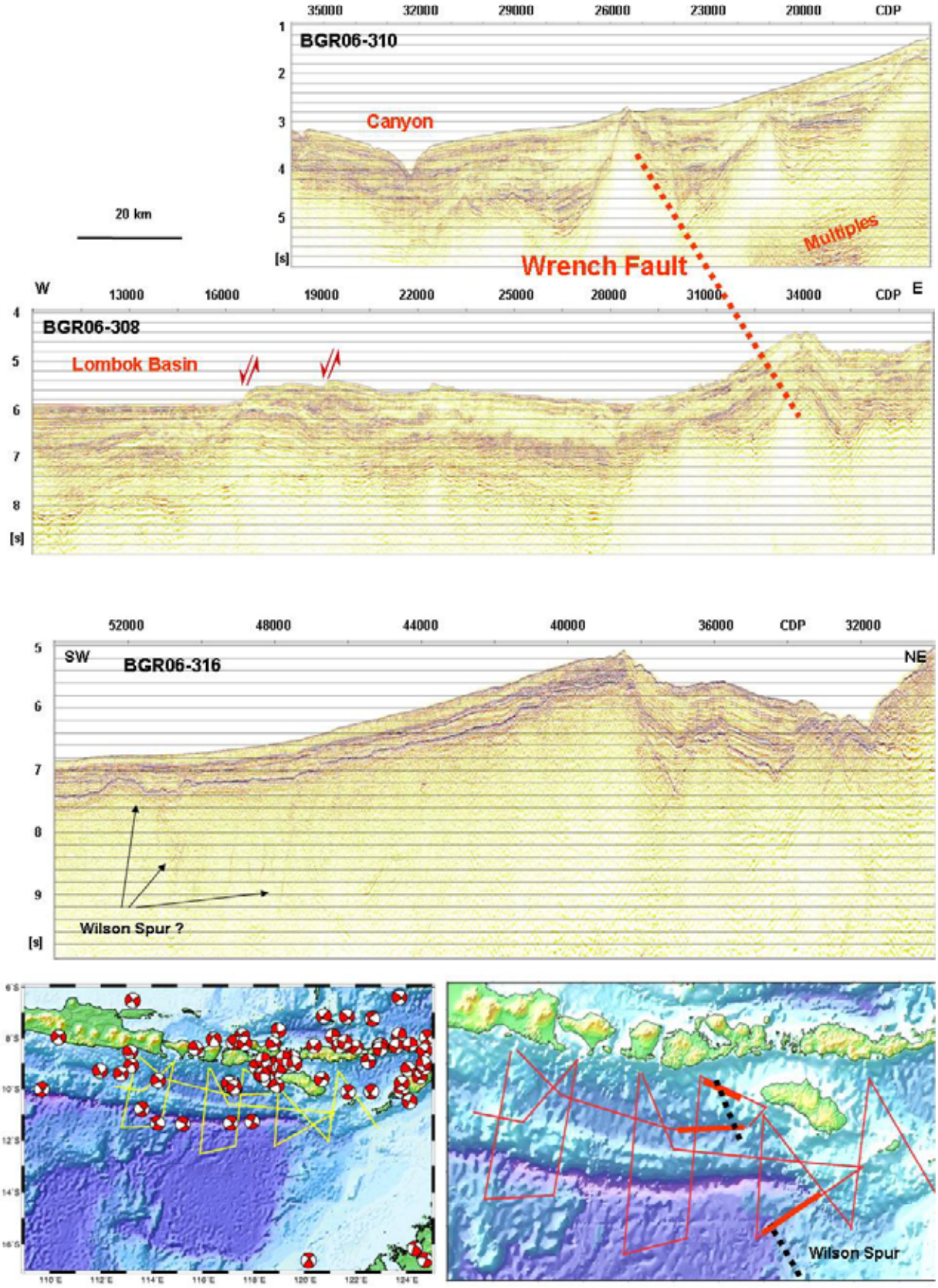

Fig. 15: Details of profiles BGR06-310 (top), BGR06-308 (middle) and BGR06-316 (bottom) in the presumed transition zone between the subduction regime in the West and the collision

regime in the East. Sections are presented in post-stack time-migrated version (4-120 Hz). See inset (lower right) for location. Arrows in the middle section mark an abrupt termination of the Lombok forearc basin, with relative uplift in the East and subsidence in the basin. Basement highs between the upper two sections correlate and may be interpreted as a wrench fault system (dashed line in location map). A continuation to the ‘Wilson Spur’ on the Scott Plateau may be suspected (see text). Focal mechanisms (Engdahl, pers. comm., 2008; lower left) show dominant right-lateral strike-slip movements in the transition area west of Sumba Island.

Crustal structure of the eastern Sunda margin, Indonesia, obtained from wide-angle seismic tomography and gravity modeling

L. Planert [1,*], H. Kopp [1], E. Lueschen [2], C. Mueller [2], E. R. Flueh [1], A. Shulgin [1], Y. Djajadihardja [3], and A. Krabbenhoeft [1]

[(1)] IFM-GEOMAR, Leibniz Institute of Marine Sciences at the University of Kiel, Wischhofstr. 1-3, D-24148 Kiel, Germany.

[(2)] BGR, Federal Institute for Geosciences and Natural Resources, Stilleweg 2, D-30655 Hannover, Germany.

[(3)] BPPT, Agency for the Assessment and Application of Technology, Jl. M.H. Thamrin No. 8, Jakarta 10340, Indonesia.

[(*)] corresponding author: Lars Planert, IFM-GEOMAR, Leibniz Institute of Marine Sciences at the University of Kiel, Wischhofstr. 1-3, D-24148, Germany, phone: +49-431-600-2337, fax: +49-431-600-2922, e-mail: lplanert@ifm-geomar.de

For submission to *Journal of Geophysical Research (JGR).*

Abstract

The Sunda-Banda arc transition at the eastern termination of the Sunda margin (Indonesia) represents a probably unique natural laboratory to study the effects of lower plate variability on related upper plate deformational segmentation. Neighbouring margin segments display a high degree of structural diversity on the incoming plate (transition from an oceanic to a continental lower plate, presence/absence of an oceanic plateau, variability of subducting seafloor morphology) as well as a wide range of corresponding forearc structures, including large sedimentary basins and an accretionary prism/outer arc high of variable size and shape. Here, we present results from a combined analysis of seismic wide-angle refraction, multichannel streamer and gravity data recorded along two trench normal corridors located offshore the islands of Lombok (116°E) and Sumba (119°E). The results reveal the seismic velocity and density structure of the incoming plate, starting 100 km seaward of the trench, and the adjoining forearc down to depths of 20-28 km, i.e. well into the upper mantle. We analyse mass transfer processes at the plate boundary to characterize the interaction between oceanic basement relief and related upper plate deformation and we resolve the differences in forearc structure offshore Lombok and offshore Sumba close to the transition to the collisional regime farther east. Our results allow a detailed view into the complex structure of both the deeper and shallower portions of the eastern Sunda margin

1. Introduction/Tectonic Setting

The Sunda-Banda arc transition comprises the portions of the Indonesian island arc where the tectonic regime changes from oceanic-island arc subduction along the eastern Sunda arc to continent-island arc collision along the Banda arc. Convergence between the Indo-Australian Plate in the south and the Eurasian Plate in the north is active since the late Oligocene [*Hamilton,* 1988; *Hall and Smyth,* 2008] and currently occurs at a rate of 7.6 cm/a almost perpendicular to the trench offshore Java [*DeMets et*

al., 1994]. The overriding plate is of continental nature off Sumatra [*Kopp et al.*, 2001] and changes to an island-arc type off Java/Lombok and farther east, although the internal structure of the islands and the adjacent forearc is still largely unknown due to the lack of deep seismic data.

The incoming oceanic seafloor can be subdivided into three different domains between 108°E and 125°E (Fig. 1): The Roo Rise (I), which is an oceanic plateau subducting off eastern Java, is characterized by rough seafloor up to 1500 m shallower compared to seafloor of the adjacent Argo Abyssal Plain (II), which is subducting off Lombok and Sumbawa. Farther east, the Scott Plateau (III) is marked by shallower seafloor depths and increased sedimentary coverage from the Australian continental shelf. Seafloor age of the oceanic crust increases towards the east from Early Cretaceous at 110°E to Late Jurassic close to 120°E where the transition to the continental seafloor of the Scott Plateau occurs [*Heine et al.*, 2004; *Mueller et al.*, 2008].

Forearc structures along this margin include a well-developed outer arc high (OAH) which is visible as a continuous bathymetric feature along the entire Indonesian forearc, starting with Simeulue island offshore northern Sumatra as its subaerial expression and continuing as a submarine bathymetric elevation from offshore western Java to offshore the island of Sumba, where the Java trench terminates (Fig. 1). The observed decrease in dimension and height of the OAH towards the east is obviously closely linked to the changes in trench sediment contribution and subducting seafloor morphology of the incoming Indo-Australian Plate. The related subduction processes at the plate boundary result in an accretionary regime offshore Sumatra and western Java [*Schlueter et al.*, 2002; *Kopp et al.*, 2003], whereas erosive processes dominate off central and eastern Java, where the subduction of the Roo Rise results in a northward retreat of the trench [*Kopp et al.*, 2006]. Farther east offshore Lombok and Sumbawa, however, the sediment input to the trench as well as the internal structure of the oceanic crust are largely unknown and as a consequence the processes governing the origin and evolution of the OAH are still unclear.

The Lombok Basin forms a major forearc basin and is located between the OAH and the volcanic arc in

the north (Fig. 1). Its termination in the west is controlled by the subduction of the Roo Rise and related uplift of the adjacent forearc [*Kopp et al.*, 2006] and in the east by the collision of the Australian continental shelf with the island of Sumba [*Shulgin et al.*, 2009a]. The origin of Sumba is still enigmatic; it is not part of the modern Banda volcanic arc but according to a number of investigators [e.g. *Rutherford et al.*, 2001; *Hall*, 2002] originated at a relict northern hemispheric arc system, situated south of West Sulawesi. The island migrated to its current position in the Middle to Late Miocene and now serves as an integral part of the forearc.

In this study we use deep penetrating seismic and shipboard gravity data to explore the internal structure of the incoming and the overriding plates in this poorly investigated part of the Indonesian margin. Seismic velocity models were obtained by a combined tomographic inversion of refracted and wide-angle reflected phases where we incorporated the well-resolved sedimentary portions from the analysis of the multichannel streamer data as a priori information. We analyse mass transfer processes at the plate boundary to characterize the interaction between oceanic basement relief and related upper plate deformation and we resolve the differences in forearc structure offshore Lombok and offshore Sumba close to the transition to the collisional regime farther east.

2. Data Acquisition

In 2006, R/V Sonne cruise SO190 explored the Sunda-Banda arc transition during two consecutive legs within the scope of the SINDBAD project (Seismic and Geoacoustic Investigations Along the Sunda-Banda Arc Transition). Almost 5000 km of multichannel streamer (MCS) seismic data and coincident gravity and magnetic data were acquired on leg 1 between 112°E and 122°E and are discussed in the work of *Lueschen et al.* [2009]. Leg 2 included the acquisition of more than 1700 km of wide-angle reflection and refraction seismic profiles in four different corridors of the margin (Fig. 1), at 113°E (offshore eastern Java), 116°E (offshore Lombok), 119°E (offshore Sumba) and 121°E (offshore Flores). Seafloor swath mapping on both legs resulted in an almost complete coverage of the trench and

the lower slope between 113°E and 121°E. The westernmost (113°E) as well as easternmost (121°E) corridors represent distinct tectonic regimes dominated by the subduction of thickened crust of the Roo Rise and Scott Plateau, respectively. These areas are discussed in the work of *Shulgin et al.* [2009a, 2009b]. In this study we present results for the corridors at 116°E and 119°E obtained from the tomographic inversion of the wide-angle reflection and refraction seismic data and from the forward modeling of coincident gravity data.

2.1 Seismic data

The seismic source used was a 64 l G-gun cluster fired at constant time intervals, resulting in a nominal shot spacing of 130 m. Data processing included the localisation of the ocean bottom instruments using the arrival time of the P-wave and the exact shot point geometry. In a second step, a time-gated deconvolution was applied to remove predictable bubble reverberations to produce a signal free of the disturbing interference of multiple and primary phases [*Wiener*, 1949]. Finally, a time and offset-variant Butterworth filter was applied in which the passband moves towards lower frequencies as record time and offset increases to consider frequency changes caused by signal attenuation.

2.2 Gravity data

Gravity data were acquired every second using the KSS31M sea gravimeter system built by Bodenseewerk Geosystem GmbH. Using the navigation information from the ship, the gravity data were corrected for the Eötvös effect and for the instrumental drift by tying it to calibrated land stations after completion of the cruise. The Free-Air Anomaly (FAA) was then obtained by substracting the WGS67 normal gravity from the corrected values.

2.3 Profile transects

Offshore Lombok at 116°E, profile 31/32 consists of two overlapping profiles and runs perpendicular

to the trench with a combined length of 354 km (Fig. 2). A total of 46 IFM-GEOMAR ocean bottom hydrophones/seismometers (OBH/S) [*Flueh et al.*, 2002] were deployed at ~6 km average instrument spacing. The line extends from 100 km seaward of the trench to close to the island of Lombok, crossing the Lombok Basin and profile 33 at ~222 km profile distance. Profile 33 runs in a trench-parallel direction and with a length of 113 km covers major portions of the Lombok Basin. On this line, 16 OBH/S were deployed at ~6 km instrument spacing. Seafloor depths in the Argo Abyssal Plain are in the range of 5.0-5.5 km and reach up to 6.8 km in the trench (Fig. 2). Seaward of the trench, some basement structures can be traced at the seafloor, aligned in a NE-SW direction and most likely related to original seafloor fabric. Landward of the trench, the OAH rises up to water depths of 2.4 km (slope angle ~5°) and is characterized by a trench-parallel tectonic fabric including two pronounced ridges spaced ~25 km apart (Fig. 2). North of the OAH, the Lombok Basin exhibits a very smooth and virtually flat seafloor with water depths of 4.4 km.

The adjacent corridor located at 119°E offshore Sumba island comprises two additional seismic profiles: the 250 km long trench-perpendicular profile 22 and the 145 km long crossing profile 21, covered with 27 and 18 OBH/S at ~6 km instrument spacing, respectively (Fig. 3). Line 21 runs parallel to the trench and covers the OAH at its highest elevation. Water depths for this corridor are slightly shallower for the oceanic plate and the trench (4.8-5.0 km and 6.5 km) and the corresponding seafloor is smoothed by a sediment blanket for distances >30 km from the trench. At the trench, however, oceanic seafloor fabric, aligned at low angles relative to the trench, crops out and subducts beneath the trench, which results in pronounced indentations of the deformation front and the adjacent slope (Fig. 3). Plate-bending likely enhances the subducting seafloor morphology. A slide with a lateral dimension of ~25 km is visible ~30 km east of where our profile crosses the trench and we speculate that this slide was caused by slope failure due to the subduction of equivalent seafloor fabric.

3. Data analysis

3.1 Tomographic Inversion of Seismic Data

We chose the tomographic method of *Korenaga et al.* (TOMO2D) [2000], which determines the 2-D velocity structure together with a floating reflector from the simultaneous inversion of refracted and reflected phases. The method employs a hybrid ray-tracing scheme combining the graph method with further refinements utilizing ray bending with the conjugate gradients method. Smoothing and damping constraints regularize the iterative inversion. An initial velocity model can be defined as an irregular grid hung below the seafloor. We employed a horizontal node spacing of 250 m and a vertical node spacing, which linearly increases from 100 m at the seafloor to 250 m at 30 km depth below seafloor. Model regularization is employed by the use of correlation lengths, which control the size of those model areas affected by a velocity update of a grid cell [*Korenaga et al.*, 2000]. We used a horizontal correlation length, which linearly increases from 1.5 km at the seafloor to 6 km at the model bottom, and a vertical correlation length with corresponding values of 0.2 km and 1.5 km, respectively. For reflector nodes, the appropriate regularization length scales are taken from the horizontal 2D velocity correlation lengths at the corresponding depths.

From the coincident MCS seismic profiles we incorporated the well resolved sedimentary portions as *a priori* structure into our starting models and fixed these areas during the iterations using spatially variable velocity damping. To make use of secondary arrivals and different reflections we employed a "layer stripping" approach and subsequently built the velocity model from top to bottom. This approach further involves the use of spatially variable velocity damping for the upper layers, e.g. when restricting the picks to the lower layers, and the incorporation of velocity jumps at prominent structural interfaces such as the plate boundary and the crust-mantle boundary (Moho). Obtained RMS travel time misfits for all velocity models shown in this study are in the order of 60 ms for a total of 9.000 (profile 21) to 26.000 (profile 31/32; cf. Fig. 4) arrivals, which were manually picked and assigned with individual pick uncertainties in the processed seismic sections (e.g. Fig. 5).

3.2 Resolution Tests

In order to demonstrate the resolving power of the data in different parts of the model, a set of synthetic tests was performed where a known model has to be resolved using the same profile geometry and data coverage as in the real experiment. A set of Gaussian velocity anomalies of ±3 % velocity perturbation and dimensions of 25 km x 5 km was imposed in a checkerboard pattern on the final velocity solution of profile 31/32 (Fig. 6). Synthetic traveltimes were computed through this model and Gaussian noise with a standard deviation equal to a quarter of the individual pick uncertainty was added to the synthetic traveltimes. The inversion was initialized using the underlying velocity model as a starting model. The ultimate aim of this approach is to test the algorithm's capability of resolving small perturbations within the original tomographic output and whether during this process structure gets mapped into different areas.

Lower and upper plates were investigated separately (Fig. 6), according to the tomographic approach chosen for these profiles. As displayed in the recovery panels of Figure 6, the incoming oceanic crust is well resolved, as is the oceanic uppermost mantle. Resolution of the upper plate diminishes at a depth of 18 km, thus the entire crust and upper mantle wedge are resolved.

3.3 Forward Modeling of Gravity Data

Forward modeling of the shipboard FAA gravity data was performed in order to verify the resolved structures obtained by our seismic tomography. We also used the TOMO2D code [*Korenaga et al.*, 2001], which adopts the method of *Parker* [1972] modified by topographic correction terms, to calculate the 2-D gravity response to a density model obtained by converting our seismically derived velocities using empirical velocity-density relations. We applied the relations of *Hamilton* [1978] for the sedimentary portions and *Carlson and Herrick* [1990] for the upper oceanic crust and – for

simplicity - we used constant densities for the lower oceanic crust and the entire mantle. Employing a constant density for the forearc crust offshore Lombok turned out to result in a satisfying fit whereas adopting a combination of linear relations including *Birch*'s formula [1961] for the lower crust proved to better fit the observed data offshore Sumba. These varying density functions are in accordance with the seismic results as described below.

4. Results

4.1 Profile 31/32

Seismic Tomography Results

The incoming oceanic crust is on average 8.6 km thick (Fig. 4) and largely devoid of sediments, except for an isolated sediment pond at ~20 km profile distance. This sediment accumulation occurs in a structural trap related to the original seafloor fabric imprinted during seafloor spreading (Fig. 2). About 50-70 km seaward of the trench velocities start to decrease in the crust and in the underlying mantle, resulting in anomalously low upper mantle velocities of 7.5 km/s (Fig. 4a). The area of reduced velocities coincides with the onset of normal faulting in the MCS seismic data (Fig. 4c).

The OAH reveals relatively low velocities of 2.5-5.5 km/s above the plate boundary, which is imaged down to 13 km depth (see Fig. 5 for data example). The downgoing slab subducts at angles of 5-8° and is traced over a distance of 70 km beneath the OAH. The plate interface is of irregular shape with several hundreds of meters vertical displacement obviously imprinted by the complex deformation of the oceanic basement (Fig. 4a, c).

Landward of the OAH, our model shows the geometry of the Lombok Basin with up to 2.8 km of sediment infill with velocities of 1.6-2.8 km/s. The underlying crust is 9-10 km thick and reveals a pronounced model portion with velocities of 6-7 km/s; the transition from the low velocity portions beneath the OAH to the oceanic-type velocity structure beneath the Lombok Basin occurs abrupt over a distance of 10-30 km around profile km 180 (Fig. 4). Velocities in the upper forearc mantle are in the

range of 7.4-7.8 km/s and thus, very similar to those observed at the incoming oceanic plate.

Gravity Modeling Results

The obtained velocity model was converted into a density model by using the velocity-to-density relation of *Hamilton* [1978] for sediments (velocity portions <4 km/s at the OAH and as inferred from MCS seismics elsewhere) and of *Carlson and Herrick* [1990] for the upper oceanic crust (crustal velocity portions <6 km/s) as well as constant densities for the major structural model units elsewhere (Fig. 7). The thickness and velocity structure of the subducting slab was held constant beyond the depth of seismic penetration and its geometry was inferred from the distribution of Wadati-Benioff hypocenters down to 100 km depth [*Engdahl and Villaseñor,* 2002]. The gravity response of the resulting density model reveals a RMS of 6.0 mGal (solid red line in Fig. 7; the black line shows the corresponding residual FAA).

In order to evaluate the method's sensitivity to small changes in density and model geometry we computed the FAA for a model comprising a 2 km deeper forearc Moho (dashed red line in Fig. 7) and in a second approach, for a model with a slightly denser forearc crust of 2.90 g/cm^3 (dotted red line in Fig. 7). Obtained results show that - compared to the initial model - none of these two models explains the observed FAA equally well; a combination of both models, however, would result again in a very close match to the observed FAA.

In summary, our seismically obtained results for profile 31/32 explain the observed FAA by adopting a combination of empirical velocity-to-density relations and constant densities for major structural model units elsewhere. Thus, the gravity modeling supports the corresponding seismic tomography results, in particular the shallow mantle wedge beneath the forearc.

4.2 Profile 33

On this line, the basement of the Lombok Basin can be traced in depths of 2.0 km to 3.7 km beneath the seafloor and resolved sediment velocities reach 2.8 km/s (Fig. 8). Since no MCS seismic data (and no gravity data) are available for profile 33 also the sedimentary portions were modeled using refracted

and wide-angle reflected seismic phases (Fig. 9). The underlying crust shows some thickness variations around average values of 10.0 km and it includes a ~6 km thick portion of velocities of 6-7 km/s and relatively low velocity gradients reminiscent of an oceanic seismic layer 3 (Fig. 8). The velocities in the uppermost mantle are in the order of 7.4 km/s, reaching 7.7 km/s in 21 km depth and thus are slightly lower compared to profile 31/32 at the line intersection.

4.3 Profile 22

Seismic Tomography Results

In the southernmost model portions the incoming oceanic plate is covered with up to 600 m of relatively undisturbed sediments; approaching the trench, however, the sedimentary cover seems to decrease to sometimes <250 m which is probably related to the reactivation of seafloor fabric and the onset of normal faulting ~30 km seaward of the trench (Fig. 3). Similar to the situation observed offshore Lombok, the onset of normal faulting coincides with a vigorous decrease of crustal and upper mantle velocities (Fig. 10a, c). The observed velocity decrease probably starts even further away from the trench at about 60 km distance where the continuous band of Moho reflections in the MCS seismic data terminates (Fig. 10c). Compared to those velocity portions located 60 km south of the trench, corresponding velocities at the trench are up to 1.2 km/s lower in the mid crust and 0.6 km/s in the lower crust directly above the Moho. The oceanic crustal thickness is 9.0 km on average and hence slightly thicker than offshore Lombok. The resolved upper mantle portions reveal velocities of 7.4-7.8 km/s (see Fig. 11 for data example), which is very close to corresponding values on profile 31/32.

The plate interface can be traced over a distance of ~100 km laterally beneath the forearc down to ~22 km depth (dipping 5-8°). The boundary is of irregular shape with pronounced indentations suggesting vertical displacements of sometimes >1 km.

On this line, the change in velocity structure associated with the transition from the OAH to the model areas further north is less pronounced: velocities beneath the OAH are <5.5 km/s down to ~11 km depth and thus, only slightly lower than corresponding velocity portions further north (Fig. 10a).

Different to the forearc setting observed offshore Lombok, there is only a thin sedimentary cover (no mature sedimentary basin) and crustal type velocities are observed down to ~25 km depth. Beneath the northern model edge, some steep seaward dipping reflections are observed in the wide-angle seismic data set (Fig. 10b). From the velocity information gained from the few rays penetrating those areas, however, it seems unlikely that this reflector is associated with a major velocity discontinuity such as the crust-mantle interface.

Gravity Modeling Results

We used the velocity-to-density relations of *Hamilton* [1978] for sediments (velocity portions <4.5 km/s at the OAH and as inferred from MCS seismics elsewhere) and *Carlson and Herrick* [1990] for the upper oceanic crust (crustal velocity portions <6 km/s). For the upper forearc crust we employed a linear velocity-to-density relation (see insect in Fig. 12) and for those model areas between the steep seaward dipping reflector and the subducting slab we used the relation of *Birch* [1961] which was originally established for the lower crust (diabase, gabbro, eclogite) at 10 kbar and room temperature. Using constant densities for the remaining structural units reveals an RMS misfit of 3.9 mGal for the residual FAA (Fig. 12). Hence, the gravity modeling confirms our obtained model geometry showing that in this sector of the margin, close to the transition to the collisional regime further east, there is a subducting oceanic plate of very similar thickness and velocity structure; but different to the situation offshore Lombok, the forearc lacks a major sedimentary unit and there is no evidence for a shallow mantle wedge.

4.4 Profile 21

Seismic Tomography Results

Compared to the previous lines data quality on profile 21 is only moderate, which is most likely related to the rather complex morphology and internal structure of the OAH close to the transition to the collisional regime. The obtained velocity model suggests significant structural changes between the western and the eastern model portions and a transition zone between ~60 km and ~100 km profile distance where the depth of the oceanic Moho increases from 19 km to 23 km (Fig. 13). In the western

model portions velocities reach 5.3 km/s above the plate boundary which can be traced as a continuous reflector in 11-12 km depth up to ~80 km profile distance (Fig. 13b). Along the entire profile, the oceanic slab is characterized by an intra-crustal reflector, which seems to be associated with the 5.5-6.0 km/s iso-velocity line. In the eastern model portions, there is evidence for two shallower reflectors, although their continuation is sometimes unclear due to the lack of reflection coverage. If the lower reflector represents the eastern continuation of the plate boundary, this would imply a ~13 km thick subducting oceanic slab in the eastern model portions versus a 8-9 km thick slab in the western model portions (Fig. 13). Resolved mantle velocities are in the range of 7.7-8.0 km/s and thus, ~0.3 km/s higher compared to corresponding velocities on profile 22 at the line intersection.

Gravity Modeling Results

The observed FAA decrease of ~70 mGal towards the east on profile 21 indicates significant trench-parallel changes within the OAH in this part of the margin (Fig. 14). Gravity modeling, using the same velocity-density relations as on the crossing line 22 and adopting the lower reflector (see above) as the eastward continuation of the plate boundary, reveals a RMS misfit of 4.0 mGal. Accordingly, we interpret the observed change towards greater thickness of the lower plate as the transition to the collisional setting comprising the promontory of the Australian continental shelf.

5 Discussion

5.1 Oceanic plate and trench

A thickened oceanic crust is observed on both trench-perpendicular profiles. In case of profile 31/32, obtained average values of 8.6 km are interpreted as the transition to the easternmost extensions of the Roo Rise and another bathymetric high near the trench close to 114.5°E (Fig. 1), which locally reveal crustal thicknesses >15 km [*Curray et al.*, 1977; *Shulgin et al.*, 2009b]. The refraction profile offshore Lombok Strait from *Curray et al.* [1977] runs ~50 km west of profile 31/32 and reveals velocities of 8.1 km/s at 23 km depth at the trench. Owing to the large shot spacing and related difficulties in

following secondary arrivals from one record to another, their evaluation of layer thickness is mainly based on the recordings of refracted arrivals, which makes their interpretation of Moho depths from these early shot records ambiguous. If there were a portion of upper mantle velocities comprising ~7.5 km/s at 17 km depth at the trench, as revealed by our data, and these layers were masked in their data, the obtained depth for the 8.1 km/s velocity layer in their model rather represents a minimum estimate. On profile 22 the obtained crustal thickness of 9.0 km is likely related to the transition to the Scott Plateau representing the promontory of the Australian continental shelf [*Shulgin et al.*, 2009a]. This is confirmed by the trench-parallel profile off Sumba which suggests structural changes of the subducting crust manifested in a thickness increase of ~5 km over a distance of 40 km to the east (Fig. 13). Most of the observed crustal thickening is related to the thickening of the upper crustal layer. The profile of *Shulgin et al.* [2009a] at 116°E (Fig.1) reveals a 15 km thick crust beneath the Scott Plateau which seems to thin out northwards when subducting beneath the Sumba Ridge. The crust shows a pronounced intra-crustal reflector at roughly mid-crustal depths and is interpreted to be of continental nature. Accordingly, we interpret the easternmost portions of profile 21 as the ocean-continent transition in the subducting plate (Fig. 13).

The oceanic crust is characterized by higher velocity gradients in the upper crust (3.5-6.0 km/s, layer2) and increasingly lower velocity gradients in the lower crust (6.0-7.2 km/s, layer3), and there is a reduction of upper mantle velocities at distances <30-50 km seaward of the trench. In order to assess the robustness of the obtained upper mantle velocities a set of resolution tests was performed where a synthetic anomaly of ±3% was confined to the oceanic mantle underneath the trench (Fig. 15). We took the same approach as described above in section 3.2. Obtained results demonstrate that the uppermost ~2 km of oceanic mantle beneath the trench are well resolved.

Additionally, we evaluated the impact of different mantle starting models upon the tomographic solution of profile 31/32 (Fig. 16). An individual mantle starting model was built by replacing the oceanic mantle portions in our final tomographic solution with a uniform mantle velocity gradient

344 constructed by a randomly generated 1-D velocity depth profile hung beneath the Moho. Using the
345 available crustal and mantle phases as well as reflections from the oceanic Moho and applying velocity
346 damping to the entire forearc, we computed the tomographic solutions for a total of 40 initial models,
347 with sub-Moho velocities ranging from 7.4 km/s to 8.1 km/s and underlying vertical velocity gradients
348 of 0.01-0.1 s^{-1}. The averaged model of all tomographic solutions and the corresponding standard
349 deviation model are shown in the upper and lower panels of Figure 16, respectively. The center panels
350 show velocity depth profiles through individual starting models (gray lines) and corresponding
351 tomographic solutions (red lines) for different parts of the oceanic plate. Obtained upper mantle
352 velocities converge to average values of about 7.9 km/s at 30 km profile distance, 7.5 km/s at 90 km
353 close to the trench and increase again to 7.7 km/s at 120 km beneath the lower slope (Fig. 16). This
354 clearly demonstrates that the reduction in upper mantle velocities at the trench is independent of the
355 employed mantle starting model and a robust feature of our tomographic solution.
356 The apparent coincidence of the observed velocity decrease with the onset of faulting in the MCS
357 seismic data, visible on both trench-perpendicular profiles, can be interpreted as the result of fracturing
358 and subsequent alteration of the oceanic crust and the underlying upper mantle. By this view, mantle
359 velocities of 7.9-7.4 km/s would imply a 0.6-2.4% increase in water content resulting in 5-19%
360 serpentinisation of mantle peridotite as a maximum estimate [*Carlson and Miller*, 2003]. On profile 22,
361 the amplitude and extent of the crustal low-velocity anomaly is stronger and occurs more tightly
362 confined to the trench, respectively. This is likely related to the stronger fragmentation of the crust as
363 indicated by the greater basement relief with vertical throws of sometimes >1 km [*Lueschen et al.*,
364 2009] and might be the result of enhanced compressional and rotational tectonic forces due to the close
365 proximity to the collisional regime farther east [*Wallace et al.*, 2009]. The strike of these features
366 oblique to the trench indicates that fracturing of the crust occurs predominantly at reactivated seafloor
367 fabric and faults; the strong Mw=8.3 earthquake seaward of the trench at 118.38°E/11.13°S on 19th of
368 August 1977 and related aftershock sequence (Centennial Earthquake Catalog:

http://earthquake.usgs.gov/research/data/centennial.php [Engdahl and Villaseñor, 2002]) may have been related to the rupture of the entire oceanic crust and thus to the opening of pathways for seawater into the mantle. Reduced upper mantle velocities within a similar range close to the trench and associated with the bending of the incoming plate prior to subduction are found e.g. at the Middle-American trench [*Grevemeyer et al.*, 2007; *Ivandic et al.*, 2008] and offshore Chile [*Ranero and Sallarès*, 2004; *Contreras-Reyes et al.*, 2007].

5.2 Outer arc high offshore Lombok

Models of arc evolution, which involve a progressive growth of the forearc by subduction accretion predict a seaward shift of the volcanic arc with age, provided that melting occurs at constant depths and the dip of the slab does not change [e.g. *Lallemand*, 1995]. In East Java the volcanic arc remained in the same position from the Eocene to the early Miocene [*Smyth et al.*, 2008]; activity then ceased, and a new arc formed ~10 Ma later, 50 km to the north, where it has remained since the late Miocene [*Hall and Smyth*, 2008]. Near the trench, our models do not show evidence for significant frontal accretion and thus do not support a progressive seaward growth of the margin. Offshore western Java, there is evidence for a young frontal accretionary wedge juxtaposed against a fossil accretionary backstop [*Kopp et al.*, 2003], whereas erosional processes accompany the subduction of the Roo Rise offshore eastern Java [*Kopp et al.*, 2006]. As a summary, these observations send a mixed message suggesting abrupt rather than progressive changes in arc-trench width and that for this margin neither subduction accretion nor subduction erosion has had a significant impact on arc history [*Hall and Smyth*, 2008]. The most striking feature of the OAH is the portion of low velocities (<5.5 km/s) above the plate interface, which intuitively points towards a sedimentary rock origin of this feature (Fig. 4). But this might actually be misleading since the incoming oceanic plate including the trench is largely devoid of sediments and a possible sediment supply from the forearc is blocked due to the higher elevation of the OAH representing an effective barrier from the depocenters of the Lombok Basin. Currently, only

394 minor sedimentary portions are involved in the formation of the OAH, comprising mainly the thin
395 (<600 m) predominantly pelagic sedimentary cover visible atop the oceanic plate and some turbiditic
396 slumps from the inner trench slope [*Lueschen et al.*, 2009]. Off eastern Java, the onset of subduction of
397 the Roo Rise resulted in an uplift of the trench and subsequent truncation of sediment supply from the
398 Bengal Fan, but the effect should be rather negligible given the relatively small amounts of sediments
399 which are now trapped west of this barrier (~1.5 km sediment thickness in the trench off western Java)
400 [*Kopp et al.*, 2002].
401 *Lueschen et al.* [2009] imaged duplexes of various modes and geometries at the interface between the
402 upper and lower plate in the MCS seismic data and concluded that significant volumes of oceanic
403 sediments and crustal material are basally accreted beneath the outer arc high and incorporated into a
404 thrust and erosion cycle (Fig. 17). Taking into account the ~25 Ma long period of subduction at the
405 eastern Sunda Arc [e.g. *Hall and Smyth*, 2008], continuous underplating of sediments could have
406 formed major portions of the OAH although involved sedimentary volumes at present might actually be
407 quite small [*Van der Werff*, 1995]. A similar mechanism of mass transfer is proposed for the formation
408 of the elevated forearc portions at the northern Hikurangi margin [*Scherwarth et al.*, 2009; *Sutherland*
409 *et al.*, 2009]. The low velocities and the lack of internal strata in the OAH bulk in our wide-angle
410 reflection and refraction data might indicate a strong alteration of this recycled melange facilitated by
411 the percolation of fluids released by dehydration processes in the subducting slab [*Bostock et al.*, 2002;
412 *Hyndman and Peacock*, 2003].
413 From the MCS seismic data, however, there is evidence for recent vertical displacements as manifested
414 in the uplift and tilting of small piggy-back basins between the two tectonic ridges atop of the OAH
415 [*Mueller et al.*, 2008; *Lueschen et al.*, 2009]. These features are associated with landward dipping splay
416 faults, which penetrate the entire OAH crust and connect to the plate interface (Fig. 17). The
417 importance of such faults for tsunami generation during great subduction zone earthquakes was
418 recently demonstrated for Sumatra [*Sibuet et al.*, 2007], North Ecuador [*Collot et al.*, 2008] and Nankai

[*Moore et al.*, 2007]. Given the continuity of these features in an along-margin dimension (Fig. 2), movement along these faults represents a tremendous tsunami potential for the entire eastern Sunda Arc [*Mueller et al.*, 2008, *Lueschen et al.*, 2009].

5.3 Forearc offshore Lombok

Profile 31/32 reveals a sharp increase of crustal velocities beneath the landward slope break of the OAH and suggests a distinct lithological change associated with the transition from the landward portions of the OAH to those forearc portions capped by the sedimentary strata comprising the Lombok Basin (Fig. 4, Fig. 17 bottom). In contrast to the low-velocity portions farther south, crustal velocities beneath the Lombok Basin rapidly increase to 5.5-6.0 km/s and then rise somewhat more gentle to ~7.0 km/s above the upper plate Moho. We favor an interpretation of this unit beneath the forearc basin as an oceanic type crust. The thickness of the crust ranges from 9 km beneath the portions of highest sedimentary infill to 11 km at ~250 km profile distance (Fig. 4). There is no distinct lateral change in crustal velocities visible in the northernmost model portions, which would be related to the forearc/volcanic arc transition, but crustal thickness likely increases to >14 km here.

Results obtained from the analysis of MCS data show an irregular topography of the Lombok forearc basement reminiscent of horst and graben structures at rifted continental margins or stacked ophiolite sheets and nappes, which could be formed by underthrusting of younger oceanic blocks and subsequent steepening due to continuous compression [*Lueschen et al.*, 2009]. From the distribution of zircon ages in sedimentary and igneous rocks from southeast Java, *Smyth et al.* [2007] inferred the presence of a Gondwana continental fragment from northwest Australia which was accreted offhore East Java in the Late Cretaceous; the eastern extend of this fragment is unknown but the oceanic type velocity structure beneath the Lombok Basin rather precludes a possible continuation into this area. As an alternative, the forearc crust in our models could be interpreted as an altered, heavily fractured piece of an older oceanic terrane, perhaps formed during the opening of the Indian Ocean during Cretaceous to middle

444 Eocene times, which was hindered from subduction due to its increased buoyancy; a similar scenario
445 was previously invoked to explain the origin of the forearc offshore Lombok Strait [*Curray et al.*,
446 1977] and western Java [*Kopp et al.*, 2002]. As mentioned above, the northern extent of this unit is not
447 resolved by our data, which would suggest a more gradual rather than a distinct change in lithological
448 composition towards the volcanic arc. The base of this unit marks the crust mantle boundary, as the
449 seismic and gravity data strongly support the existence of a shallow mantle material here.
450 The presence of a shallow mantle wedge off Java was already proposed by *Kopp et al.* [2002] based on
451 seismic wide-angle and refraction data, and a possible continuation farther east of this feature was
452 suggested by *Grevemeyer and Tiwari* [2006] on the basis of gravity modeling. The profile of *Curray et*
453 *al.* [1977] conducted ~50 km west of profile 31/32 shows a forearc Moho at ~18 km depth and upper
454 mantle velocities of 7.8-8.4 km/s in the forearc off the Lombok Strait. Hence, their obtained Moho
455 depths are ~2 km deeper and observed mantle velocities are 0.4-0.6 km/s higher than the results of this
456 study.
457 A serpentinized mantle wedge implies some important consequences for the seismic velocity structure
458 and the mechanical strength, which controls the ability to support seismogenic stick-slip behavior.
459 During subduction the downgoing oceanic plate experiences increased temperatures and pressures. As
460 a result, significant volumes of water trapped in the crust and in the mantle are gradually expelled by
461 dehydration and infiltrate the overlying forearc resulting in a change in forearc mantle composition
462 from dry minerals into a variety of hydrous minerals including serpentine [*Bostock et al.*, 2002;
463 *Hyndman and Peacock*, 2003]. Our study suggests a possible degree of 5-19% serpentinization,
464 according to *Carlson and Miller* [2003], within the resolved forearc mantle portions.
465 From the velocity model of profile 31/32 it seems that velocities in the subducting slab and in the
466 underlying oceanic mantle increase again beneath the OAH (Fig. 16). A similar conclusion could be
467 drawn from the relatively normal mantle velocities observed on profile 21 (Fig. 13). In summary, these
468 observations can be interpreted as the onset of dehydration and thus, indicate the possible source

469 regions of the fluid release.

470 *Grevemeyer and Tiwari* [2006] suggest that for the Sunda-Andaman margin the lower limit and
471 therefore the width of the seismogenic coupling zone, which controls the potential magnitude of large
472 megathrust earthquakes, may be governed by the depth of the intersection of the thrust with the forearc
473 mantle and the presence of weak hydrous minerals in the mantle wedge, which do not support
474 seismogenic stick-slip behavior: a shallow serpentinized mantle wedge underlying the forearc basin
475 would limit the width of the coupling zone to only 30-40 km offshore Java, compared to >120 km
476 offshore of Sumatra. Thermal modeling shows that the updip limit of the seismogenic zone (~100°C
477 isotherm [*Hyndman and Wang*, 1993]) offshore Java is located ~80 km from the trench [*Grevemeyer*
478 *and Tiwari*, 2006]. Offshore Lombok, the similar trench-normal convergence rate and dip [*Kopp et al.*,
479 2002] but the older age of the subducting plate [e.g. Mueller et al., 2008] suggest a thermally defined
480 coupling zone that reaches farther from the trench and thus the width of the seismogenic coupling zone
481 is likely to be even smaller here. The distribution of earthquake hypocenters off Lombok and Sumbawa
482 shows a band of extensional mechanisms closely confined to the trench and some events revealing
483 compressional mechanisms beneath the forearc basin and the volcanic arc [*Spicák et al.*, 2007]. The
484 OAH belongs to a >100 km wide zone in between characterized by virtually no teleseismically
485 recorded earthquakes related to the plate boundary (down to a regional threshold magnitude of ~5.5)
486 [e.g. *Engdahl and Villaseñor*, 2002]. These observations strongly contrast with the adjacent Sumatra-
487 Andaman margin where the recent and historic earthquake record suggests a much larger potential for
488 destructive subduction zone megathrust earthquakes than for Java and Lombok [*Lay et al.*, 2005;
489 *Newcomb and McCann*, 1987]. Thus, the shallow serpentinized mantle wedge, which is absent offshore
490 Sumatra [*Kieckhefer et al.*, 1980; *Kopp et al.*, 2002], might be the major factor limiting the magnitude
491 of rupture offshore Java and Lombok. The well-developed system of splay faults in the outer arc high,
492 however, demonstrates that potential movements can be transmitted to shallow seafloor portions and
493 thus this margin is nevertheless prone to a serious tsunami hazard [*Mueller et al.*, 2008, *Lueschen et al.*,

494 2009] (Fig. 17).

495

496 **5.4 Outer arc high and forearc offshore Sumba**

497 Offshore Sumba, the lateral and vertical dimensions of the outer arc high are smaller and the transition
498 in seafloor topography from the elevated portions towards the adjacent forearc is much more subdued
499 (Fig. 3). The strong relief of the plate boundary imaged in both the wide-angle and MCS seismic data
500 (Fig. 10) suggests significant vertical steps between dissected oceanic blocks, probably further
501 increased due to plate bending during subduction [*Lueschen et al.*, 2009]. Where these asperities
502 subduct beneath the trench they entrain lower slope material and cause slope failure in their wake (see
503 annotated slide in Fig. 3) and thus, may unbalance the mass budget of this margin towards local
504 erosion.
505 Compared to the geometry offshore Lombok, velocities in the upper crustal forearc portions suggest a
506 greater heterogeneity and related vertical velocity gradients are lower (velocities do not reach 6 km/s
507 within the uppermost 6-10 km beneath the basement, compared to ~5 km offshore Lombok) and thus,
508 the transition in velocity structure from the OAH towards the forearc is less pronounced (Fig. 10). In
509 the absence of drilling and more detailed geophysical sampling it is impossible to unequivocally define
510 the internal composition of the forearc, but from the similar velocity structure it seems that the
511 processes which form the OAH (and which are discussed in section 5.2) might also contribute to the
512 formation of adjacent forearc portions in this part of the margin.
513 The base of the forearc crust in our models is marked by the steep seaward dipping reflector identified
514 in the wide-angle seismic data set. The seismic refraction data, however, do not support the presence of
515 mantle velocities directly below this reflector and the gravity data reveals densities of ~3.0 g/cm^3
516 between the reflector and the plate interface and in depth of 15-29 km (Fig. 12). We interpret this unit
517 as the westward extension of the crystalline basement beneath the Sumba Ridge in the seismic profile
518 of *Shulgin et al.* [2009a] at 121°E and eventually as the onset of the *Sumba block* [e.g. *Rutherford et*

519 *al.*, 2001]. In the structural interpretation of *Shulgin et al.* [2009a], the seaward dipping interface
520 separates the Paleo Accretionary Prism from the Sumba Ridge crust, which extends down to the crust-
521 mantle boundary at 26-28 km depth. Hence, these models do not support the presence of a shallow
522 mantle wedge south and east of the island of Sumba.
523

524 ## 6 Conclusions

525 The tomographic analysis of wide-angle reflection and refraction data, supported by the modeling of
526 coincident shipboard gravity data, reveals the crustal and upper mantle velocity structure of the
527 incoming oceanic plate and the adjoining forearc offshore Lombok and offshore Sumba at the transition
528 from the oceanic to the collisional regime farther east.
529 **Offshore Lombok,** (1) the incoming oceanic crust is on average 8.6 km thick and largely devoid of
530 sediments. Seismic velocities in the crust and in the uppermost mantle are reduced within 50 km
531 seaward of the trench, which coincides with the onset of normal faulting in the MCS seismic data.
532 Assuming that these faults provide the pathways for seawater to percolate down into the upper mantle,
533 observed velocities of 7.4-7.9 km/s in the uppermost ~2 km beneath the Moho would imply 5-19%
534 serpentinisation of mantle peridotite as a maximum estimate.
535 (2) Velocities of the outer arc high do not exceed 5.5 km/s down to the top of the subducting slab,
536 which is traced over minimum 70 km length beneath the forearc down to ~13 km depth. If the present
537 growth of the outer arc high is due to duplex formation and underplating of oceanic sediments and
538 crustal material at the plate boundary, as previously suggested from the analysis of MCS seismic data
539 and supported by the complex shape of the plate boundary in our models, the relatively low bulk
540 velocities would indicate a strong alteration, likely facilitated by the percolation of fluids released from
541 the subducting slab by dehydration processes.
542 (3) In the Lombok Basin up to 3.7 km of sedimentary strata overlies a 9-11 km thick crust, which
543 reveals an oceanic type velocity structure. Velocities of 7.4-7.8 km/s suggest a hydrated mantle wedge

beneath the Moho at ~16 km depth, which is also supported by the gravity modeling for this corridor. Because serpentinites are expected at shallow depths in the mantle wedge, they may control, at least partially, the seismological stick-slip behavior of the megathrust; in particular, they may reduce the width of the seismic coupling zone and thus limit the potential magnitude of large subduction megathrust earthquakes offshore Lombok. The system of splay faults in the outer arc high, however, demonstrates that potential movements can be transmitted to shallow seafloor portions and thus poses a serious tsunami threat for this margin.

Offshore Sumba, (4) the oceanic crust is on average 9.0 km thick and at greater distance from the trench comprises a thin (<600 m) largely undisturbed sedimentary cover. Within 30 km seawards of the trench, intense fracturing of the crust coincides with a vigorous decrease of crustal velocities. Here, upper mantle velocities reach 7.4-8.0 km/s.

(5) Slope indentations and the presence of a slide in the trench suggest that subduction of pronounced seafloor asperities such as on profile 22 locally contribute to the frontal erosion of the lower slope, although the net mass budget may be close to zero over greater periods.

(6) From West to East the subducting slab thickens from ~9 km to ~13 km beneath the outer arc high, which we interpret as the transition from the oceanic crust of the Argo Abyssal Plain to the promontory of the Australian continental shelf of the Scott Plateau.

(7) Our seismic and gravity models do not support the presence of a shallow mantle wedge beneath the forearc. A steep seaward dipping reflector in the northernmost model portions of profile 22 may be related to the transition to the Sumba block farther north.

Acknowledgments: The SINDBAD project was funded by the German Federal Ministry of Education and Research (BMBF) under grants 03G0190A and 03G0190B. We would like to thank the master and crew of R/V Sonne for their professional assistance during cruise SO190 and the SINDBAD scientific party for their enormous help in collecting of the data.

References:

Birch, F. (1961), The velocity of compressional waves in rocks to 10 kilobars, *J. Geophys. Res., 66,* 2199-2224.

Bostock, M. G., R.D. Hyndman, S. Rondenay and S.M. Peacock (2002), An inverted continental Moho and the serpentinization of the forearc mantle, *Nature, 417*, pp. 536–538.

Carlson, R. L., and C. N. Herrick (1990), Densities and porosities in the oceanic crust and their variations with depth and age, *J. Geophys. Res., 95(B6),* 9153–9170.

Carlson, R. L., and D. J. Miller (2003), Mantle wedge water contents estimated from seismic velocities in partially serpentinized peridotites, *Geophys. Res. Lett., 30(5),* 1250, doi:10.1029/2002GL016600.

Curray, J. R., G. S. Shor, R. W. Raitt, and M. Henry (1977), Seismic Refraction and Reflection Studies of Crustal Structure of the Eastern Sunda and Western Banda Arcs, J. Geophys. Res., 82, 2479-2489.

Collot, J.-Y., W. Agudelo, A. Ribodetti, and B. Marcaillou (2008), Origin of a crustal splay fault and its relation to the seismogenic zone and underplating at the erosional north Ecuador-south Colombia oceanic margin, *J. Geophys. Res., 113,* B12102, doi:10.1029/2008JB005691.

Contreras-Reyes, E., I. Grevemeyer, E. R. Flueh, M. Scherwath, and M. Heesemann (2007), Alteration of the subducting oceanic lithosphere at the southern central Chile trench–outer rise, *Geochem. Geophys. Geosyst., 8,* Q07003, doi:10.1029/2007GC001632.

DeMets, C., R. G. Gordon, D. F. Argus, and S. Stein (1994), Effect of recent revisions to the

geomagnetic reversal time scale on estimates of current plate motions, *Geophys. Res. Lett., 21*, 2191-2194.

Engdahl, E.R., and A. Villaseñor (2002), Global Seismicity: 1900–1999, in *International Handbook of Earthquake and Engineering Seismology*, edited by W.H.K. Lee, H. Kanamori, P.C. Jennings, and C. Kisslinger, Part A, Chapter 41, pp. 665–690, Academic Press.

Flueh, E. R., D. Klaeschen, and J. Bialas (2002), Options for multi-component seismic data acquisition in deep water, First Break, 20, p. 764-769.

Grevemeyer, I., V. M. Tiwari (2006), Overriding plate controls spatial distribution of megathrust earthquakes in the Sunda–Andaman subduction zone, *Earth Planet. Sc. Lett., 251,* 3-4, 199-208.

Grevemeyer, I., C. R. Ranero, E. R. Flueh, D. Klaeschen, and J. Bialas (2007), Passive and active seismological study of bending-related faulting and mantle serpentinization at the Middle America trench, *Earth Planet. Sc. Lett., 258*, 528-242, doi:10.1016/j.epsl.2007.04.013.

Hall, R. (2002), Cenozoic geological and plate tectonic evolution of SE Asia and the SW Pacific: computer-based reconstructions, model and animations, *J. Asian Earth Sciences, 20*, 353-431.

Hall, R., and H. R. Smyth (2008), Cenozoic arc processes in Indonesia: identification of the key influences on the stratigraphic record in active volcanic arcs, in *Formation and Applications of the Sedimentary Record in Arc Collision Zones,* edited by A. E. Draut, P.D. Clift, and D.W. Scholl, *Geol. Soc. America Spec. Pap., 436*, p. 27-54, doi: 10.1130/2008.2436(03).

Hamilton, E. L. (1978), Sound velocity–density relations in sea-floor sediments and rocks, *J. Acoust. Soc. Am, 63,* Issue 2, pp. 366-377.

Hamilton, W. B., (1988), Plate tectonics and island arcs, *Geol. Soc. Am. Bull. 100,* 1503-1527.

Heine, C., R. D. Mueller, and C. Gaina (2004), Reconstructing the lost Tethys Ocean basin: Convergence history of the SE Asian margin and marine gateways, in *Continent-Ocean Interactions Within East Asian Marginal Seas. Geophys. Monogr. Ser.*, Vol. 149, edited by P Clift et al., pp. 37-54, American Geophysical Union, Washington D.C.

Hyndman, R. D., and S.M. Peacock (2003), Serpentinization of the forearc mantle, *Earth Planet. Sci. Lett., 212,* pp. 417–432.

Hyndman, R. D., and K. Wang (1993), Thermal constraints on the zone of major thrust earthquake failure: the Cascadia subduction zone, *J. Geophys. Res., 98*, 2039-2060.

Ivandic, M., I. Grevemeyer, A. Berhorst, E. R. Flueh, and K. McIntosh (2008), Impact of bending related faulting on the seismic properties of the incoming oceanic plate offshore of Nicaragua, *J. Geophys. Res., 113*, B05410, doi:10.1029/2007JB005291.

Kieckhefer, R. M., G. G. Shor Jr., J. R. Curray, W. Sugiarta, and F. Hehuwat (1980), Seismic refraction studies of the Sunda Trench and forearc basin, *J. Geophys. Res., 85,* 863–890, doi:10.1029/JB085iB02p00863.

Kopp, H., and N. Kukowski (2003), Backstop geometry and accretionary mechanics of the Sunda

644 margin, *Tectonics, 22*, doi: 10.1029/2002TC001420.
645
646 Kopp, H., E. R. Flueh, D. Klaeschen, J. Bialas, and C. Reichert (2001), Crustal structure of the central
647 Sunda margin at the onset of oblique subduction, *Geophys. J. Int., 147*, 449-474.
648
649 Kopp, H., D. Klaeschen, E. R. Flueh, and J. Bialas (2002), Crustal structure of the Java margin from
650 seismic wide-angle and multichannel reflection data, *J. Geophys. Res., 197*, B2,
651 doi:10.1029/2000JB000095.
652
653 Kopp, H., E. R. Flueh, C. J. Petersen, W. Weinrebe, A. Wittwer, and Meramex Scientists (2006), The
654 Java margin revisited: Evidence for subduction erosion off Java, *Earth and Planetary Science Letters,*
655 *242*, 130-142.
656
657 Korenaga, J., W. Holbrook, G. Kent, P. Kelemen, R. Detrick, H.-C. Larsen, J. Hopper, and T. Dahl-
658 Jensen (2000), Crustal structure of the southeast Greenland margin from joint refraction and reflection
659 seismic tomography, *J. Geophys. Res., 105(B9*), 21591-21614.
660
661 Korenaga, J., W. S. Holbrook, R. S. Detrick, and P. B. Kelemen (2001), Gravity anomalies and crustal
662 structure across the Southeast Greenland margin, *J. Geophys. Res., 106*, 8853-8870.
663
664 Lallemand, S. (1995), High rates of arc consumption by subduction processes: Some consequences,
665 *Geology, 23*, no. 6, p. 551-554, doi:10.1130/0091-7613.
666
667 Lay, T., H. Kanamori, C. J. Ammon, M. Nettles, S. N. Ward, R. C. Aster, S. L. Beck, S. L. Bilek, M.
668 R. Brudzinski, R. Butler, H. R. DeShon, G. Ekström, K. Satake, and S. Sipkin (2005), The Great

669 Sumatra-Andaman Earthquake of 26 December 2004, *Science, 308*, 5725, p. 1127-1131,
670 doi:10.1126/science.1112250.
671
672 Lueschen, E., C. Mueller, H. Kopp, M. Engels, R. Lutz, L. Planert, A. Shulgin, and Y. Djajadihardja
673 (2009), Structure, evolution and tectonic activity at the Eastern Sunda forearc, Indonesia, from marine
674 seismic investigations, submitted to *Tectonophysics*.
675
676 Moore, G. F., N. L. Bangs, A. Taira, S. Kuramoto, E. Pangborn, and H. J. Tobin (2007), Three-
677 dimensional splay fault geometry and implications for tsunami generation, *Science, 318*, 1128-1131.
678
679 Mueller, C., H. Kopp, Y. S. Djajadihardja, U. Barckhausen, A. Ehrhardt, M. Engels, E. R. Flueh, C.
680 Gaedicke, H. Keppler, R. Lutz, E. Lueschen, S. Neben, L. Seeber, and D. P. S. Dzulkarnaen (2008),
681 From subduction to collision: The Sunda-Banda arc transition, *EOS Trans. AGU*, 89, No.6, 49-60.
682
683 Newcomb, K. R., and W. R. McCann (1987), Seismic history and seismotectonics of the Sunda arc, *J.*
684 *Geophy. Res.*, *92*, pp. 421–439.
685
686 Parker, R. L. (1974), The rapid calculation of potential anomalies, *Geophys. J. R. Astron. Soc.*, *31*, 447-
687 455.
688
689 Ranero, C. R., and V. Sallarès (2004), Geophysical evidence for hydration of the crust and mantle of
690 the Nazca plate during bending at the north Chile trench, *Geology*, *32*, no. 7, p. 549-552, doi:
691 10.1130/G20379.1.
692
693 Rutherford, E., K. Burke, and J. Lytwyn (2001), Tectonic history of Sumba Island, Indonesia, since the

694 Late Cretaceous and its rapid escape into forearc in the Miocene, *J. Asian Earth Sciences, 19*, 453-479.
695
696 Scherwath, M., H. Kopp, E. R. Flueh, S. A. Henrys, R. Sutherland, V. M. Stagpoole, D. H. N. Barker,
697 M. E. Reyners, D. G. Basset, L. Planert, and A. Dannowski, Fore-arc deformation and underplating at
698 the northern Hikurangi margin, New Zealand, submitted to *J. Geophys. Res.* in 2009.
699
700 Schlueter, H. U., C. Gaedicke, H. A. Roeser, B. Schreckenberger, H. Meyer, C. Reichert, Y.
701 Djajadihardja, and A. Prexl (2002), Tectonic features of the southern Sumatra-western Java forearc of
702 Indonesia, *Tectonics, 21*, doi:10.1029/2001TC901048.
703
704 Shulgin, A., H. Kopp, C. Mueller, E. Lueschen, L. Planert, M. Engels, E. R. Flueh, A. Krabbenhoeft,
705 and Y. Djajadihardja (2009), Sunda-Banda arc transition: Incipient continent-island arc collision
706 (northwest Australia), Geophys. Res. Lett., 36, L10304, doi:10.1029/2009GL037533.
707
708 Shulgin, A., H. Kopp, C. Mueller, E. Lueschen, L. Planert, M. Engels, Y. Djajadihardja, E. R. Flueh,
709 and A. Krabbenhoeft (2009b), Subduction of the Roo Rise offshore East Java, submitted soon...
710
711 Sibuet, J.-C., C. Rangin, X. Le Pichon, S. Singh, A. Cattaneo, D. Graindorge, F. Klingelhoefer, J.-Y.
712 Lin, J. Malod, T. Maury, J.-L. Schneider, N. Sultan, M. Umber, H. Yamaguchif and “Sumatra
713 aftershocks” team (2007), 26th December 2004 great Sumatra–Andaman earthquake: co-seismic and
714 postseismic motions in northern Sumatra, *Earth Planet. Sci. Lett., 263*, p. 88-103,
715 doi:10.1016/j.epsl.2007.09.005.
716
717 Smyth, H. R., P. J. Hamilton, R. Hall, and P. D. Kinny (2007), The deep crust beneath island arcs:
718 Inherited zircons reveal a Gondwana continental fragment beneath East Java, Indonesia, *Earth Planet.*

719 *Sci. Lett., 258*, 269-282, doi:10.1016/j.epsl.2007.03.044.
720
721 Smyth, H. R., R. Hall, and G. J. Nichols (2008), Cenozoic volcanic arc history of East Java, Indonesia:
722 The stratigraphic record of eruptions on an active continental margin, in *Lessons from the Stratigraphic*
723 *Record in Arc Collision Zones*, edited by A. E. Draut, P.D. Clift, and D.W. Scholl, *Geol. Soc. America*
724 *Spec. Pap., 436*, p. 27-54, doi: 10.1130/2008.2436(10).
725
726 Spicák, A., V. Hanus, and J. Vanek (2007), Earthquake occurrence along the Java trench in front of the
727 onset of the Wadati-Benioff zone: Beginning of a new subduction cycle? *Tectonics*, *26*,
728 doi:10.1029/2005TC001867.
729
730 Sutherland, R., V. Stagpoole, C. Uruski, S. Henrys, B. Field, S. Toulmin, D. Barker, S. Bannister, F.
731 Davey, C. Kennedy, D. Basset, T. Stern, M. Scherwath, E. Flueh, and H. Kopp, Reactivation of
732 tectonics, crustal underplating and uplift after 60 Myr of passive subsidence, Raukumara Basin,
733 Hikurangi-Kermadec forearc, New Zealand: implications for global growth and recycling of continents,
734 accepted in *Tectonics* in 2009.
735
736 Van der Werff, W. (1995), Structure and morphotectonics of the accretionary prism along the Eastern
737 Sunda-Western Banda Arc, *Journal of Southeast Asian Earth Sciences*, *11*, 309-322.
738
739 Wallace, L. M., S. Ellis, and P. Mann (2009), Collisional model for rapid fore-arc block rotations, arc
740 curvature, and episodic back-arc rifting in subduction settings, *Geochem. Geophys. Geosyst.*, *10*,
741 Q05001, doi:10.1029/2008GC002220.
742
743 Wiener, N. (1949), *Extrapolation, interpolation, and smoothing of stationary time series*, New York,

744 John Wiley and Sons.

745

746

Figures:

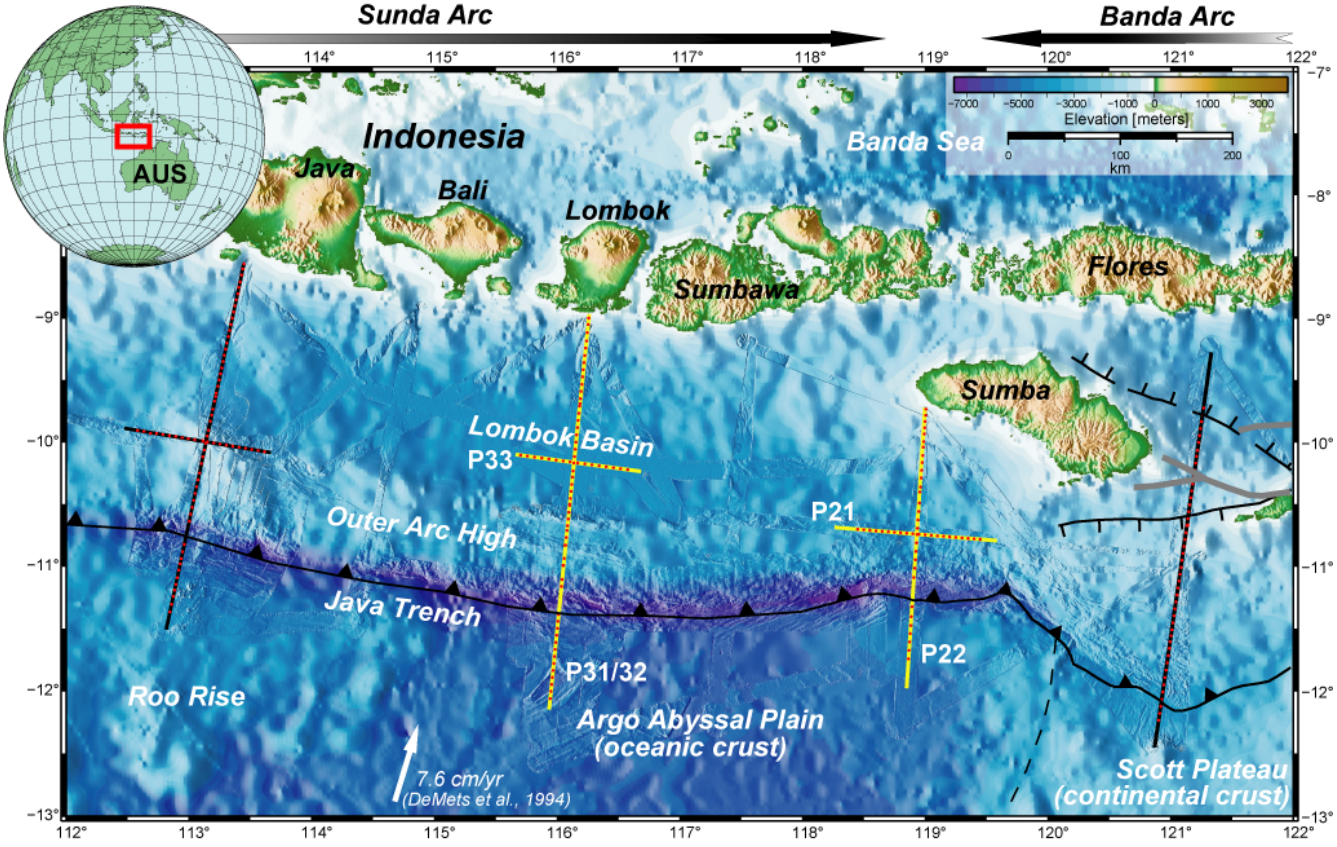

Fig. 1: *Work Area and profile distribution of the SINDBAD seismic refraction experiment. Red circles mark the the locations of ocean bottom seismic recorders. In this study we present results for the corridors at 116°E and 119°E (yellow profiles) characterized by the subduction of oceanic crust of the Argo Abyssal Plain. The westernmost (113°E) as well as easternmost (121°E) corridors (black profiles) represent distinct tectonic regimes dominated by the subduction of thickened crust of the Roo Rise and Scott Plateau, respectively. These areas are discussed in Shulgin et al. [2009a, 2009b].*

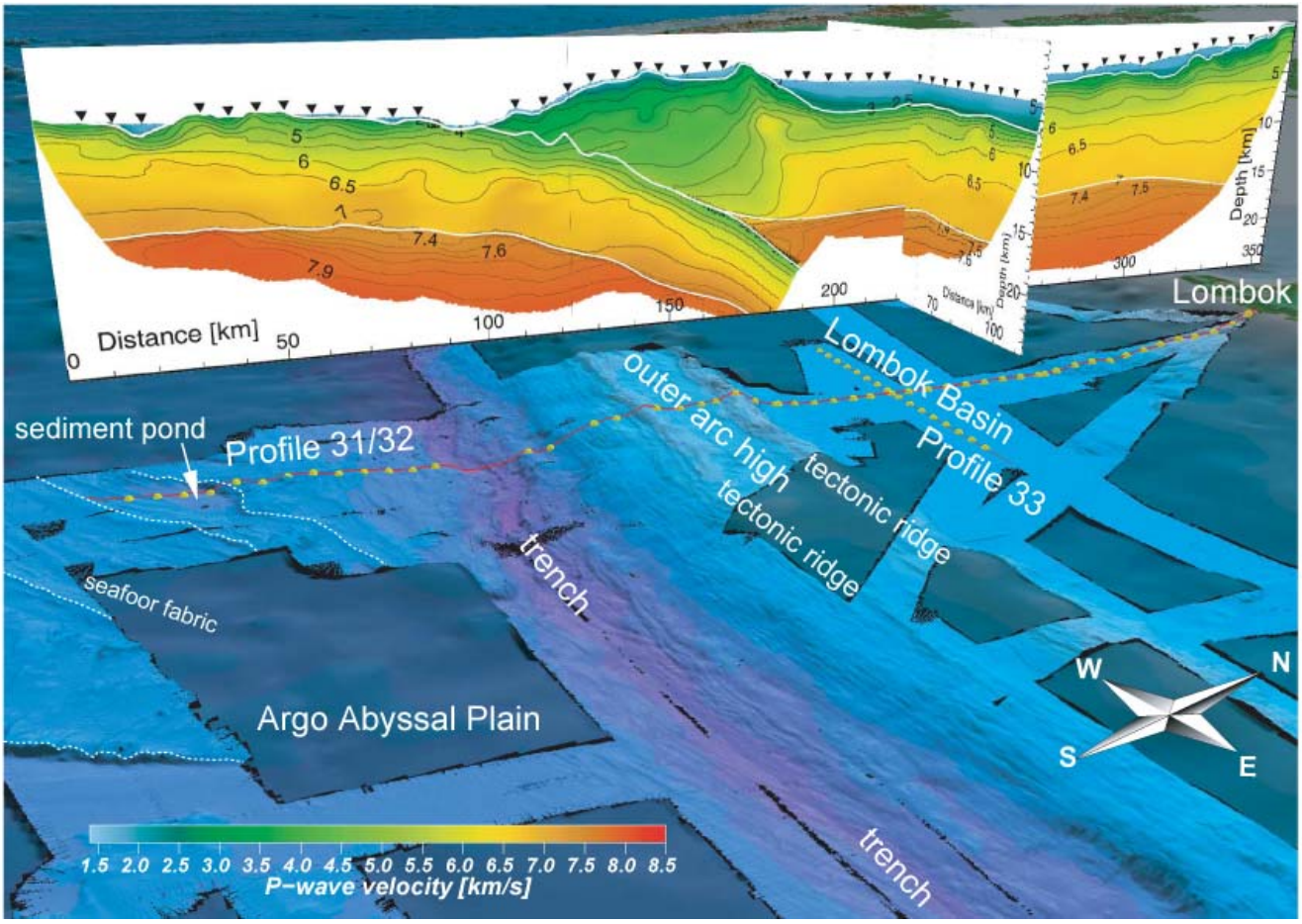

Fig.2: *116°E corridor offshore Lombok: perspective view including acquired seafloor bathymetry (light blue) and seismic velocity profiles (velocities are color coded). The red lines are seafloor projections of the seismic shots, yellow spheres mark the instrument locations. Seafloor fabric locally crops out as basement structures on the oceanic plate. The trench is largely devoid of sediments. A well-developed outer arc high comprises pronounced ridge structures. The Lombok Basin is characterized by a virtually flat seafloor. Annotated features are discussed in the text.*

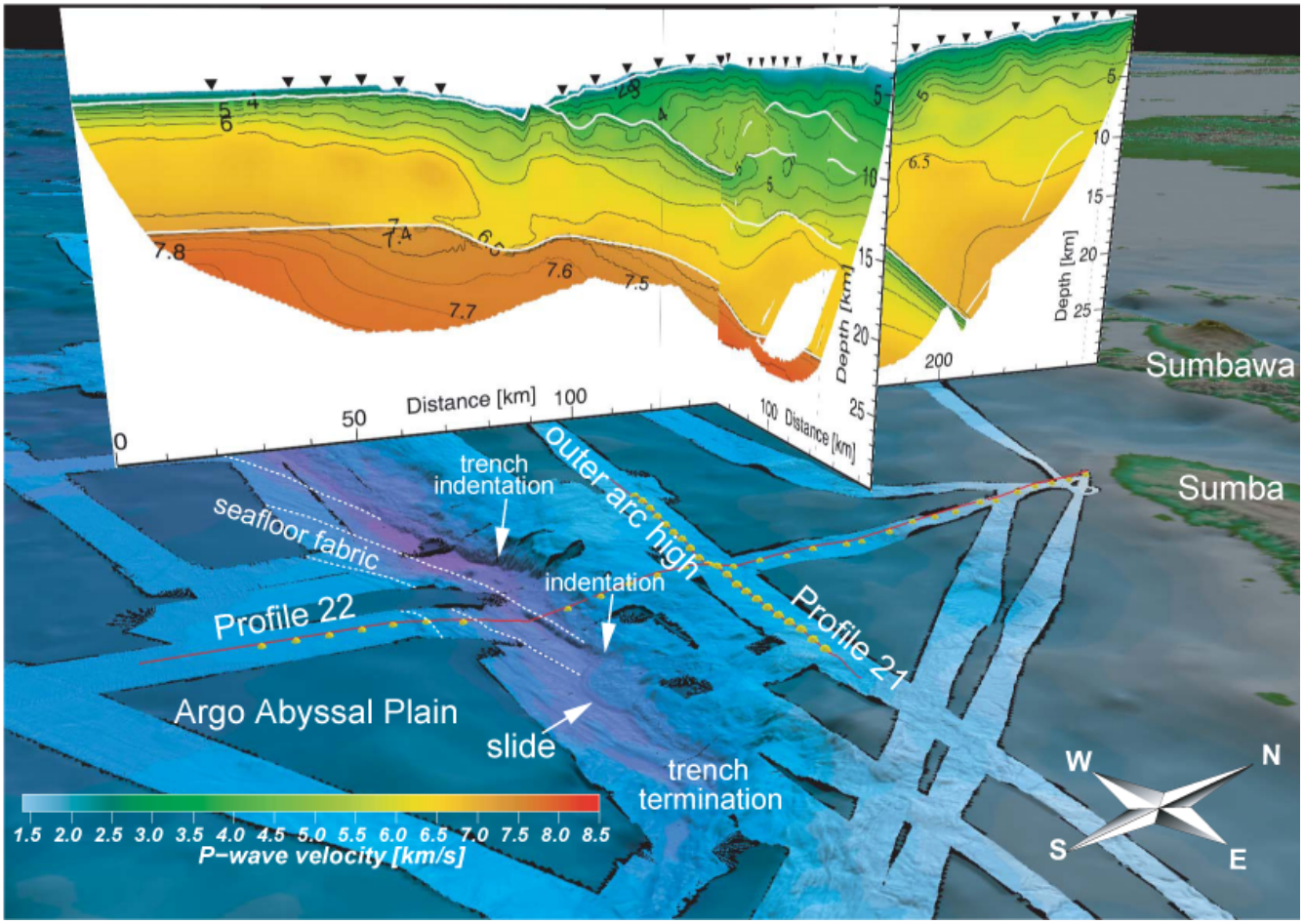

763

764 ***Fig.3:*** *119°E corridor offshore Sumba: perspective view including acquired seafloor bathymetry (light*
765 *blue) and seismic velocity profiles (velocities are color coded). The red lines are seafloor projections of*
766 *the seismic shots, yellow spheres mark the instrument locations. The subduction of reactivated seafloor*
767 *fabric, aligned at high angles relative to the trench, locally results in the erosion of the lower slope and*
768 *subsequent slope failure (note the coincidence of the eastern indentation and the slide). Annotated*
769 *features are discussed in the text.*

770

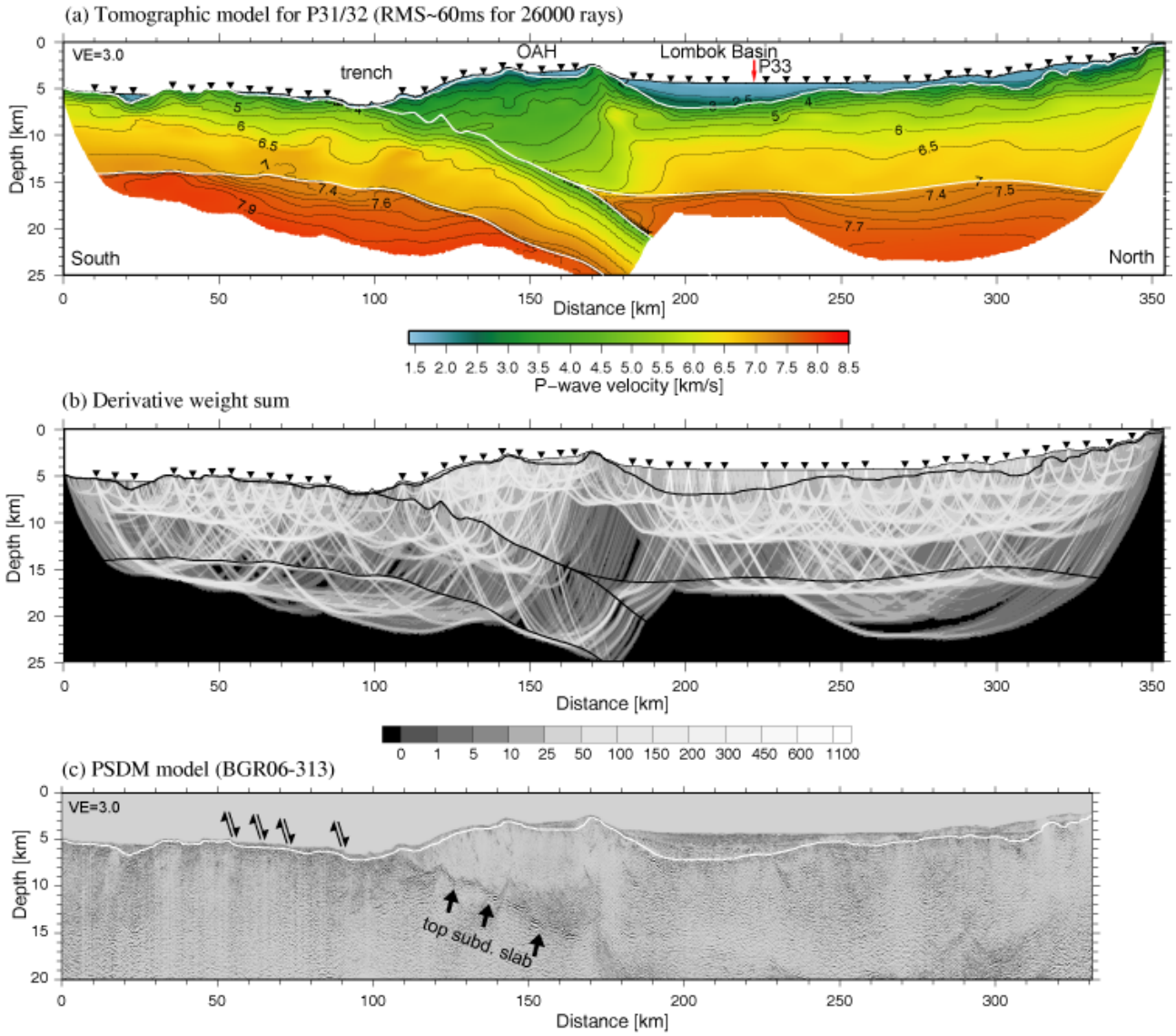

771

772 ***Fig. 4:*** *(top): Final tomographic velocity model for profile 31/32. Triangles indicate locations of ocean*
773 *bottom seismographs. Red arrow displays line intersection with profile 33. White lines mark structural*
774 *interfaces: sedimentary portions are derived from the analysis of high-resolution MCS seismic data;*
775 *plate boundary, oceanic Moho and forearc Moho are obtained from the joint refraction and wide-angle*
776 *reflection tomography. (center): Derivative weight sum for the final tomographic velocity model.*
777 *(bottom): Coincident prestack depth-migrated MCS line BGR06-313 from Lueschen et al. [2009]. Line*
778 *drawing shows sedimentary basement (white line) and area of normal faulting. All models are plotted*
779 *with 3× vertical exaggeration. OAH=outer arc high.*

780

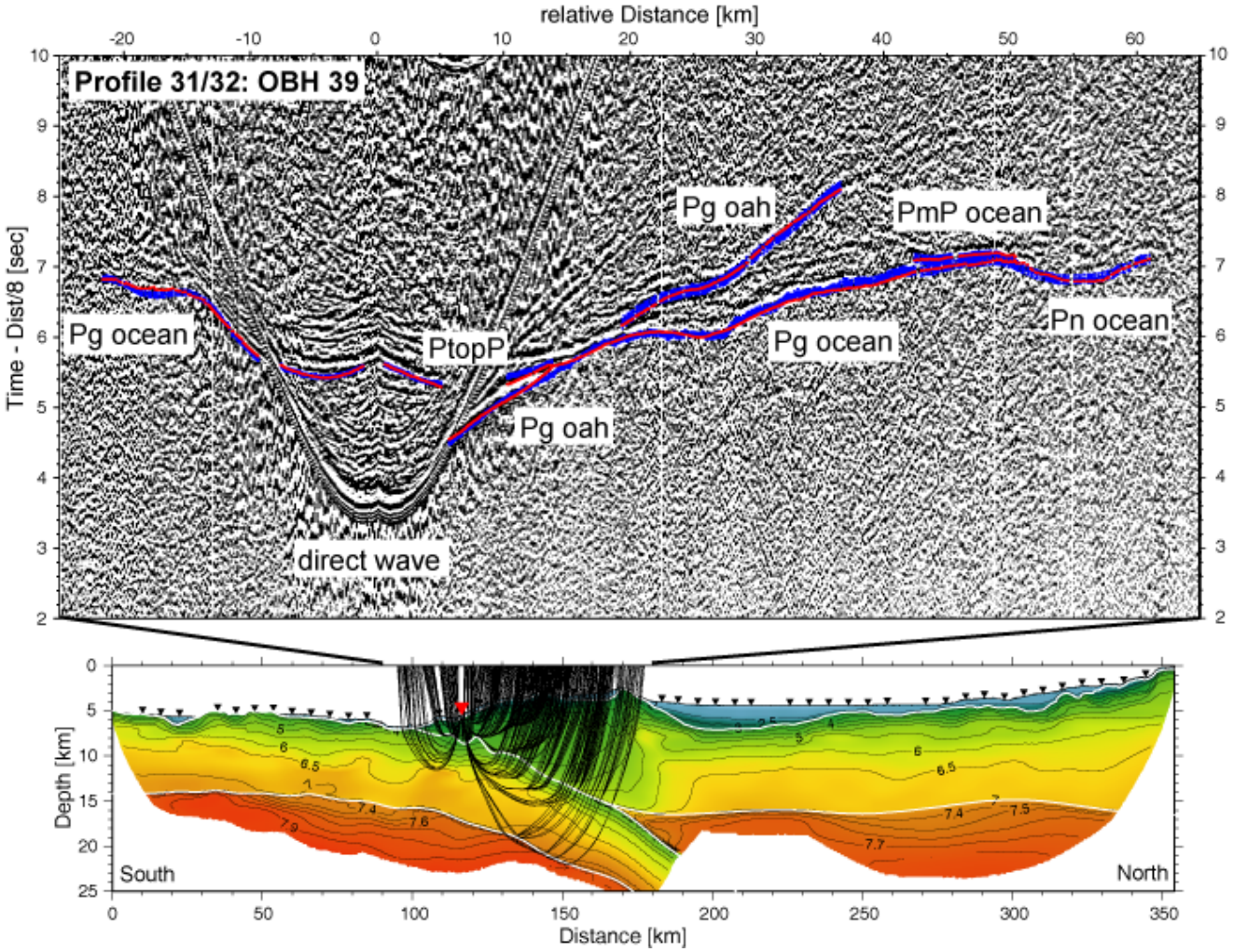

781

782 ***Fig. 5:*** *Record section of OBH 39, located at the lower OAH slope on profile 31/32, and constraining*
783 *the velocity structure of the OAH and the downgoing oceanic plate. (top): Computed traveltimes (red*
784 *dots) and associated pick uncertainties (blue bars). Interpreted seismic arrivals are labeled: Pg oah*
785 *(turning rays within the outer arc high), Pg ocean (turning rays within the oceanic crust), Pn ocean*
786 *(turning rays in the upper oceanic mantle), PtopP (reflected rays at the plate boundary), and PmP*
787 *ocean (reflected rays at the oceanic Moho). (bottom): Corresponding ray paths through the final*
788 *tomographic solution of Profile 31/32. Velocity contours are annotated in km/s.*

789

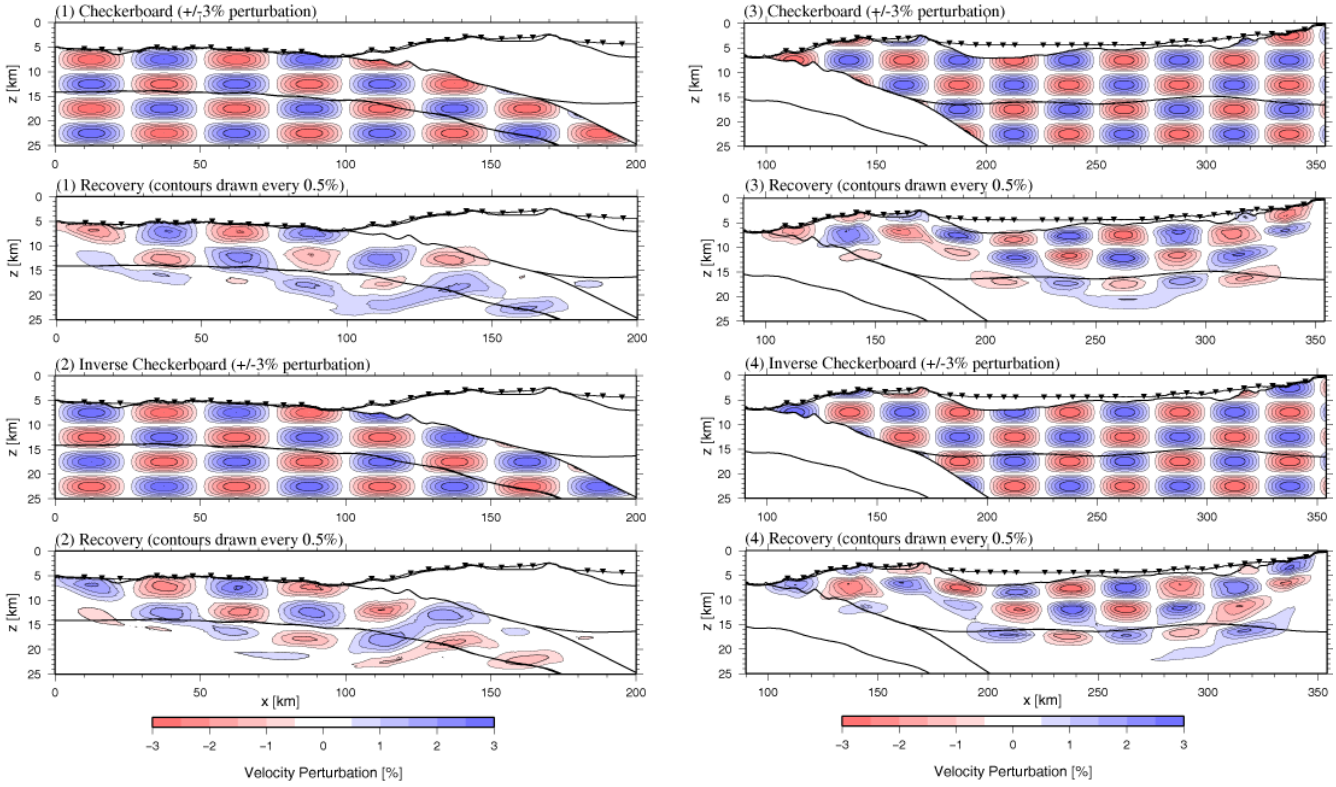

790

791 ***Fig. 6:*** *Resolution tests using a ±3 %, 25 km x 5 km checkerboard pattern of synthetic velocity*

792 *anomalies within the oceanic model portions (left) and within the forearc model portions (right) of*

793 *profile 31/32. Tests show normal and inverse checkerboard patterns, original perturbation model and*

794 *recovery after three iterations, respectively. The background model for the anomalies is the*

795 *tomographic velocity model of figure 4 (top). See text for discussion.*

796

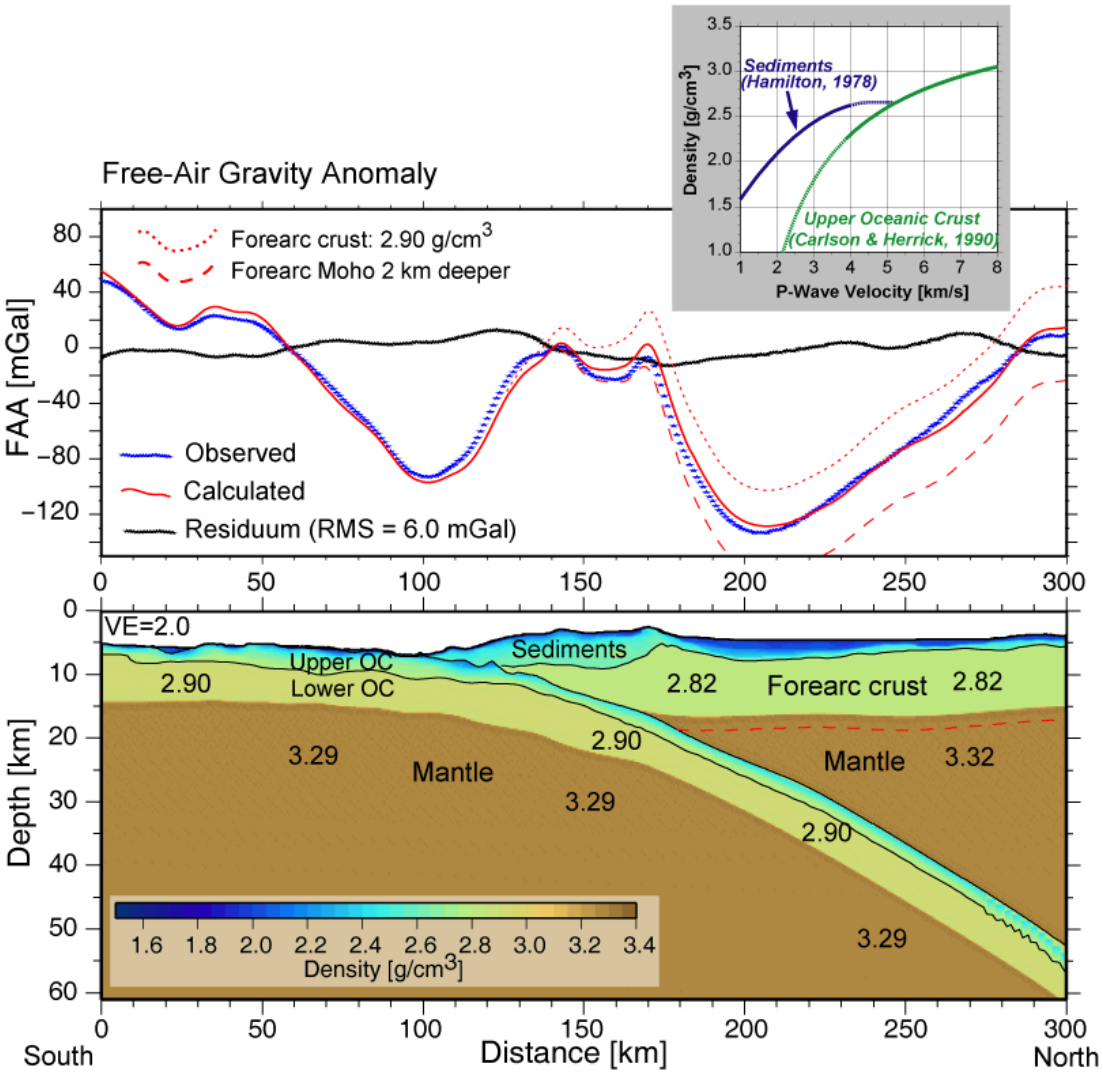

797

798 ***Fig. 7:*** *Gravity modeling for profile 31/32. (top): Free-air gravity anomaly, observed (blue stars) and*
799 *calculated (red lines) for different density models: the solid red line (best fit) and corresponding*
800 *residuum (black stars; RMS=6 mGal) are obtained for the density model below, the dashed red line is*
801 *obtained by assuming a 2 km thicker forearc crust (see red dashed forearc Moho in the density model*
802 *below), and the dotted red line is obtained by assuming a density of 2.90 g/cm^3 for the forearc crust.*
803 *(bottom): Densities are converted from seismic velocities using empirical velocity-density relations for*
804 *major structural units and constant densities elsewhere (see insect and text for details).*

805

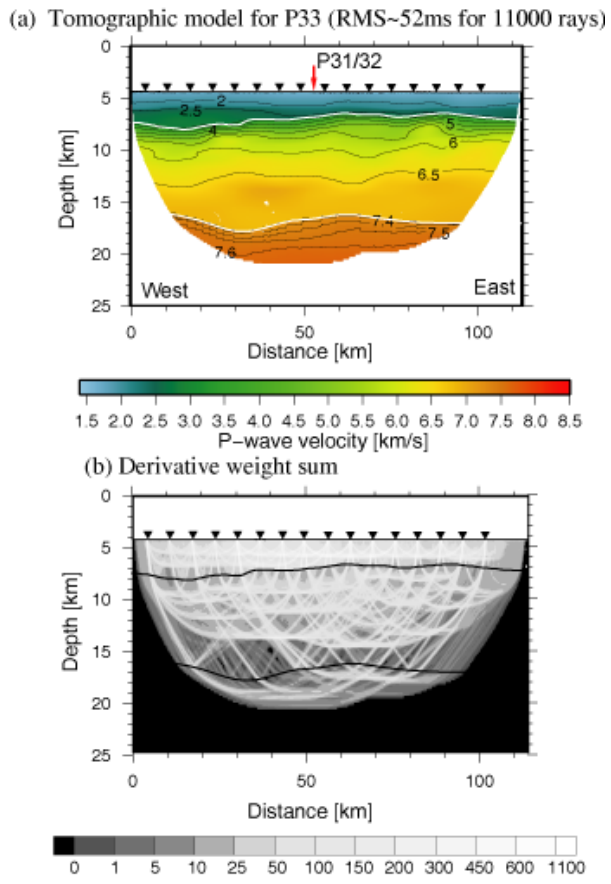

806

807 ***Fig. 8:*** *(top): Final tomographic velocity model for profile 33 (Lombok Basin). Triangles indicate*

808 *locations of ocean bottom seismographs. Red arrow displays line intersection with profile 31/32. White*

809 *lines mark structural interfaces: basement and forearc Moho are obtained from the joint refraction and*

810 *wide-angle reflection tomography. (bottom): Derivative weight sum for the final tomographic velocity*

811 *model.*

812

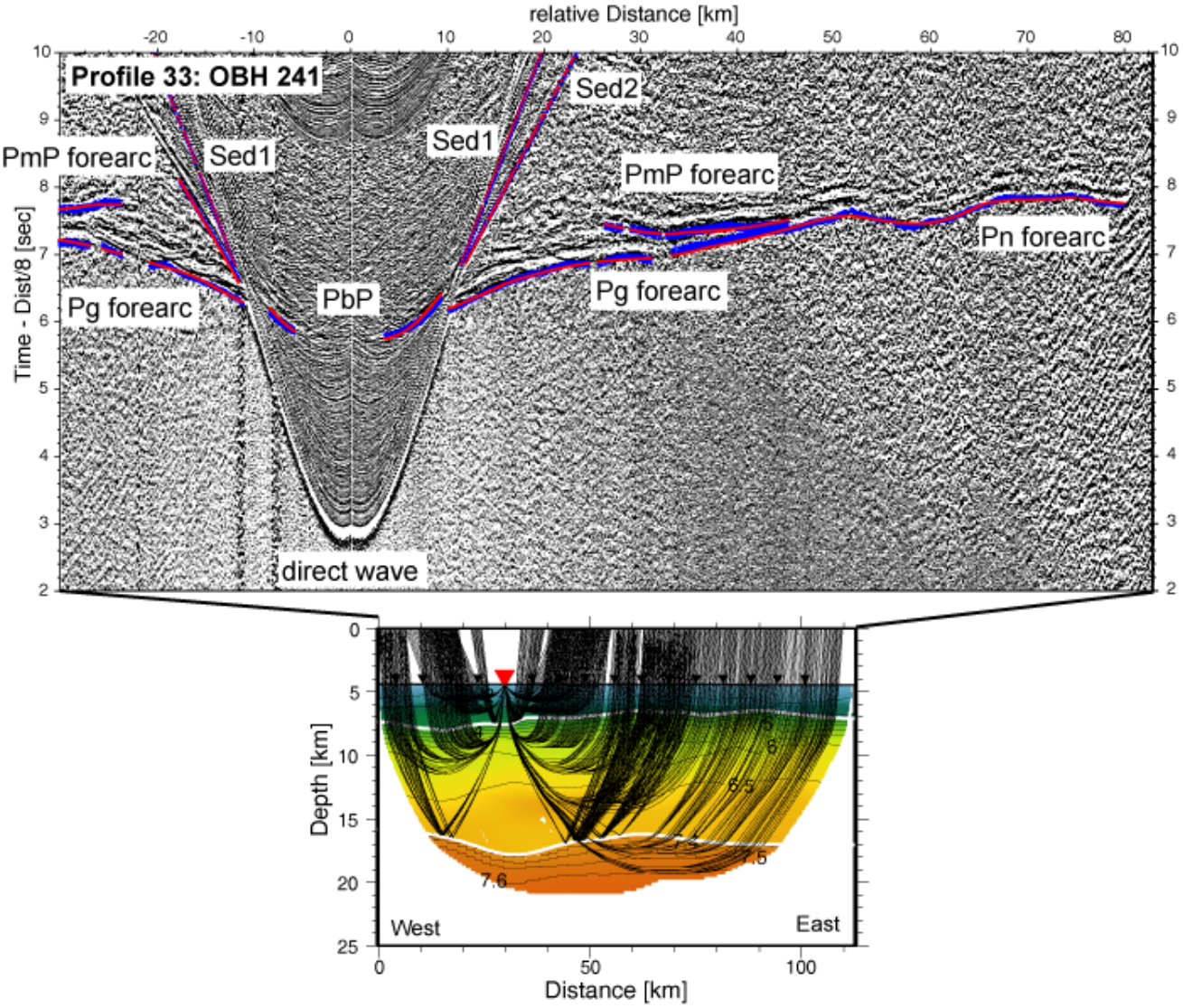

Fig. 9: *Record section of OBH 241, located on profile 33, constraining the sedimentary portions of the Lombok Basin as well as the underlying crust and forearc mantle. Note the strong PmP reflection from the shallow forearc Moho. (top): Computed traveltimes (red dots) and associated pick uncertainties (blue bars). Interpreted seismic arrivals are labeled: Sed1 (turning rays within the upper sediments), Sed2 (turning rays within the lower sediments), Pg forearc (turning rays within the forearc crust), Pn forearc (turning rays in the upper forearc mantle), PbP (reflected rays at the basement), and PmP forearc (reflected rays at the forearc Moho). (bottom): Corresponding ray paths through the final tomographic solution of Profile 33. Velocity contours are annotated in km/s.*

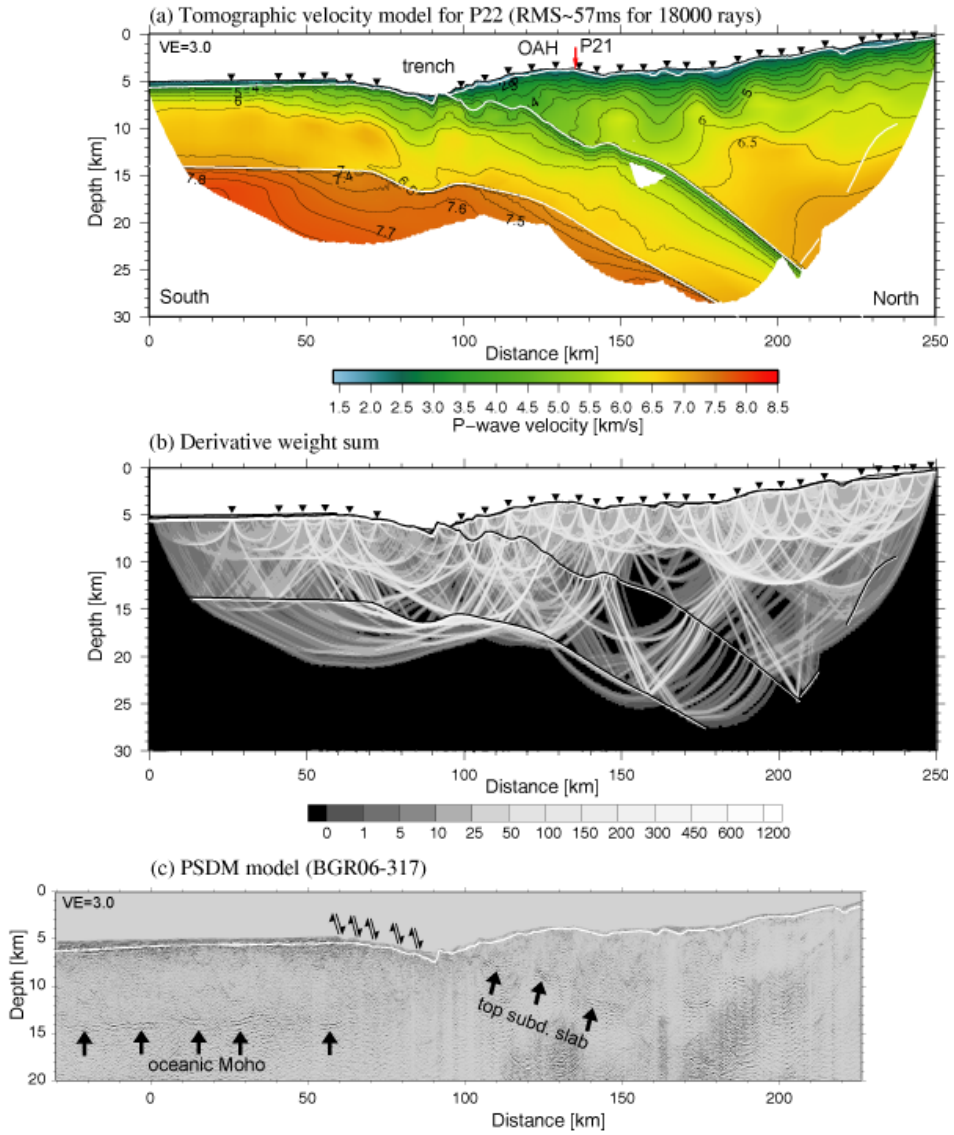

Fig. 10: *(top): Final tomographic velocity model for profile 22. Triangles indicate locations of ocean bottom seismographs. Red arrow displays line intersection with profile 21. White lines mark structural interfaces: sedimentary portions are derived from the analysis of high-resolution MCS seismic data; plate boundary, oceanic Moho and seaward dipping forearc reflector are obtained from the joint refraction and wide-angle reflection tomography. (center): Derivative weight sum for the final tomographic velocity model. (bottom): Coincident prestack depth-migrated MCS line BGR06-317 from Lueschen et al. [2009]. Line drawing shows sedimentary basement (white line) and area of normal faulting. All models are plotted with 3× vertical exaggeration. OAH=outer arc high.*

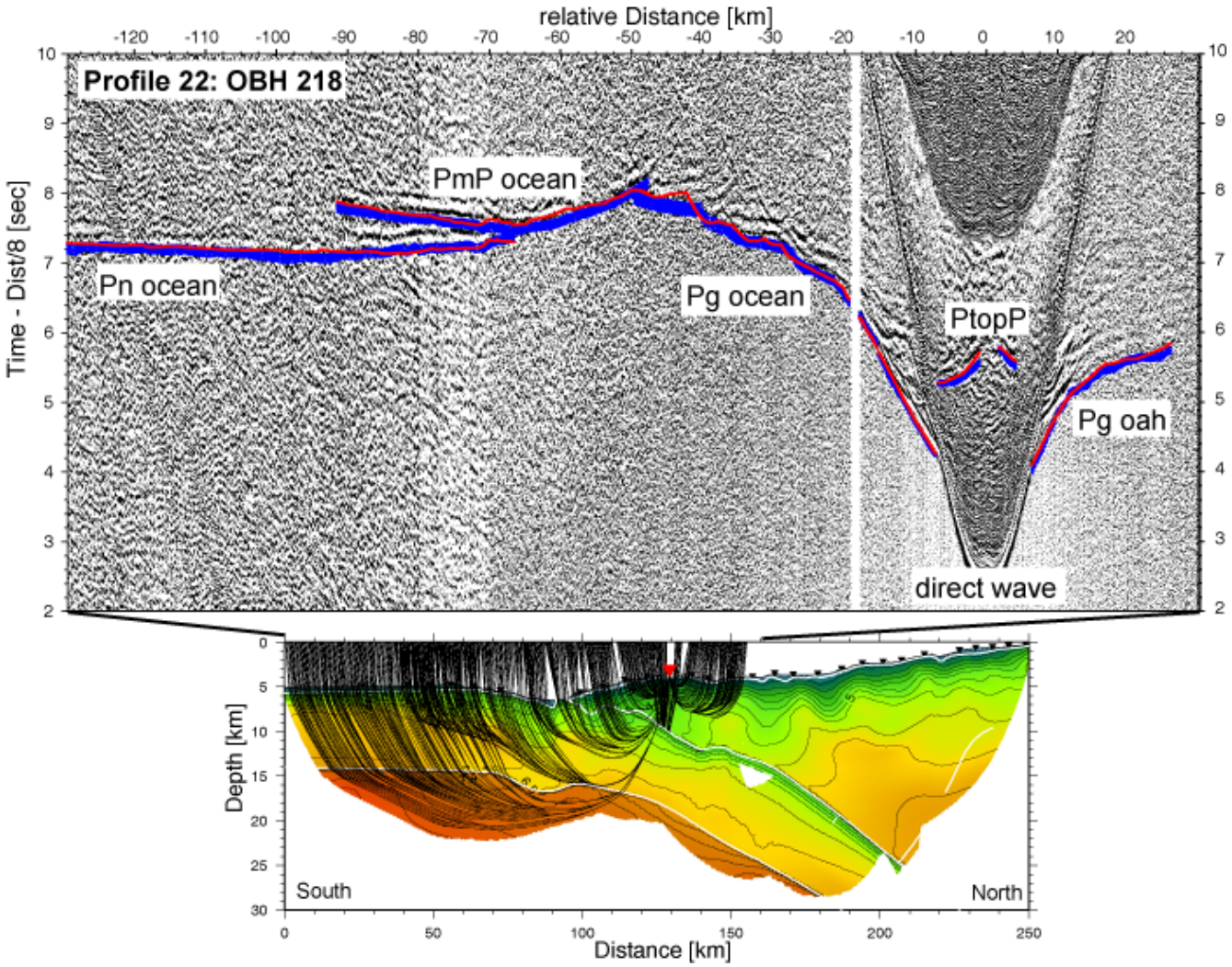

833

834 ***Fig. 11:*** *Record section of OBH 218, located at the OAH on profile 22, constraining large portions of*
835 *the incoming oceanic crust and mantle. (top): Computed traveltimes (red dots) and associated pick*
836 *uncertainties (blue bars). Interpreted seismic arrivals are labeled: Pg oah (turning rays within the*
837 *outer arc high), Pg ocean (turning rays within the oceanic crust), Pn ocean (turning rays in the upper*
838 *oceanic mantle), PtopP (reflected rays at the plate boundary), and PmP ocean (reflected rays at the*
839 *oceanic Moho). (bottom): Corresponding ray paths through the final tomographic solution of Profile*
840 *22. Velocity contours are annotated in km/s.*

841

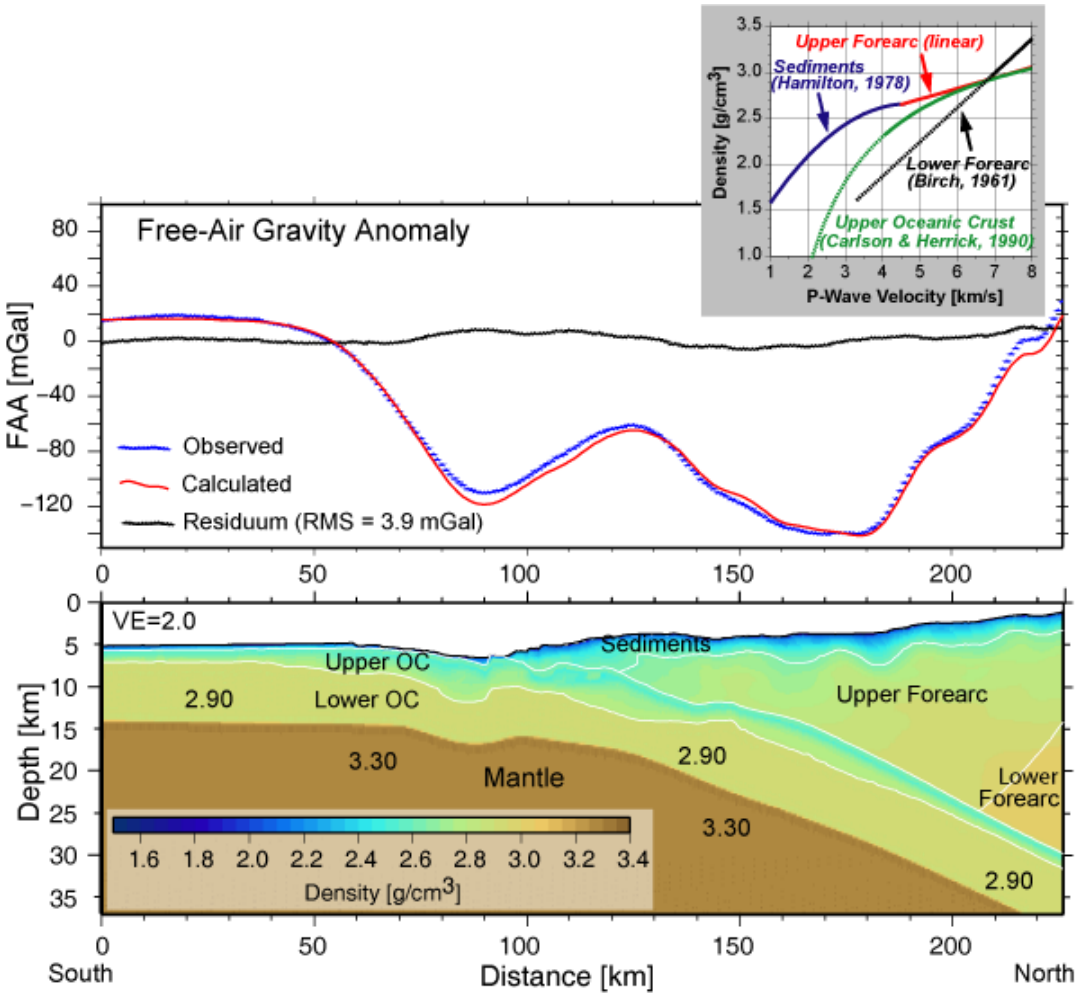

842

843 ***Fig. 12:*** *Gravity modeling for profile 22. (top): Observed (blue stars) and calculated (red line) free-air*

844 *gravity anomaly for the density model below. Black stars show corresponding residuum (RMS=3.9*

845 *mGal). (bottom): Densities are converted from seismic velocities using empirical velocity-density*

846 *relations for major structural units and constant densities elsewhere (see insect and text for details).*

847

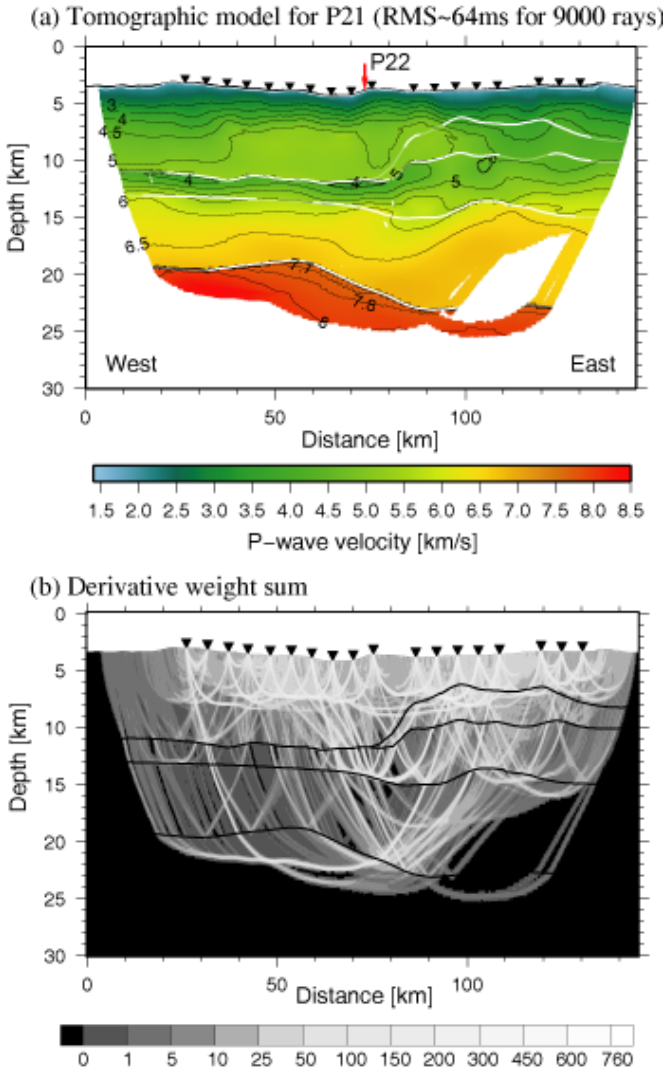

Fig. 13: *(top): Final tomographic velocity model for profile 21 (outer arc high). Triangles indicate locations of ocean bottom seismographs. Red arrow displays line intersection with profile 22. White lines mark structural interfaces obtained from the joint refraction and wide-angle reflection tomography (see text for details). (bottom): Derivative weight sum for the final tomographic velocity model.*

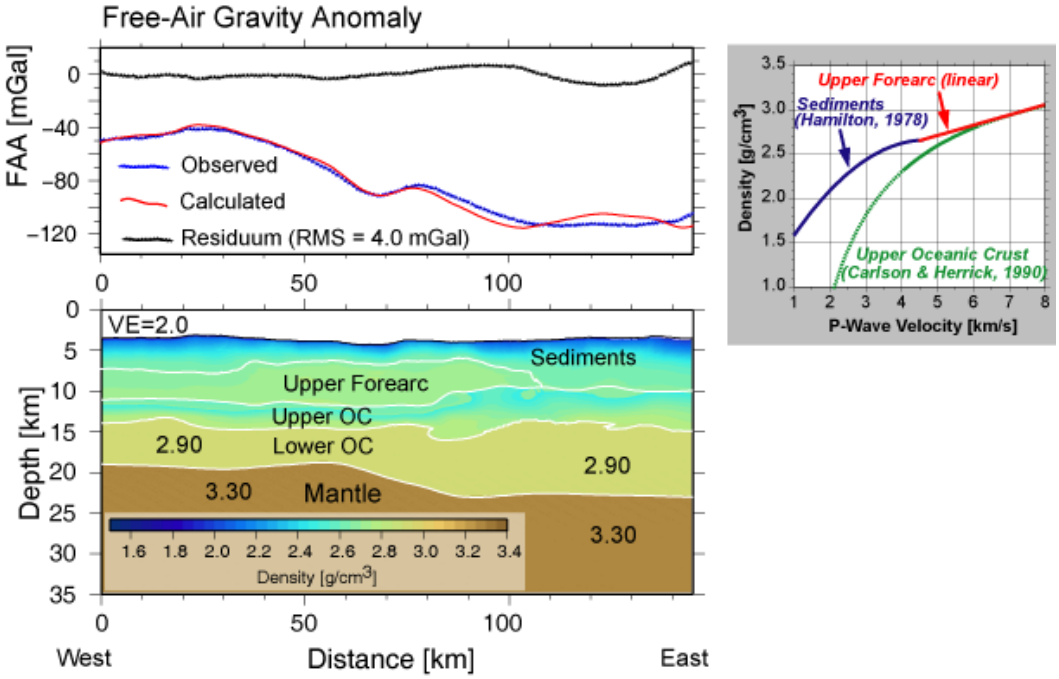

855

856 ***Fig. 14:*** *Gravity modeling for profile 21. (top): Observed (blue stars) and calculated (red line) free-air*

857 *gravity anomaly for the density model below. Black stars show corresponding residuum (RMS=4.0*

858 *mGal). (bottom): Densities are converted from seismic velocities using empirical velocity-density*

859 *relations for major structural units and constant densities elsewhere (see insect and text for details).*

860

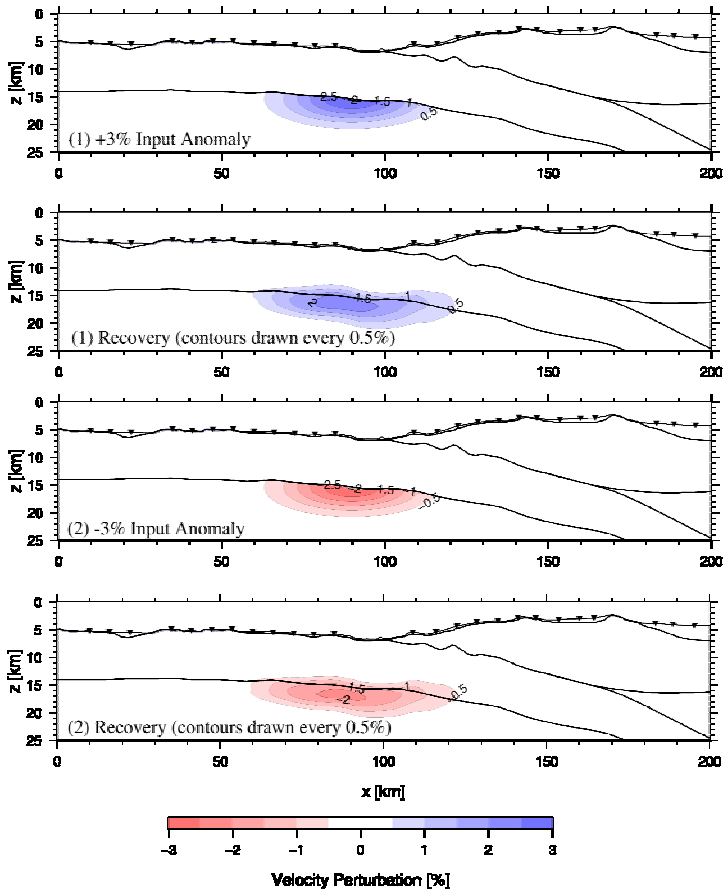

Fig. 15: *Resolution tests for profile 31/32. We use a 3 % synthetic velocity anomaly within the oceanic mantle at the trench. Recovery after three iterations is shown for normal and inverse perturbational model. Results demonstrate that the uppermost ~2 km beneath the Moho at the trench are well resolved. The background model for the anomalies is the tomographic velocity model of figure 4 (top).*

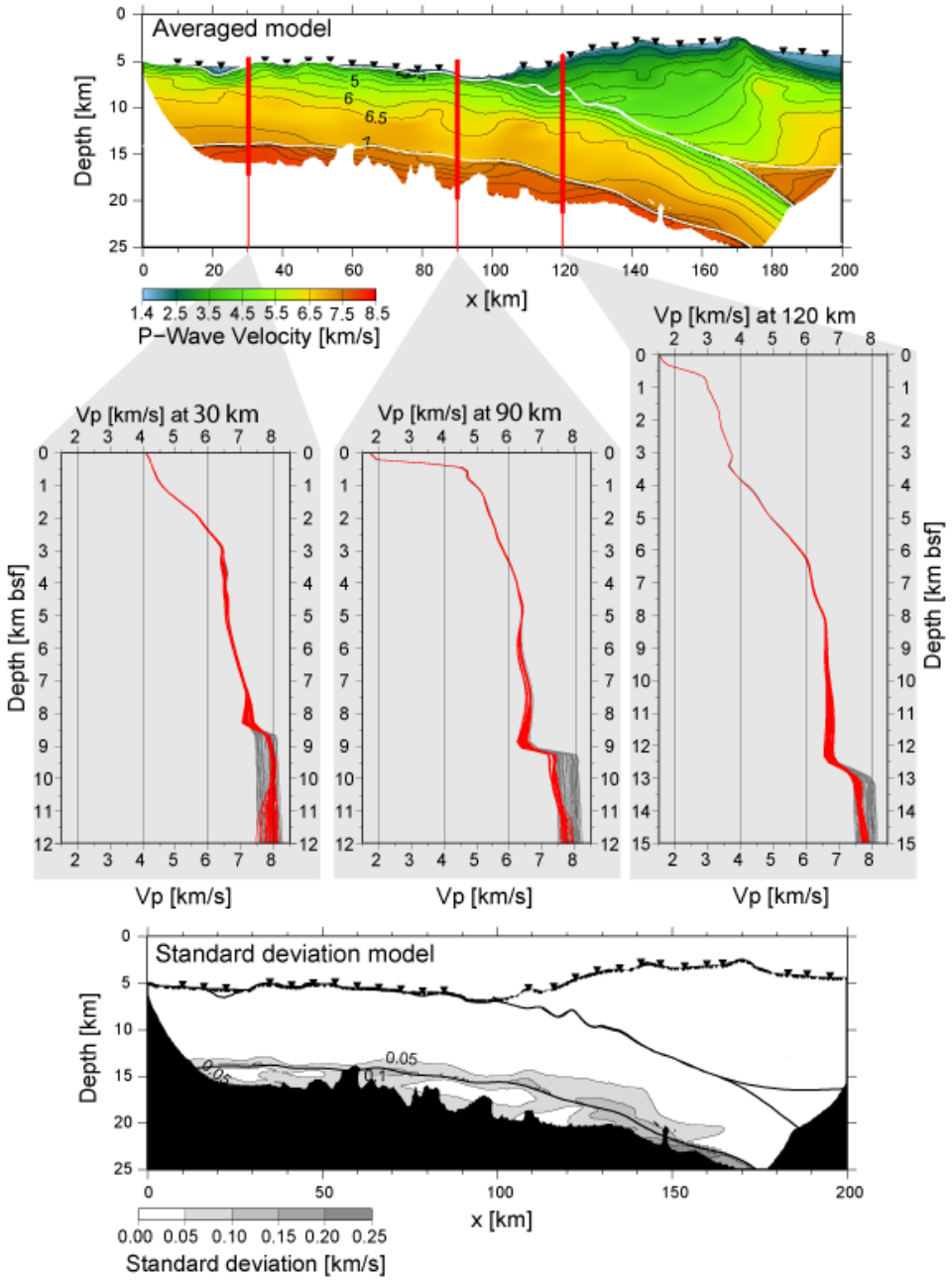

867

868 ***Fig. 16:*** *Test of 40 different mantle starting models on the tomographic solution of profile 31/32, high-*
869 *lighting the robustness of the obtained upper mantle velocities (see text for details). Individual initial*
870 *models were built by laterally expanding a 1-D velocity depth profile beneath the Moho (see text for*
871 *details). (top): Model obtained by averaging the 40 output models. Only model areas with ray coverage*
872 *in all solutions are shown. (center): Velocity depth profiles through starting models (gray lines) and*
873 *final solutions (red lines) at three different locations. (bottom): Standard deviation model.*

874

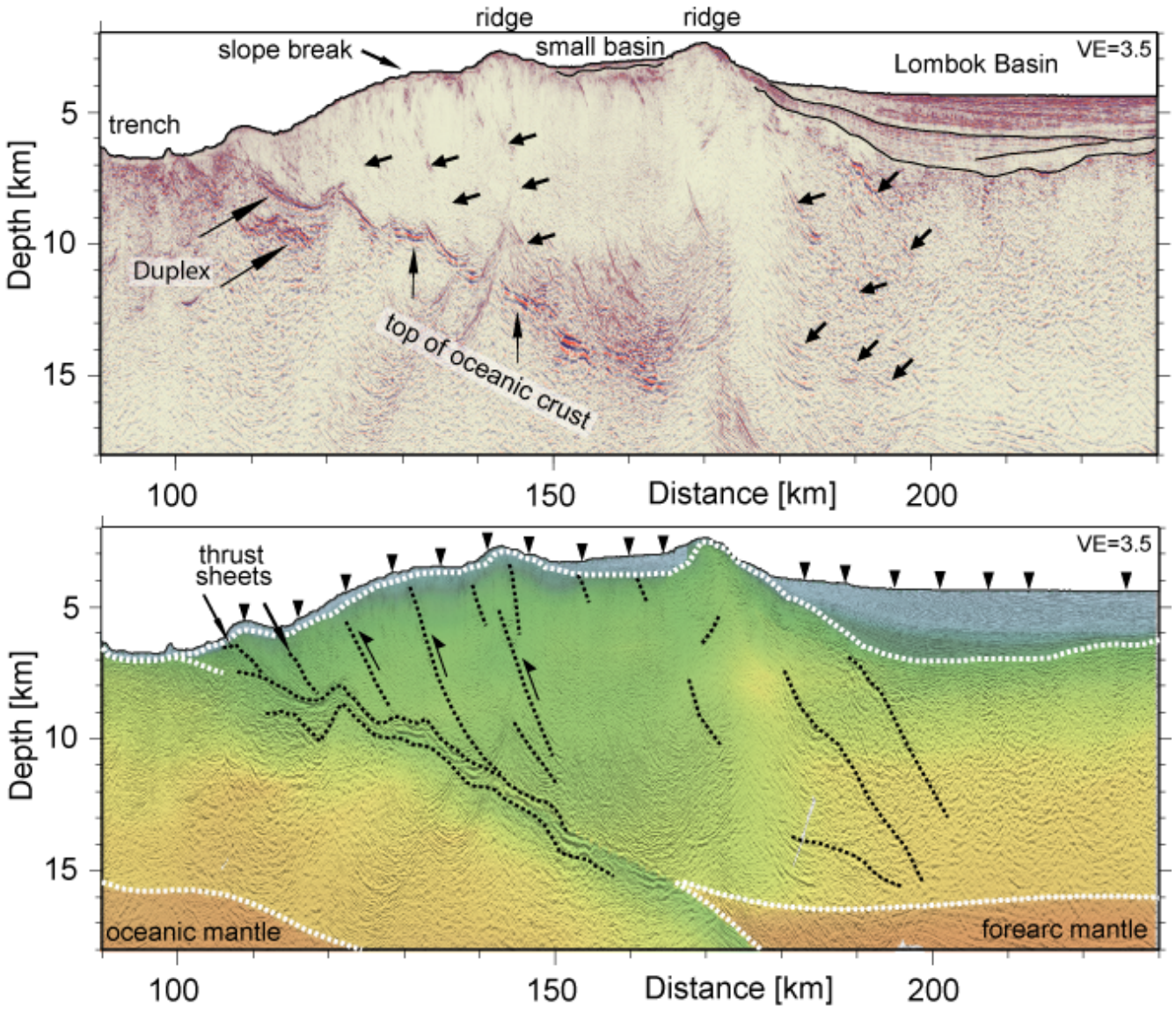

875

876 ***Fig. 17:*** *(top): Color coded close-up of prestack depth-migrated MCS line BGR06-313 (modified from*
877 *Lueschen et al. [2009]). The plate interface reveals a pronounced vertical relief and a duplex structure.*
878 *The outer arc high is characterized by landward dipping faults. (bottom): Final tomographic velocity*
879 *model and line drawing overlain over PSDM image. Splay faults originate from the plate boundary at*
880 *places where it changes shape and dip abruptly. The faults connect to the seafloor, where they are*
881 *associated with changes in slope angle and a tectonic ridge. Triangles along seafloor indicate*
882 *locations of ocean bottom stations. Models are plotted at 3.5× vertical exaggeration.*

883